Electronic Theses and Dissertations   Graduate School

1-1-2014

Reconfigurable microstrip antennas with tunable radiation pattern characteristics

Ahmed Khidre
University of Mississippi

RECONFIGURABLE MICROSTRIP ANTENNAS WITH TUNABLE

RADIATION PATTERN CHARACTERSTICS

A Dissertation

Presented in partial fulfillment of the requirements for

Doctor of Philosophy

Degree

Electrical Engineering

The University of Mississippi

Ahmed Khidre

May, 2014

ABSTRACT

Reconfigurable beam antenna systems are capable of changing their radiation characteristics in real time, such as beam direction, beam shape, beamwidth, etc. Such antenna system is desired for various wireless applications because of many reasons among them; it helps to enhance signal strength received from an intended target, mitigates interference, and accommodates sudden changes in traffic demand of wireless networks. It might also help to reduce the deployment cost of wireless networks infrastructures.

In this dissertation, designs for reconfigurable beam microstrip antennas with tunable radiation characteristics have been proposed. The method to achieve these designs is the reconfigurable parasitic element (s) of tunable electrical size, placed in close proximity to the driven patch. A tuning mechanism with the aid of Varactor diodes is introduced for the parasitic patch that effectively allows for controlling its electrical size. This (these) reconfigurable parasitic patch (es) is (are) then applied in different fashions to devise several antenna designs with dynamic electronic control over certain radiation specifications. The accomplished antenna designs in the dissertation are:

- Circularly polarized (CP) beam scanning antenna, where two elements microstrip Yagi-Uda antenna is used. The first element is a square patch driven with two probe feeds of quadrature phase for CP excitation. The second element is a parasitic square patch with narrow square-shaped slot carved on its surface. The parasitic patch is adjacent to the driven patch with a small separation distance. Four varactor diodes are placed on the middle of each side of the square slot to facilitate tuning of its electrical size. The parasitic patch

electrical size is allowed to be effectively tuned by varying the applied reverse biasing DC voltage to the varactors (capacitance value). The CP beam direction is scanned from $-36°$ to $32°$ with gain variation from 5.7 to 8.2 dBic, and efficiency from 54% to 75.58% along the scanning range.

- Two-dimensional beam scanning antenna, where two orthogonal crossed Yagi-Uda antenna configuration is utilized. The driven element is a square patch excited with a probe coaxial feed. The other two parasitic patches are closely placed along the *E & H* planes of the driven patch. Each parasitic patch has a narrow rectangular slit at its center, where a varactor diode is placed to allow for tuning its electrical size. The beam direction is permitted to be scanned in both the elevation and azimuth planes. The achieved scan range in the elevation plane is from $0°$ to $32°$, whereas in azimuth plan is from $0°$ to $90°$. Along the scanning range, the attained gain changes from 8.1 to 8.9 dBi, and efficiency changes from 86% to 93%.

- Tunable beamwidth antenna, with a dynamic control over the radiation beam focusing is proposed. The antenna consists of a square patch excited by a coaxial probe feed, and other two square parasitic patches placed on both sides of the driven along its H-plane. Each parasitic patch has a narrow slit at its center loaded with lumped varactor diode to tune its electrical size. Upon changing the parasitic patches size, the antenna effective aperture is altered, and hence the beamwidth in the H-plane is controlled. The achieved beamwidth tuning range is from $52°$ to $108°$, whereas the gain changes from 6.5 to 8.1 dBi.

Throughout the dissertation, 2.45 GHz is chosen, as an example, to be the target frequency. All the designs are validated through experimental measurements for fabricated prototypes, and good agreement is observed between the predicted and measured results.

DEDICATION

This dissertation is dedicated to my *Mom, dad, brothers, uncles, and cousins*, for their love, motivation, prayers and bless. I'm also dedicating it to my *wife* for her patience enduring difficulties and hardship during my study for this dissertation to exist.

ACKNOWLEDGEMENT

I'd like to acknowledge Rogers Corporation for supplying samples of microwave dielectric substrates, Skyowrks Inc., Murata Inc., and Aeroflex Metelics Inc. for supplying varactors, and capacitors SMD components, which all are used for antenna prototyping**.**

I'd like in addition to sincerely thank my advisors Professor Atef Z. Elsherbeni, and Fan Yang for their guidance, patience, attention, valuable discussion, and most important being my friends during my graduate studies. We work together as a one team, other than being just a research assistant under them, which is found to be very helpful in tackling my research challenges and difficulties. They helped me a lot to improve my presentation skills, and have been always open for my ideas, motivate me to execute it, follow up and give suggestions to my results and findings. They also gave me the chance to conclude and decide the next steps in light of their mentorship. I'm in addition, very grateful for their advices and undeniable help in my career development first steps.

I'd like also to specially thank my wife for her support, quite patience, understanding, and tolerance for me being busy most of the time with my doctoral studies, volunteer activities, and professional work. I also thank my parents and brothers for understanding my ambition, encouragement, and help to undergo the graduate studies.

TABLE OF CONTENTS

LIST OF FIGURES

LIST OF TABLES

LIST OF ABBREVIATIONS

ARBW   Axial Ratio beam width

CP   Circularly Polarized

DC   Direct Current

GPS   Global Positioning System

HFSS   High Frequency Structure Simulation

LHCP   Left-Hand Circular Polarization

LTE   Long Term Evolution

MEMS   Micro Electro Mechanical System

MIMO   Multiple Input Multiple Output

RHCP   Right-Hand Circular Polarization

RF   Radio Frequency

UMTS   Universal Mobile Telecommunication Systems

VNA   Vector Network Analyzer

WLAN   Wireless Local Area Network

1. INTRODUCTION

Pattern reconfigurable antennas are capable of altering one of their radiation properties in real time, such as beam direction, null positions, side lobe level, and beamwidth. The antenna reconfiguration can be realized with the aid of mechanical actuation (e.g. rotors, and springs), different switching (e.g. PIN diode, and MEMs) or tuning (e.g. varactor, and variable inductor) radio frequency devices. Exotic materials (e.g. liquid crystal, and magnetic) were also used to provide reconfiguration. Such antenna systems help to avoid noisy environment, mitigate fading, and strengthen the signal detection from an intended target, which is desired in some communication systems, such as airborne remote sensing, low-orbit satellite, and ground tracking terminals. They are also useful for some wireless networks (e.g. UMTS, LTE cellular systems) to enhance the traffic capacity limits [1].

The recent demand of compact, and low cost wireless devices propels the development of pattern reconfigurable antennas, other than conventional antennas of fixed radiation characteristics. Classically, the radiation beam properties were manipulated with antenna phased arrays, which might be large, heavy, or complex to meet the demands of compactness, low power consumption, light weight, and low cost of the antenna terminals. Substantial efforts toward the realization of pattern reconfigurable antennas have been reported in the last two decades. They could be generally classified into two types of designs: a) parasitic elements based; b) non-parasitic elements based. Different examples of both design types will be discussed in the following sections.

1.1. Parasitic-Element Based Pattern Reconfigurable Antennas

Microstrip Yagi-Uda antenna was first introduced in [2], where it offers tilted beam with an excellent efficiency, reduced profile, and less design complexity compared to planar phased arrays that require complex feed network. For these reasons, many pattern reconfigurable antenna designs rely on the Yagi-Uda configuration, which require parasitic elements closely placed to the driven antenna element.

The first example among these design types is the antenna proposed in [3], whose geometry is shown in Figure 1-1. It consists of a driven metallic strip with coaxial pin feed, and two parasitic strips placed to the left and right of the driven strip. The lengths of the parasitic strips are slightly longer than the driven one. Each parasitic strip is loaded with two switches at its edge as shown in the figure. The role of these switches is to change the parasitic strips lengths along their switching states. When the switches are in the ON state, the parasitic strip length is longer than the driven strip and acts as a reflector.
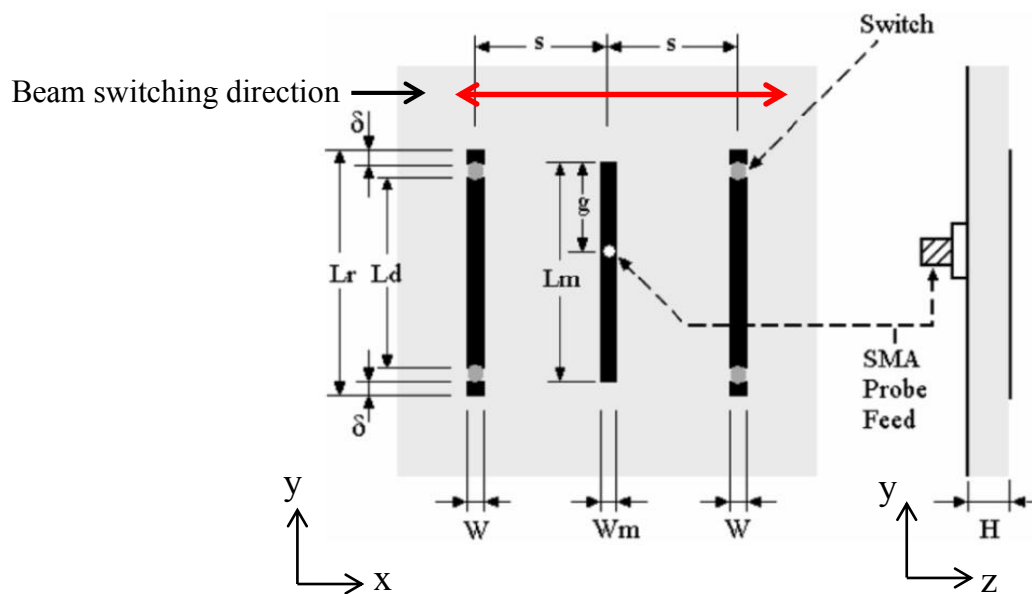
Figure 1-1. Three strips pattern reconfigurable antenna [3].
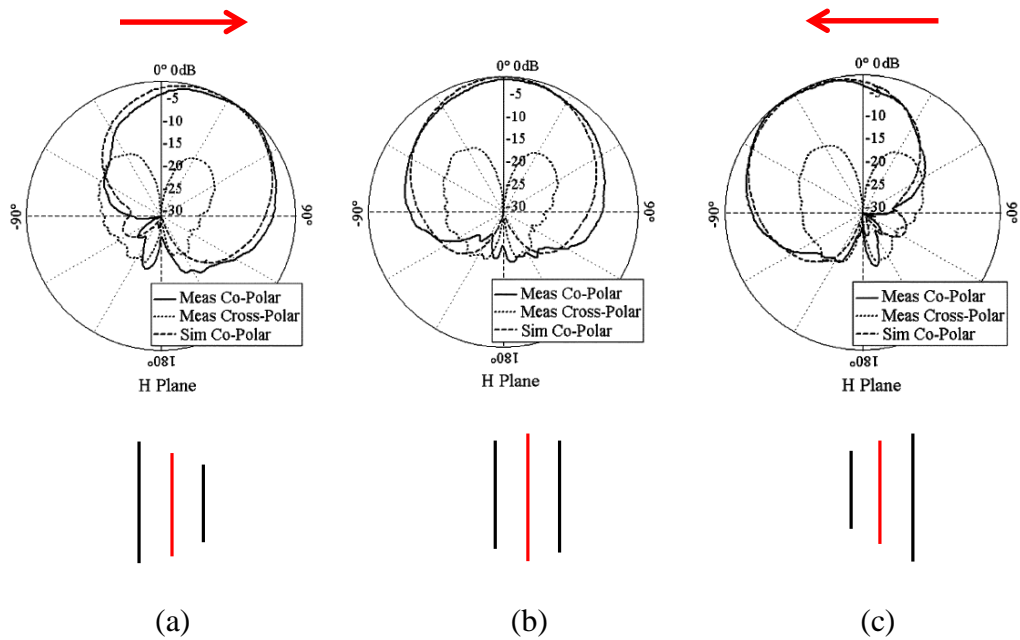
Figure 1-2. Radiation pattern in the xz plane of the three strips pattern reconfigurable antenna in [3] at different switching modes: (a) RD mode; (b) DD mode; (c) DR mode.

On the other hand, when the switches are in the OFF state, the parasitic strip is shorter than the driven strip and acts as a director. The shown antenna has three modes of operations, the RD mode, where the right parasitic strip is director and left parasitic strip is reflector. Second is the DD mode, where the two parasitic strips are directors. The third mode is the DR mode, which is opposite to the DR mode. The radiation patterns in the *xz* plane at these three modes are shown in Figure 2. The results in the figure agree with the discussion in [1] (Yagi-Uda concept), which emphasize the radiation beam tends to deflect toward the director element side, and opposite to the reflector element side. When both parasitic strips are directors, broadside beam is obtained. In this example, the beam is only allowed to be switched in the xz plane, and at three fixed directions. The attained deflection angle is ~35°. The switches are realized with metallic pads for sake of simplicity and proving the concept. The radiation beam is linearly polarized.

The second example extends the Yagi-Uda concept for beam switching to patch antenna as shown in Figure 1-3 [4], [5], where the antenna geometries are shown. In Figure 1-3a, the parasitic patches have slots carved on their surfaces and the slot of each patch has three switches as shown in the figure. The switches allow for an effective re-sizing mechanism of the parasitic patch electrical size. Therefore, the parasitic patch can be a director when the outer two switches are ON, whereas it can be a reflector if all the switches are OFF. However, if all the switches are ON, the parasitic patch will be ineffective at all.
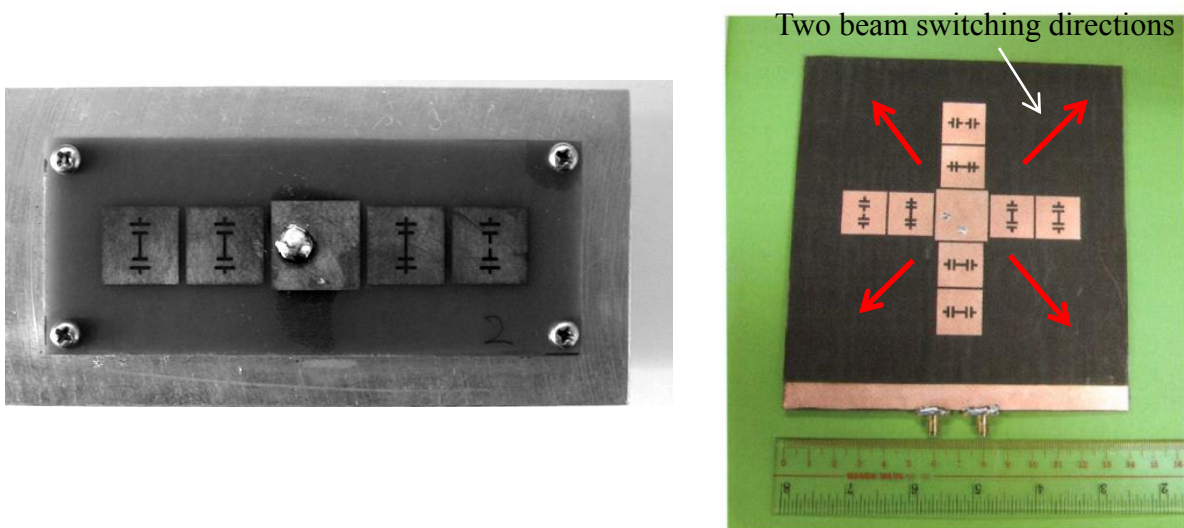
(a)   (b)
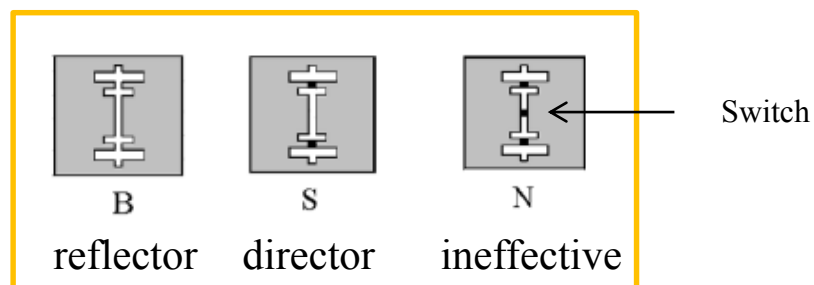
Modes of the parasitic patch

Figure 1-3. Pattern reconfigurable Yagi-patch antenna: (a) linearly polarized beam switching in elevation plane [4]; (b) circularly polarized beam switching in elevation and azimuth planes [4][5].

With these different switching states of the parasitic patches, the beam direction can be switched into three directions, -x (left), +x (right), and broadside as discussed before in the previous example. This antenna provides linear polarization. The switches here are also realized with metallic pads to prove the validity of the concept. For circularly polarized (CP) beam switching, crossed Yagi-patch antenna is used with the driven patch fed with two orthogonal feeds of quadrature phase as shown in Figure 1-3b [4][5]. This configuration results four possible directions of CP beam switching.

In the previous two examples, the radiation beam is only allowed to be switched into certain directions based on the switching states of the parasitic elements, which is not a continuous beam scanning within certain range. More switches are required if more directions are needed to be covered, which would increase the design complexity and limit its practicality. Therefore, continuous beam scanning antenna systems would provide better advantage over the beam switching in terms of beam coverage, design simplicity, and practicality.

Recently, antennas with continuous beam scanning feature have been achieved by loading the antenna with variable reactive elements [6], [7]. In [6], the Yagi-Uda concept is also used for linear polarized beam scanning. An example for an antenna geometry supporting this concept is shown in Figure 1-4. It consists of a half-wave metallic strip fed with a coaxial pin feed, and a parasitic strip of the same length placed close to the driven element (0.2 λ). The parasitic strip is loaded with a variable reactive element (inductance/capacitance) at its center to allow for tuning its electrical length. Therefore, at some instances the parasitic strip is a director and the antenna beam is scanned to the +x direction, whereas at other instances it is a reflector and the beam direction is in the –x. The radiation patterns versus the capacitance value (when a varactor is used) are shown in Figure 1-4b, and the beam direction versus the capacitance/inductance values are also shown in Figure 1-5. The scanning range in the H-plane

(a)   (b)
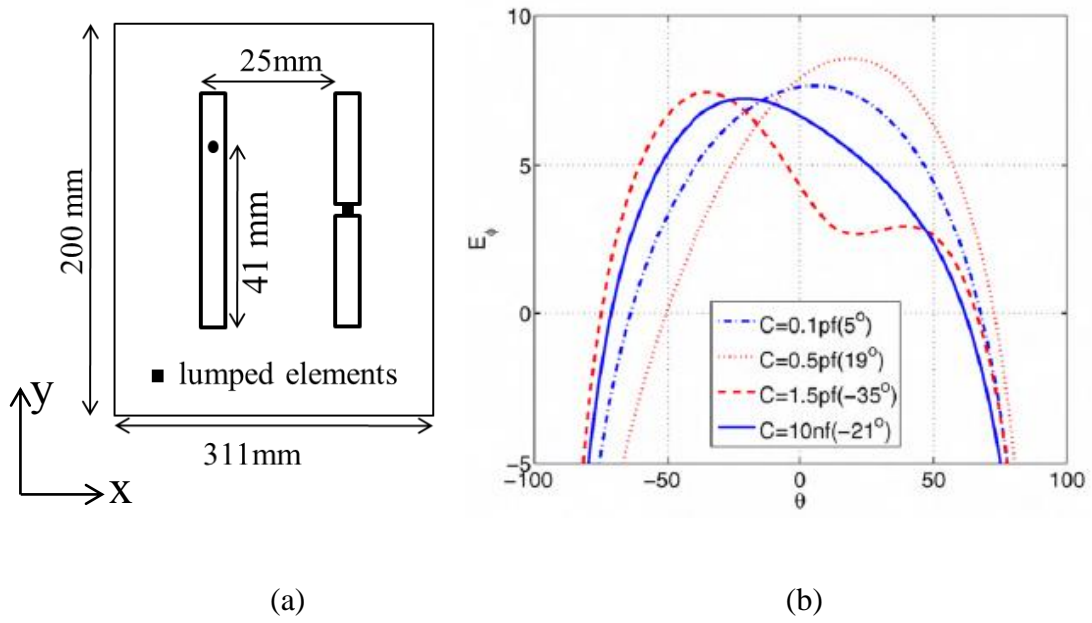
Figure 1-4. Dual-strip beam scanning antenna proposed in [6]: (a) antenna geometry; (b) radiation pattern vs. different capacitance values.

(a)   (b)
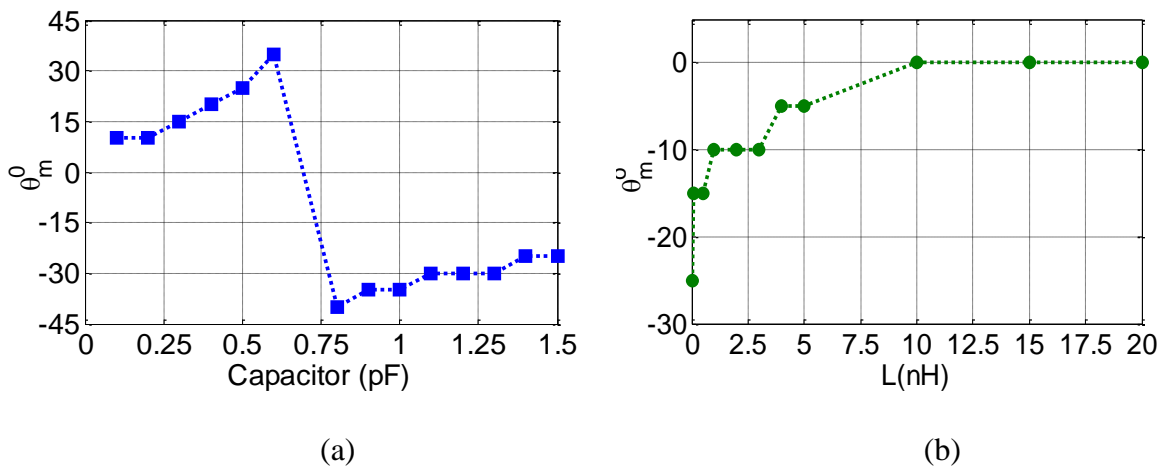
Figure 1-5. Radiation beam direction in the xz plane of the antenna in figure 4: (a) capacitor is used (b) inductor is used.

of the proposed antenna is from -45° to 35° using capacitor, whereas it is from -15° to 0° using inductor.

In a similar fashion, beam scanning is achieved in [7] with a square loop antenna of one wavelength perimeter, placed over a perfectly conducting ground plane as shown in Figure 1-6. For a square loop whose perimeter is one wavelength, it is well known that the two sides, AB, and CD are responsible for radiation in the xz plane, whereas the sides BC, and AD don't contribute for beam radiation in that plane. Therefore, in the xz plane, the antenna could be seen as dual-strip antenna of $\lambda/4$ length similar to the one shown in Figure 1-4a. The amplitude ratio and differential phase of the currents on both strips can be controlled through the reactive elements on the non-radiating sides of the loop, hence beam scanning is achieved.

1.2. Non Parasitic-Element Based Pattern Reconfigurable Antennas

In this design type, no parasitic elements exist, and a dynamic mechanism in the driven radiator geometry is required to provide changes in the radiation characteristic. An example for such type of design is the antenna introduced in [8], where the spiral shape is utilized as shown in Figure 1-7. Spiral antenna provides a CP beam whose direction changes with the physical length of its arm.
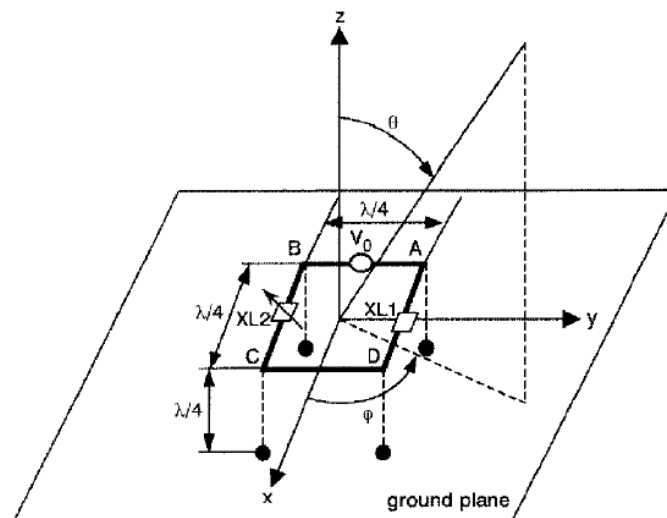
Figure 1-6. Square loop beam scanning antenna loaded with variable reactive elements on the non-radiating sides [7].
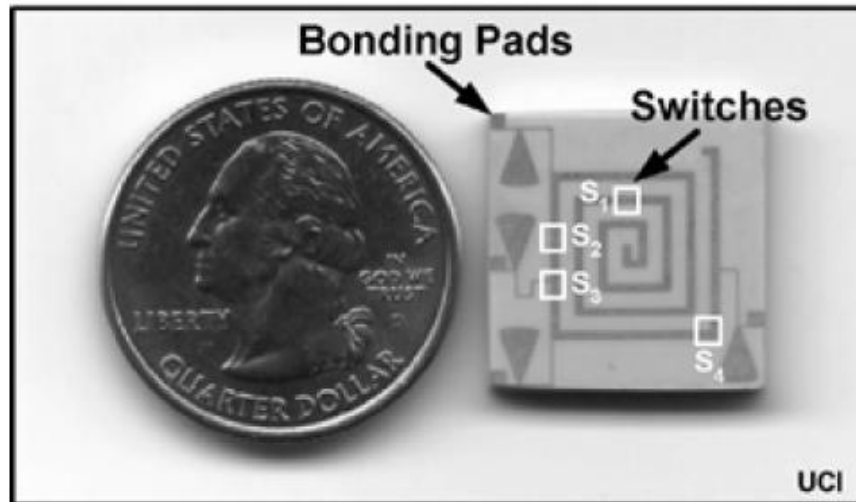
Figure 1-7. Reconfigurable CP scan-beam spiral antenna using switches [8].

Thus, tilted beam switching with respect to the spiral center axis is achieved by loading the spiral arm with several switches to change its length.

Another example introduced in [9], exploited metallic cubical cavity with a slot cut from the center of each of its faces as shown in Figure 1-8. The cavity is excited with a coaxial pin probe. A switch is placed at the center of each slot, such that the cavity radiates from the slot whose switch is in the OFF state. The radiation beam is normal to the face of the corresponding slot. On the other hand, the slots with the ON switches are inductive loads to the cavity. With switching ON one slot at a time, beam switching is realized.

As mentioned earlier, pattern reconfigurable antennas with non-parasitic elements require a mechanism to change the geometry of the driven radiator. However, it should be pointed out that in some cases, the modification in the main antenna geometry to alter its radiation beam characteristics, might affect its other aspects, such as frequency, polarization purity, matching, etc. Examples for such cases are reported in [10].
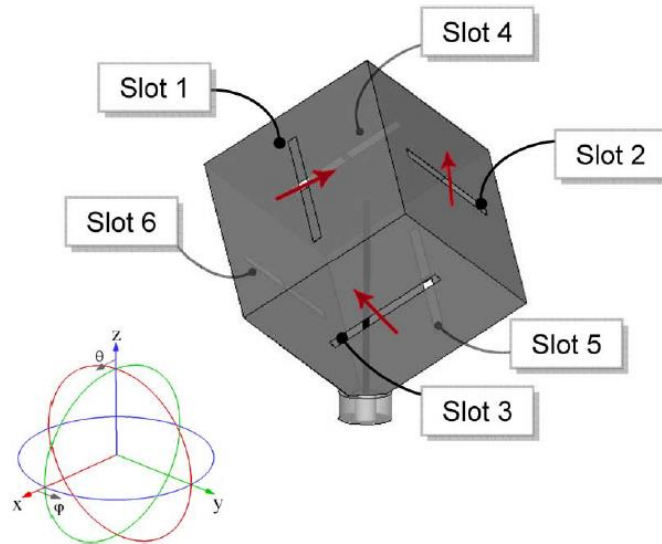
Figure 1-8. Pattern reconfigurable cubical antenna [9].

1.3. Motivation

Although many research work for pattern reconfigurable antennas of different design types is reported in the literature, several challenges haven't been maturely addressed yet, and more advances are still needed. Table 1-I summarizes the research status, or number of publications for different types of pattern reconfigurable antennas with switched, and tunable beams, versus the beam dynamic feature, as well as its polarization. As can be noticed, electronic tuning for the radiation beam characteristics, other than switching is one of the main challenges that need to be advanced further. For instance, CP beam-scanning antenna (one–dimensional), other than the LP is more suitable for some wireless application, such as satellite communication, remote sensing, etc., as illustrated in Figure 1-9. Other challenge is the two-dimensional beam scanning, which is an attractive characteristic for vehicular and land mobile tracking terminals. Moreover, dynamic zooming or focusing of the antenna coverage is desired for the traffic upper limit enhancement in wireless network. Such antenna systems are rarely

9

reported in literature and more investigations and research work are needed for their development.

Table 1-I. The research status for different types of reconfigurable beam antennas.

Radiation beam feature	Polarization	Switched	Tunable
beam direction in (one plane)	LP	mature in literature	few in literature (4)
	CP	few in literature (4)	none
beam direction in (two planes)	LP	few in literature (4)	none
	CP	few in literature (4)	none
Beamwidth	LP	few in literature (3)	few in literature (1)
	CP	none	none
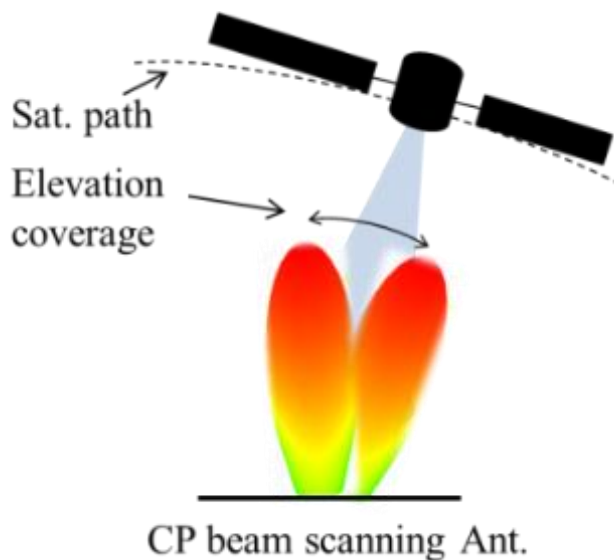
Figure 1-9. A schematic diagram of a proposed CP beam-scanning antenna, whose main beam (elevation coverage zone) is being adjusted to coincide with the foot print of a low-orbit satellite.

The dissertation purpose is to investigate CP one-dimensional beam scanning, LP two dimensional beam scanning, and dynamic focusing antenna systems. As discussed earlier, pattern reconfigurable antennas can be realized with two methods; non-parasitic elements method, and parasitic elements method. Figure 1-10 illustrates schematically the two methods and the main difference between them. The non-parasitic method might lead to a significant change in the antenna other aspects (e.g. frequency, x-pol, etc.) during the continuous tuning process of its geometry. This problem on the other hand is less significant in the second method, because the parasitic element is the one exposed to changes other than the main radiator. Accordingly the second method implies more simplicity in the design and it is the one that would be used throughout the dissertation.
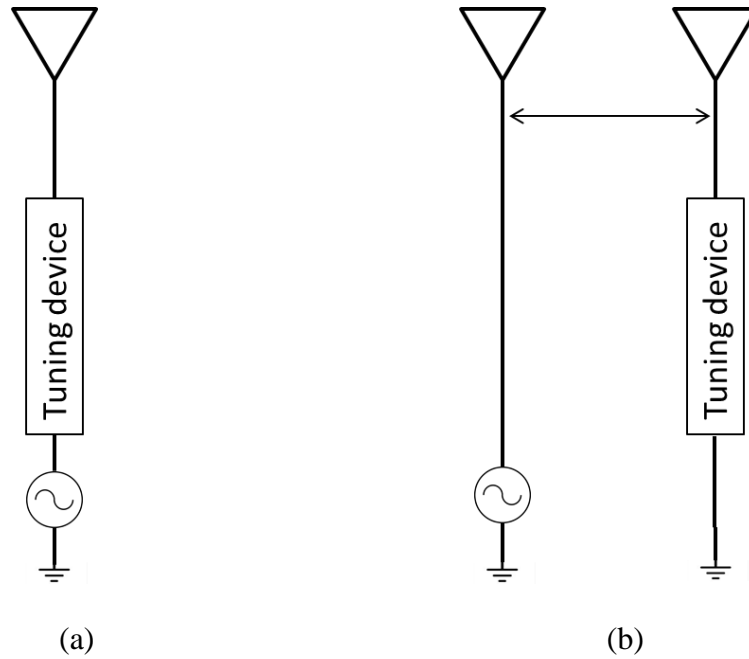
Figure 1-10. Schematic diagram for the methods of pattern reconfigurable antenna: (a) non-parasitic elements method, (b) parasitic elements method.

1.4. Overview

In light of the above discussion in section 1.3, a flow chart overview for the dissertation is shown in Figure 1-11, illustrating the research direction and organization. First, the reconfigurable patch antenna with tunable electric size is studied and proposed. A dual-band operation with tunable frequency ratio is also discussed as an attractive application for the proposed antenna. From there, the concept for tuning the radiation beam using parasitic patch (es) of reconfigurable size is introduced and researched to achieve, CP beam scanning, two-dimensional beam scanning, and dynamic control for the beamwidth (focusing), respectively.
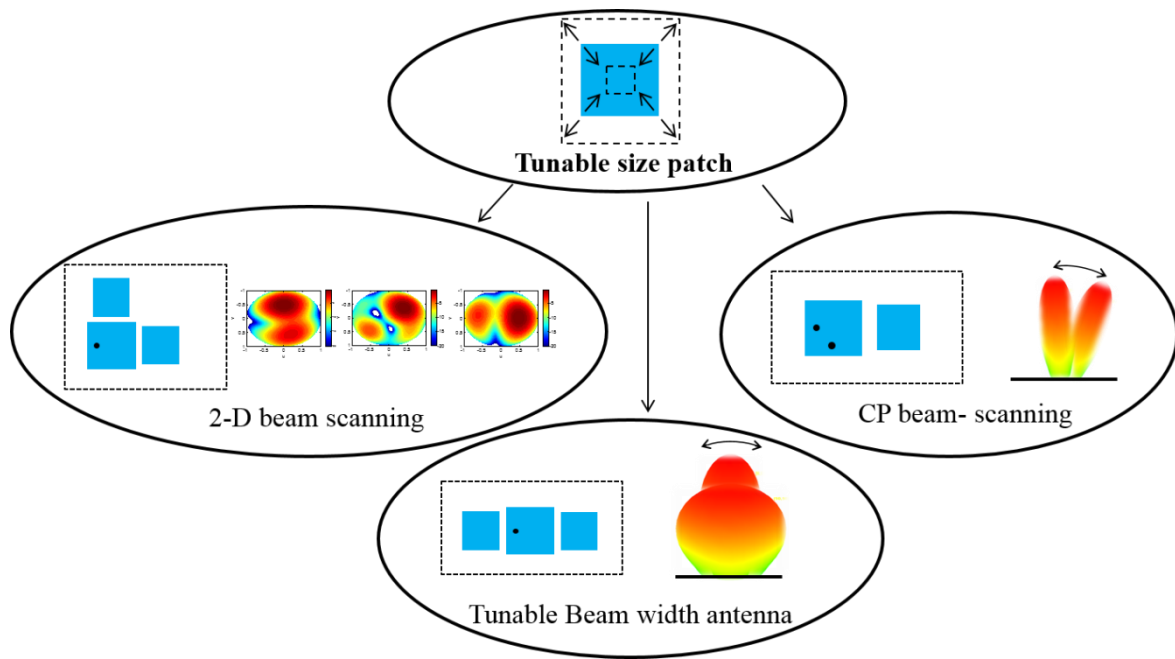
Figure 1-11. A flow chart overview for the dissertation.

2. TUNABLE ELECTRICAL SIZE PATCH ANTENNA

2.1. Introduction

Dual-band antennas are of interest for wireless communication systems that use two bands of frequencies. They are desirable in the simultaneous operation of two wireless services at different frequencies, such as GPS and WLAN (Wi-Fi). They could substitute for two individual antennas, which would reduce the implementation size, cost, and complexity. Also, they provide an advantage over wideband antennas by rejecting the interference on the spectrum between the two operating frequencies. Many techniques have been reported for designing low cost, small profile, and efficient dual-band antennas as in [11]-[18]. Some techniques used a patch antenna at the higher order mode that has a quasi-similar radiation pattern of the fundamental mode, and through the manipulation of the current distribution, the higher order resonant frequency could be reduced to achieve a certain range of frequency ratio [11]-[13]. Meanwhile, a slot antenna, which is another category of low cost small-profile antennas, is designed to provide dual-resonance in [14]-[16]. Other techniques for dual-band designs used parasitic elements in the proximity of the radiating element [17], multi-radiating elements [18], and stubs attached to the radiating elements [19]. These approaches are for fixed dual-band operation and do not allow for electronic tuning.

Frequency reconfigurable antennas are capable of changing their resonant frequency to operate at specific band along the multi-serviced radio spectrum. Therefore, they require less area for antenna terminals, and are more versatile for wireless devices. Such capability is also of interest for cognitive radio systems [20]. Significant advancements on frequency agile

antennas were reported in the last few decades, such as in [21]-[26]. In [21]-[22], the patch antenna radiating edges are loaded with varactor diodes to allow for electronic tuning, whereas in [23] a PIN diode switch controls the length of the current path on the patch surface, producing frequency reconifgurability. Both methods have been employed together to a differential-fed patch antenna for a wider tuning range [24]. Similarly, frequency agile PIFA antennas have also been reported in [25]-[26].

Lately, some works have focused on the development of electronically tunable dual-band antenna designs. Tunable dual-band PIFA antennas are devised in [27]-[32], and the tuning mechanism is based on varactors or switches. In [33]-[34], a varactor loaded-slot antenna is used at $\lambda/2$ and λ modes for the two resonant frequencies, which imposes some complications to obtain similar radiation patterns at both bands. Tunable dual-band antenna using PIFA and slot configurations are amenable for integration with hand-held devices due to their small sizes. However, they have smaller gain than their patch antenna counterpart that is more suitable for stationary terminals, base stations, and high gain antenna arrays.

In this chapter, a new approach to design a fixed and reconfigurable dual-band microstrip patch antenna is introduced. The antenna geometry is a slotted patch with a capacitor loaded in the middle of the slot. The antenna dimensions and the capacitance value determine the two frequencies and their ratio. Consequently, tuning the frequencies ratio is allowed by choosing the proper capacitor value. Moreover, if a varactor with an adequate biasing network is used instead, electronic tuning would be attained by changing the applied DC voltage. Because both resonant frequencies are due to the fundamental radiating mode, similar radiation patterns are obtained at both bands. Transmission line theory with the Wheeler incremental volume concept [35] is utilized to build an equivalent circuit model that explains the dual-resonance behavior of the proposed antenna. The circuit model is validated with full wave

simulations. Antenna prototypes operating within 2 - 4.5 GHz have been fabricated and measured, and the results show good agreement with the full wave simulations.

2.2. Antenna Design and Analysis

2.2.1. Antenna Geometry and Resonance Mechanism

The geometry of the proposed antenna design, labeled with dimensions, is shown in Figure 2-1. It is a probe-fed patch antenna with a narrow rectangular slot carved on the center of the patch surface. The substrate is Rogers RT/duroid 5880 of permittivity $\varepsilon_r = 2.2$, thickness $h = 3.175$ mm, and loss tangent $tan\delta = 0.0009$. The slot is loaded with a lumped
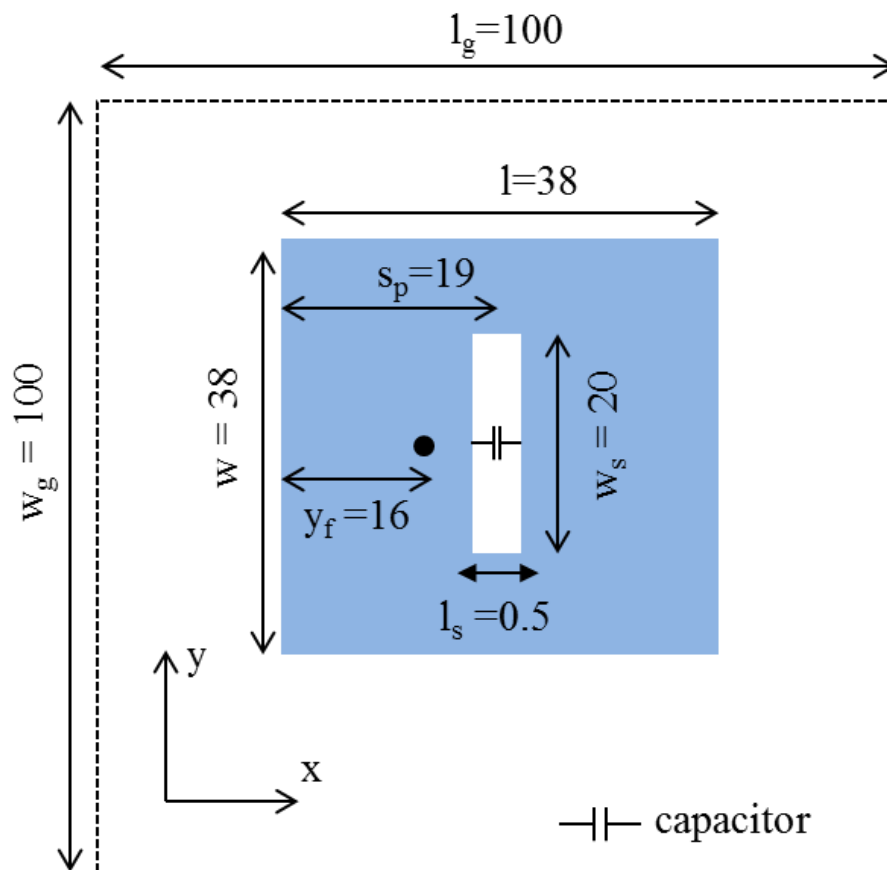
Figure 2-1. Proposed patch antenna geometry with a slot centered on the patch loaded with a capacitor in the middle. (Units: mm)

capacitor of value C on its middle to control the current path length on the patch surface; hence, continuous frequency tuning is expected by changing the capacitance value C.

Full wave simulations reveal that a dual-resonance behavior occurs when a proper capacitor is used. For instance, at $C = 0.5$ pF, two resonant frequencies $f_1 = 2.275$ GHz and $f_2 = 3.95$ GHz are observed. As a reference, the patch resonant frequency without the slot and the capacitor is $f_0 = 2.45$ GHz. The full wave simulations on the proposed antenna are carried out using Ansoft HFSS [36]. The current distribution at each frequency has been inspected and plotted in Figure 2-2. From the figure, it is observed that at the lower frequency, the current distribution is similar to the one of a plain patch but it detours around the slot, where the current path becomes longer. This explains why the first frequency is smaller than the original resonant frequency ($f_1 < f_o$). At the higher frequency, the currents pass through the capacitor in the middle of the slot. Thus, the lumped capacitor is equivalently seen in series with the antenna capacitance; hence, the second frequency is higher than the original resonant frequency ($f_2 > f_o$). Because the current distribution of the

(a)   (b)
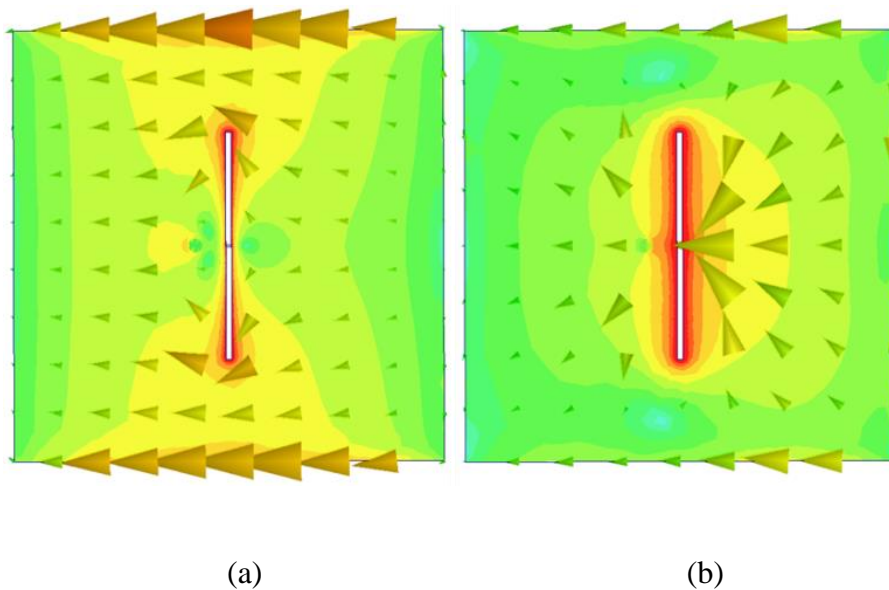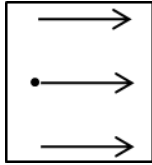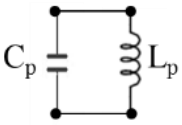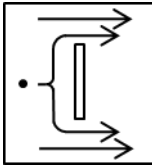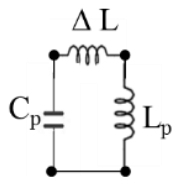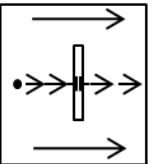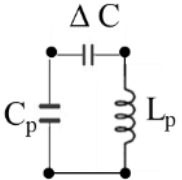
Figure 2-2. Simulated current distributions of the proposed antenna with $C = 0.5$ pF at two resonant frequencies: (a) $f_1 = 2.275$ GHz; (b) $f_2 = 3.95$ GHz.

Table 2-I. Dual-resonance mechanism of a patch antenna with a capacitor loaded–slot

Patch configuration	Frequency	Current	Equivalent Circuit
No Slot	f_o		
Slot effect	$f_1 < f_o$		
Capacitor effect	$f_2 > f_o$		

second frequency has one maximum, it is still operating at the fundamental mode. The dual-resonance mechanism has been qualitatively summarized in Table 2-I.

A plain patch antenna could be represented with a parallel $L_P C_p$ circuit that resonates at f_o, whereas a patch with a capacitor-loaded slot inheres dual-resonance. The first resonance is mainly due to the slot that has an inductive effect and is represented by an additional inductance ΔL in series with L_p, resulting in $f_1 < f_o$. The second resonance is mainly due to the lumped capacitor that equivalently adds a capacitor ΔC in series with C_p, resulting in $f_2 > f_o$.

2.2.2. Equivalent Circuit Model

To better understand the dual-resonance behavior of the proposed antenna, an equivalent circuit model is built using the transmission line theory, as shown in Figure 2-3.

A parallel connection of a resistor R_e and a capacitor C_e accounts for radiation and fringing fields at the patch edges ($x = 0, x = l$). They are calculated from the formulas given in [37]. The parameters β (propagation constant) and Z_c (characteristic impedance) are evaluated using the quasi-static formulas provided in [38]. The slot with the capacitor is modeled by a reactance M, where L_s represents the inductance accompanied by the current detour around the slot [39], and C is the value of the capacitor placed in the middle of the slot. An additional inductance L_c is added serially to the capacitor to account for the effect of the current crowded around the capacitor. The parameters L_s and L_c are deduced using the Wheeler incremental volume concept introduced in [35]. The resonant frequency f_r as a function of capacitance C is evaluated by applying the resonance condition (1), where Y_{in} is the total input port admittance, $\vec{Y}$ is the right input admittance, and $\overleftarrow{Y}$ is the left input admittance. Details about the parameters L_s, L_c, and f_r calculations are presented in Appendix 0.

$$\text{Im}\left\{Y_{in}\left(f_r,C\right)\right\} = \text{Im}\left\{\overleftarrow{Y}+\vec{Y}\right\} = 0. \tag{2-1}$$
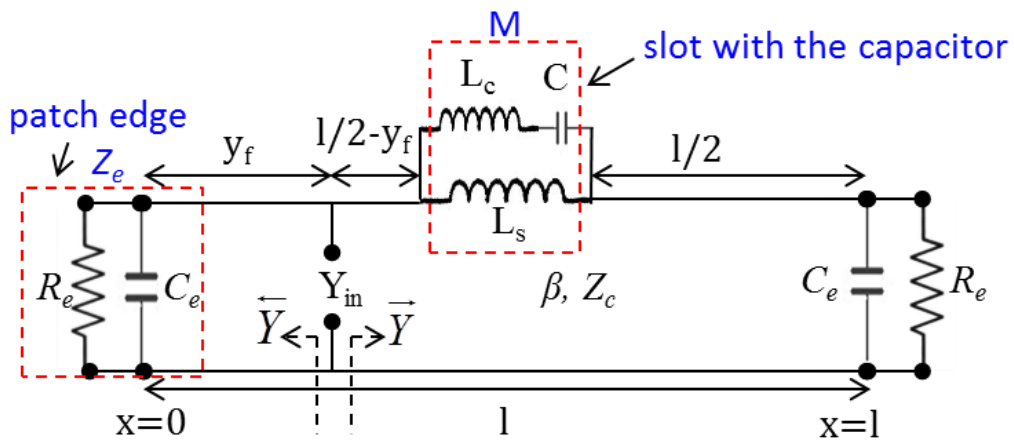
Figure 2-3. Transmission line model of a patch antenna of length l with a capacitor-loaded slot.

19

The numerical solution of (1) is plotted in Figure 2-4, where it is compared with the full wave HFSS simulation results. Good correlation is observed between the circuit model results and HFSS results. Some deviations exist due the approximations in the empirical and quasi-static formulas used in the circuit model. Nevertheless, the circuit model gives a clear insight and understanding for the dual-resonance mechanism of the proposed design.
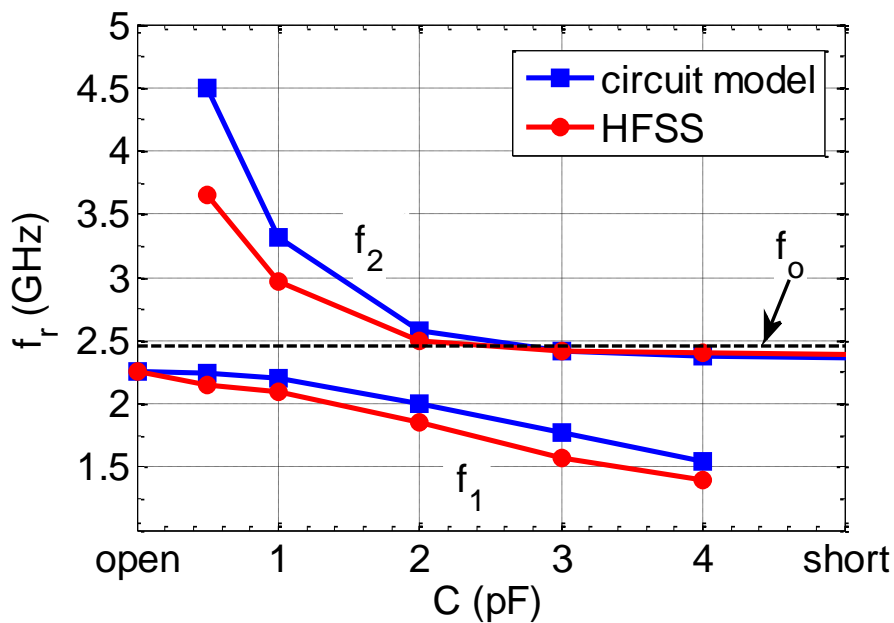
Figure 2-4. Resonant frequencies of the proposed design versus the lumped capacitance value C.

Basically, the reactance M that models the slot with the capacitor is a resonant circuit, which is inductive at low frequency, and capacitive at high frequency. Hence, at certain capacitance value C, there exist two solutions for (1) that satisfy the resonance condition at the fundamental mode. The circuit model analysis is consistent with the qualitative explanation summarized in Table 2-I. It is also observed that, at the open circuit condition ($C = 0$ pF), the antenna has single resonant frequency ($f_1 = 2.25$ GHz) lower than the original f_o, whereas at the short circuit condition ($C = \infty$ pF) the resonant frequency ($f_2 = 2.4$ GHz)

gets closer to the f_o as concluded in [23]. The curve in Figure 2-4 could be divided into three regions:

- Region 1, where $0 < C < 1$ pF: f_1 is relatively constant but f_2 varies significantly with C.

- Region 2, where $1 < C < 3$pF: both frequencies are dependent on C.

- Region 3, where $3 < C < \infty$ pF: f_1 changes with C but f_2 is almost constant.

It is also observed that the frequency ratio can go higher than 1.7, which is a quite high value for a dual-band antenna design using the fundamental mode of a single resonator. The reason for such a high ratio is the more pronounced change in the current path length with this new configuration compared to the one in [20], [21].

2.2.3. Antenna Performance

To demonstrate the radiation characteristics of the proposed antenna, the antenna in Figure 2-1 has been fabricated and a photo is shown in Figure 2-5, where a surface-mount capacitor of 0.5 pF is used. The reflection coefficient is shown in Figure 2-6. Good agreement is observed between the simulated and measured results. The antenna performance from the simulation and measurements is summarized in Table 2-II, where its resonant frequencies, realized gain, and frequency ratio are listed. A slight downward frequency shift is observed in the measured results, and it is more noticeable at

Figure 2-5. A photograph of the proposed patch antenna with a capacitor loaded-slot for dual-band operation.
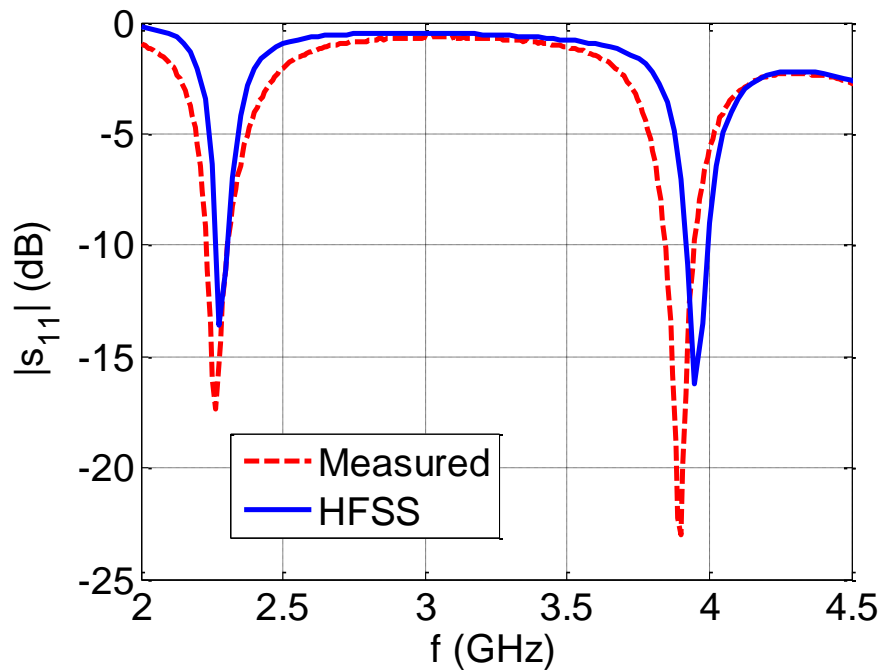
Figure 2-6. Simulated and measured results for the power reflection coefficient of a dual-band patch antenna with a capacitor-loaded slot.

22

Table 2-II. Performance of the proposed dual-band patch antenna with a capacitor-loaded slot

Quantity	Simulated		Measured	
	f_1	f_2	f_1	f_2
Frequency (GHz)	2.275	3.950	2.268	3.898
Frequency shift (%)	---	---	-0.3%	-1.3%
Gain (dBi)	7.46	7.01	7.05	5.01
Gain loss (dB)	---	---	0.41	2
Ratio (f_2/f_1)	1.74		1.72	

the higher band than the lower one. The larger tolerance in the capacitance value at the

higher frequency is considered to be the main reason for this noticeable shift. The measured

realized gain at the lower band agrees reasonably with the simulation result (-0.45 dB

difference) considering the limited accuracy ($\pm$ 0.5 dBi) of the far-field gain measurements

facility. At the higher band, the difference between the simulated and measured realized

gain is 2 dB, which is due to the inherent resistive loss (I^2R loss) in the lumped capacitor.

It has been previously shown in Figure 2-2b that a large current is passing through the

lumped capacitor at f_2; hence the capacitor loss has a significant effect at the higher band.

The capacitor loss is proportional to its capacitance value, therefore in order to attain higher

antenna efficiency at f_2, the antenna operation in regions 2 and 3 ($1 < C < \infty$) is not

suggested. It was also found that matching the antenna to 50 Ω is much easier in region 1

than in region 2, and 3 without the need of an additional matching circuit.

The antenna radiation patterns at both bands in the E-plane (xz) and H-plane

(yz) are presented in Figure 2-7. Good agreement is observed between the simulated and

measured results. The maximum measured x-pol level is -16.7 dB that occurs at the higher

band.
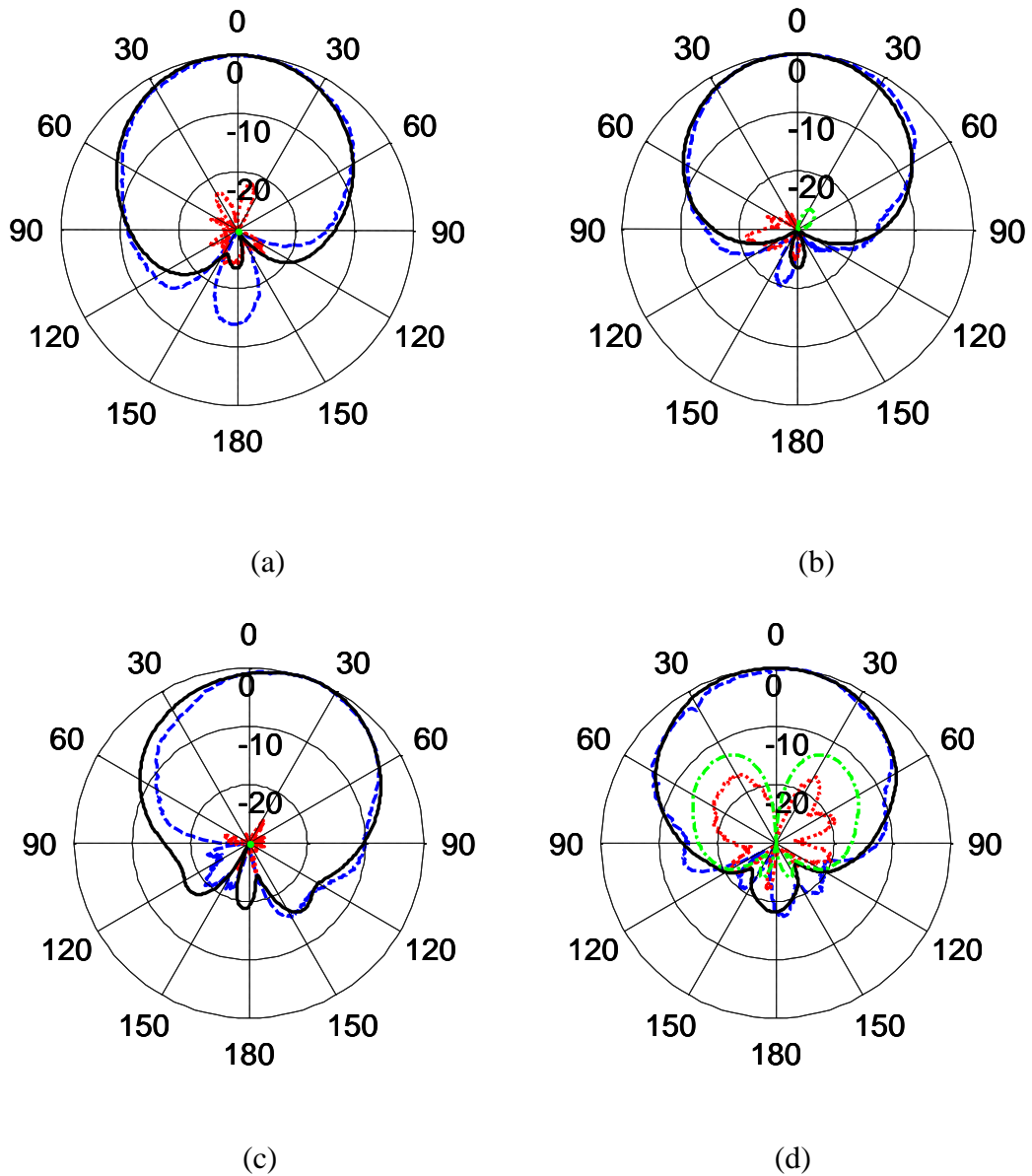
Figure 2-7. Simulated co-pol radiation pattern (solid), simulated x-pol radiation patterns (dashed-dotted), measured co-pol radiation pattern (dashed), and measured x-pol radiation pattern (dotted) results in the principle cuts at both bands: (a) E-plane (xz) at 2.26GHz; (b) H-plane (yz) at 2.268 GHz; (c) E-plane (xz) at 3.89 GHz; (d) H-plane (xz) at 3.898 GHz.

2.3. Reconfigurable Dual-Band Design

In the previous design, a fixed dual-band microstrip patch antenna has been achieved with the newly proposed antenna configuration in Figure 2-1. One of the significant virtues of
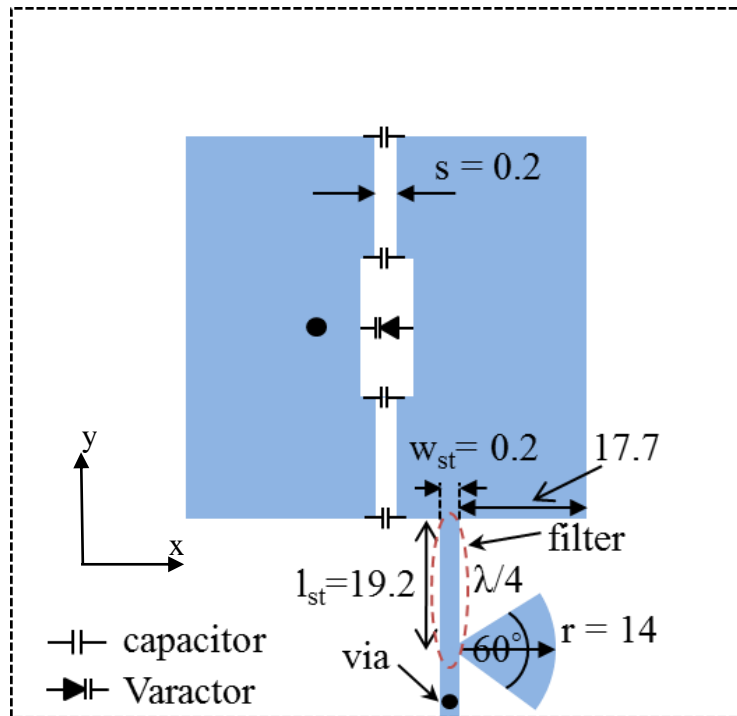
Figure 2-8. Antenna geometry of a reconfigurable dual-band patch antenna with an integrated DC biasing network. (Units: mm)

this new approach is the feasibility of electronic tuning by replacing the capacitor with a varactor diode plus a proper DC biasing circuit. Accordingly, a modification on the geometry in Figure 2-1 has been done as shown in Figure 2-8. A high quality varactor (SMV 1430) from Skyworks is used, whose tuning range of $0.31 \leq C \leq 1.24$ pF with $30 \geq V_{dc} \geq 0$ V, as shown in Figure 2-9 [40]. It is picked to cover Region 1 of the curve in Figure 2-4. Region 1 is selected to avoid the efficiency drop at the higher band, as discussed in section 2.2.3. To build the DC biasing circuit, the patch is divided into two parts by a narrow slit, in order to avoid the DC short across the varactor diode terminals. Four low-loss surface-mount 68 nF capacitors are placed on the slit to maintain the RF continuity. The DC control signal will be supplied through the probe feed with a bias Tee that superimposes both RF and DC signals with high isolation (30 dB). For the completion of the DC path, the right part of the patch is grounded through a
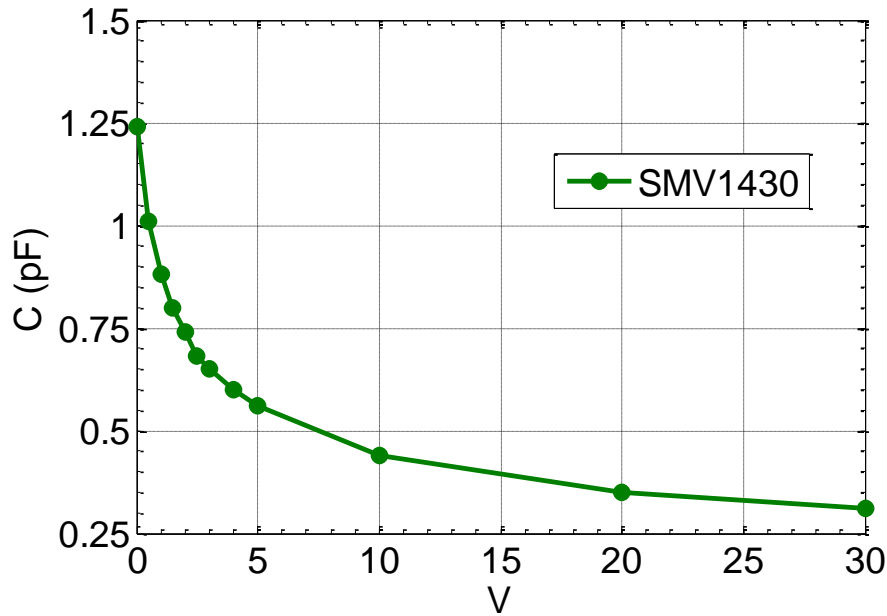
Figure 2-9. Capacitance vs. reverse biasing voltage of the varactor SMV1430 generated from the data sheet [40].

shorted transmission line with a metallic via. The transmission line is stubbed with a radial sector at $\lambda_g/4$ (referred to 3 GHz) from the patch edge, to form high impedance at that edge (RF choke). The dimensions of the transmission line and the radial stub were carefully designed to serve as a wideband stop filter with 20 dB isolation in the entire antenna operational band 2 – 4.5 GHz. A photo for the fabricated antenna prototype is shown in Figure 2-10.

The antenna reflection coefficient at different DC voltages is shown in Figure 2-11. Good agreement between the simulated and measured results is observed. As expected, by changing the biasing voltage from 0 to 30 volts that corresponds to changing the capacitance C from 2.24 to 0.31 pF, the second resonance f_2 is being tuned, whereas the first resonance f_1 is relatively constant (operation in region 1). The simulated reflection coefficient at different DC voltages is obtained by matching the diode reverse voltage with its associated capacitance,
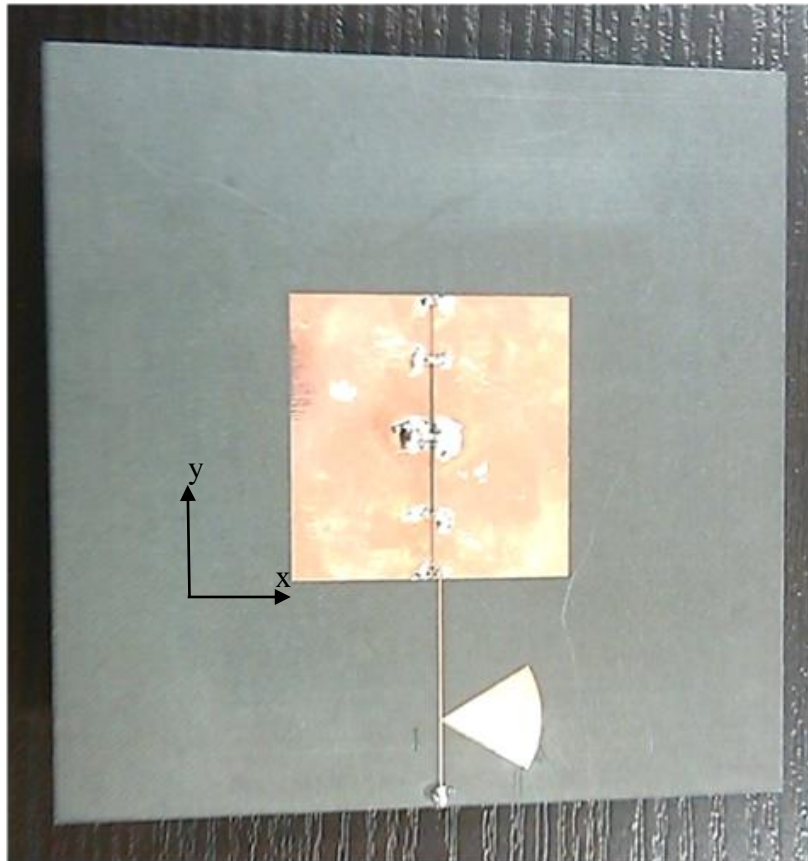
Figure 2-10. Photo for the proposed reconfigurable dual-band patch antenna.
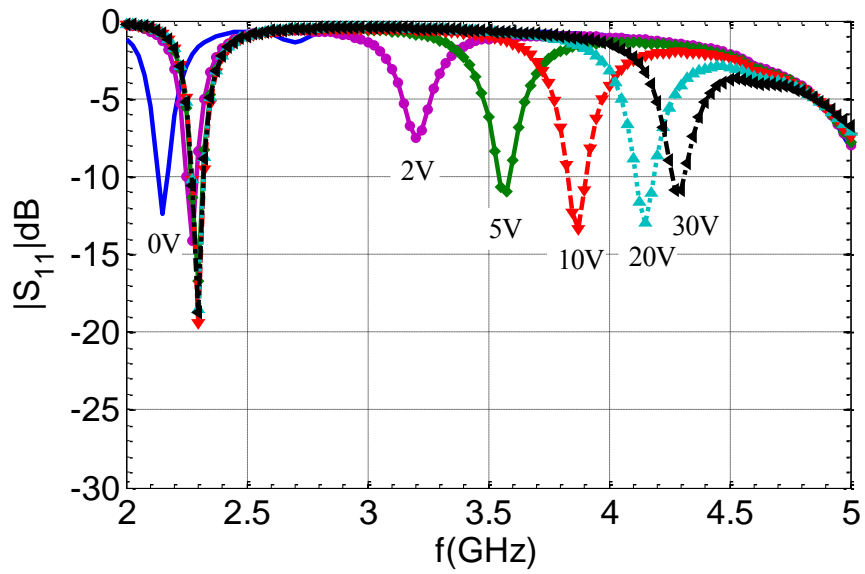
(a)
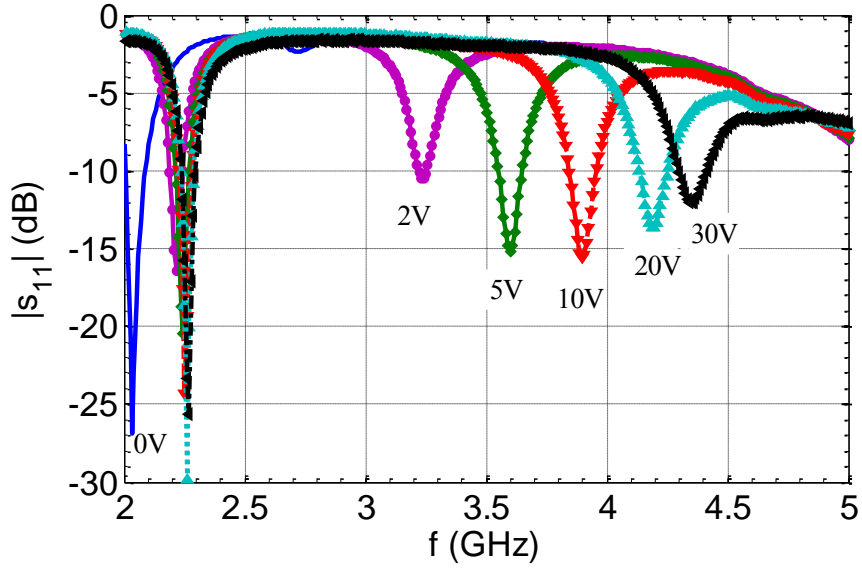
(b)

Figure 2-11. The reflection coefficient of the proposed reconfigurable dual-band patch antenna versus the frequency at different DC biasing voltages: (a) simulation with HFSS; (b) measured with VNA.

as determined in Figure 2-9 (C-V curve) [40]. From Figure 2-11b, it is clear that the useful tuning range is from 2 to 30 volts, where the antenna is well matched ($S_{11} \leq$ -10 dB).

The resonant frequencies versus the reverse bias voltages are plotted in Figure 2-12. A small deviation is observed between the simulated and measured results. This is attributed to the minor deviation of the capacitance value C from the C-V curve in Figure 2-9 [30], which is given at low frequency (< 500 MHz). Along the useful tuning range $2 \leq V_{dc} \leq 30$, the measured f_1 changes from 2.22 to 2.26 GHz, whereas the measured f_2 changes from 3.24 to 4.35 GHz.

The ratio (f_2/f_1) between the two resonant frequencies is plotted in Figure 2-13. It exhibits good agreement between the simulated and measured results, where the measured ratio changes from 1.45 to 1.93, which is a significantly large tuning ratio with $2 \leq V_{dc} \leq 30$ V that corresponds to 0.74 $> C >$ 0.31 pF.
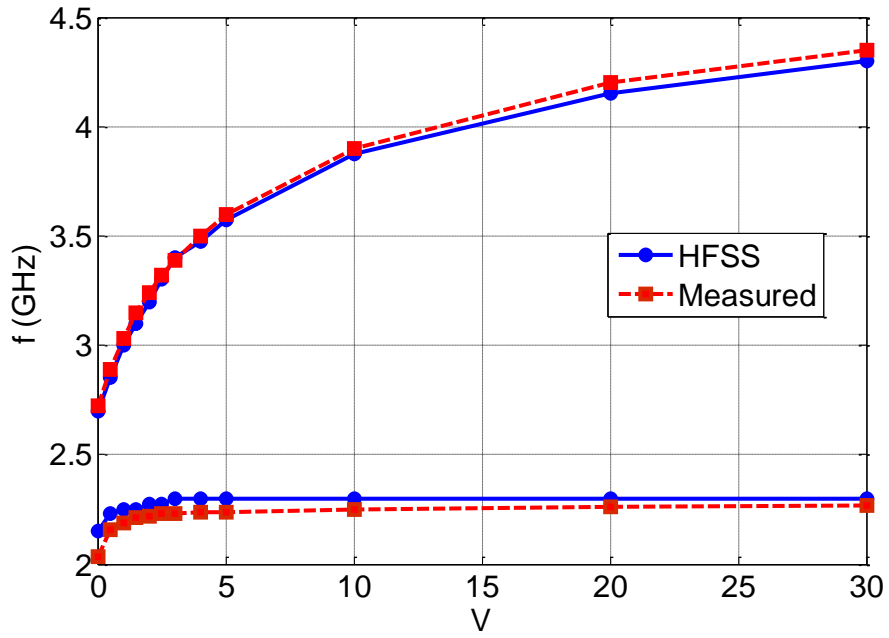
Figure 2-12. The simulated and measured results for the first and second resonant frequencies of the proposed reconfigurable dual-band patch antenna versus the reverse DC biasing voltage.
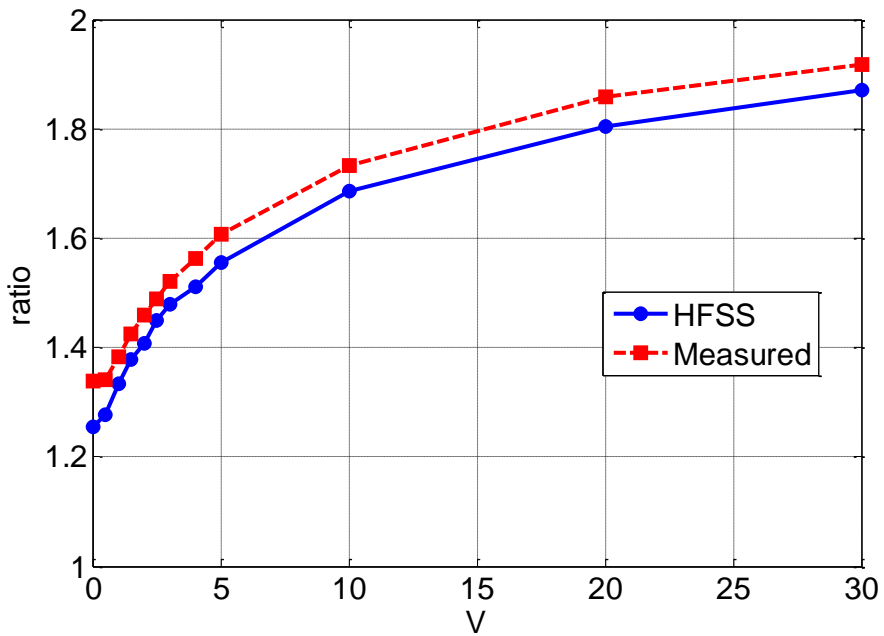
Figure 2-13. Simulated and measured results for the frequency ratio of the proposed reconfigurable dual-band patch antenna versus the revers DC biasing voltage.

The antenna radiation patterns in the principle planes at different applied DC biasing voltages have been measured and plotted in Figure 2-14. The co-pol patterns are similar at both bands because radiations at both bands are due to the fundamental TM_{01} mode. The cross polarized level within the 3 dB beam width is < -20 dB for the lower band, whereas for the higher band it is -10.6 dB at most. Pattern stability along different voltages at both bands is observed.

(a)

(b)

10 V
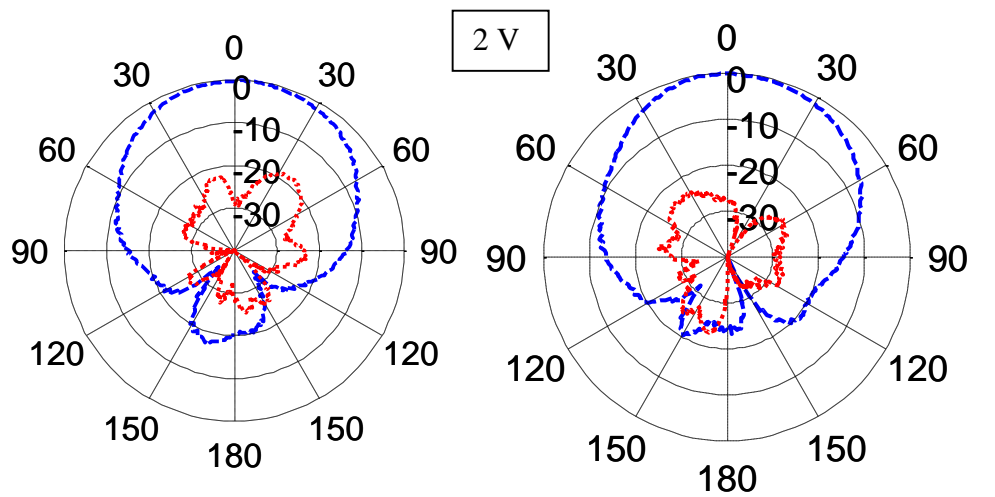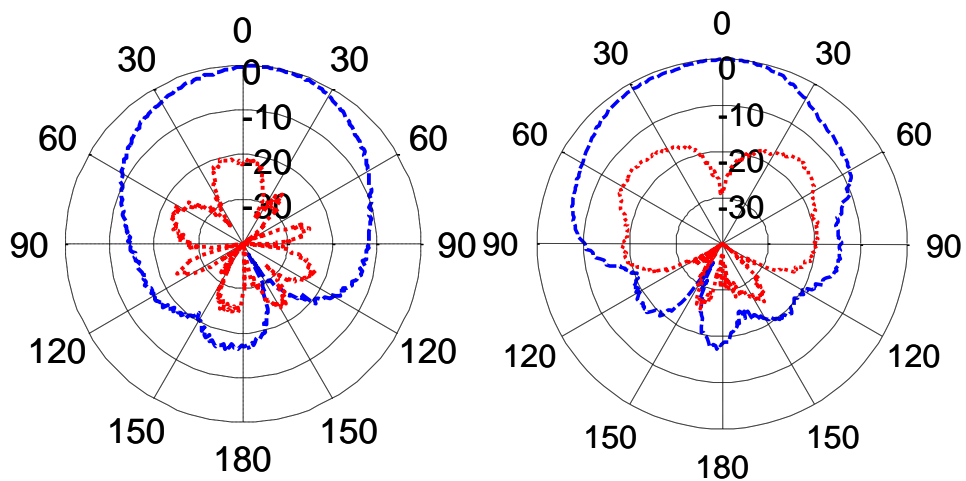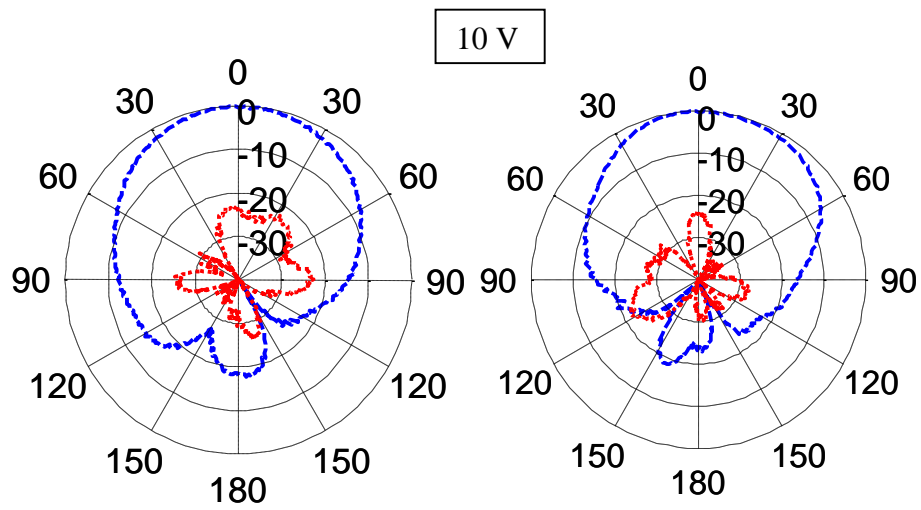
(c)
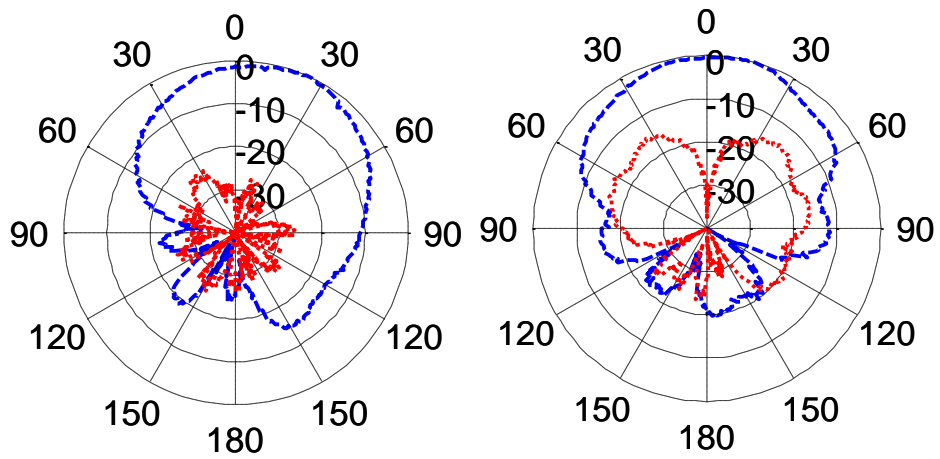
(d)
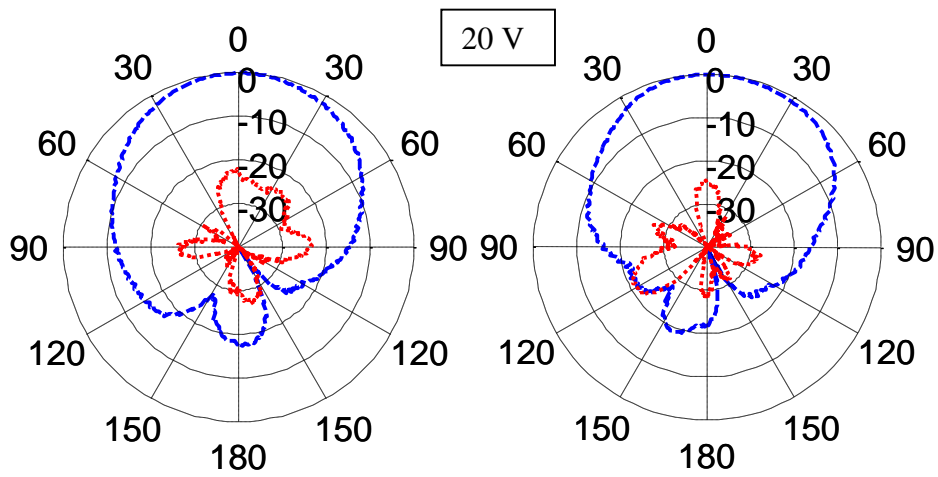
(e)
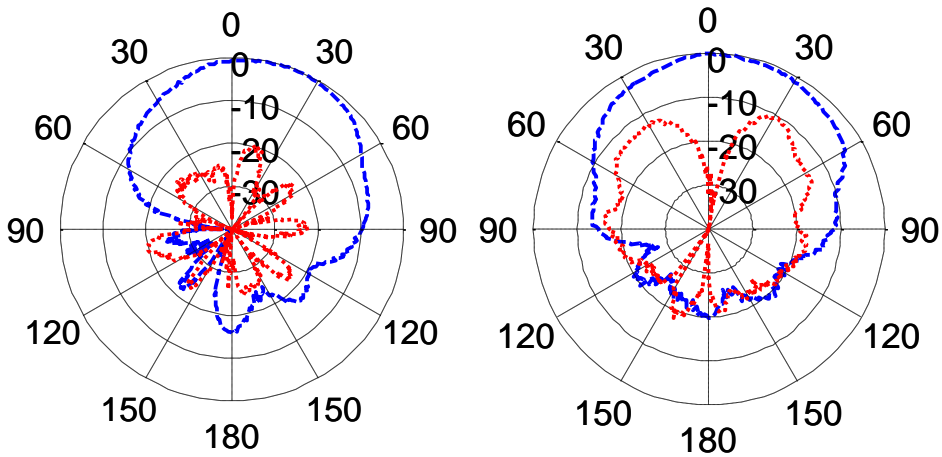
(f)

Figure 2-14. Measured results for co-pol radiation pattern (dashed), and x-pol radiation pattern (dotted), in both xz plane (left) and yz plane (right) at different voltage: (a) 2.2 GHz (2V); (b) 3.24 GHz (2V); (c) 2.26 GHz (10V); (d) 4.1 GHz (10V) ; (e) 2.26 GHz (20V); (f) 4.2 GHz (20V).
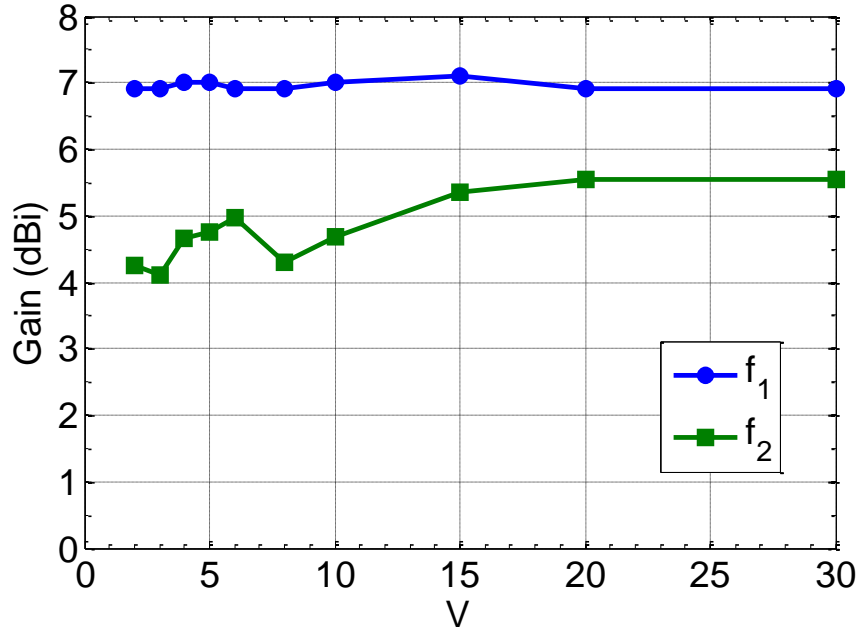
Figure 2-15. The measured gain of the proposed reconfigurable dual-band patch antenna at both bands versus the reverse DC biasing voltage.

The realized gain at both bands is measured along the entire tuning range $(2 - 30 \text{ volts})$, and the results are shown in Figure 2-15. The average gain at the lower band is 7 dBi, whereas at the higher band, the gain varies from 4.3 to 5.5 dBi. Also, the antenna efficiency at both bands is calculated using the simulated directivity and the measured realized gain. Its value across the tuning range is almost 89% at the lower band, and varies from 38% to 90% at the higher band. The gain and efficiency are almost constant with the biasing voltage for the lower band because f_1 is almost constant. However, for the higher band as the voltage increases (capacitance decreases) the efficiency and the gain increase. The efficiency and consequently the gain enhancement with the voltage growth are because the varactor loss decreases as the voltage increases, which agrees with the inversely proportional relation between the varactor loss and its capacitance value [24]. Another reason that contributes to the gain enhancement with the voltage growth is the increase of the second resonant frequency f_2, and, hence, the antenna electrical size becomes larger. This enlargement of the antenna's electrical size

(aperture) enhances the antenna directivity and hence the gain [41]. Regarding the higher band, better antenna efficiency could be attained if a higher quality varactor is used. Newly emerged technologies are needed to enable high-quality varactors for high frequency applications.

2.4.   Patch Antenna with Reconfigurable Electrical Size

The previous sections have discussed the dual-band operation of a patch antenna with a varactor loaded slot, which exhibits tunable resonant frequencies by changing the diode capacitance value as shown in Figure 2-4. Tuning the resonant frequency of a microstrip patch antenna, provides the fundamental mechanism to change its electrical size. Therefore, the equivalent electrical size of the proposed antenna would behave as illustrated schematically in Figure 2-16. At a small capacitance C close to the open circuit condition ($C \leq 0.5$ pF), the patch has two electrical sizes: one is slightly larger than its physical size, denoted by patch 3, and the other is much smaller, denoted by patch 1. Upon increasing C, patches 1 and 3 start to increase until C approaches the short circuit condition ($C \geq 5$ pF), where patch 3 becomes extremely large and denoted by patch 4, and patch 1 approaches the physical size to become patch 2. In summary, one can change the capacitance value to effectively tune the electrical size of the patch.
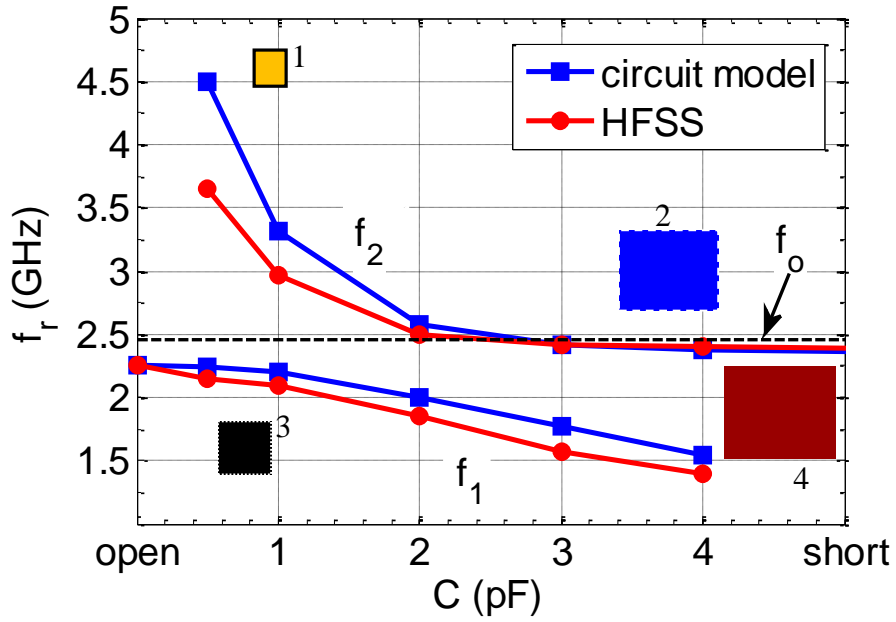
(a)
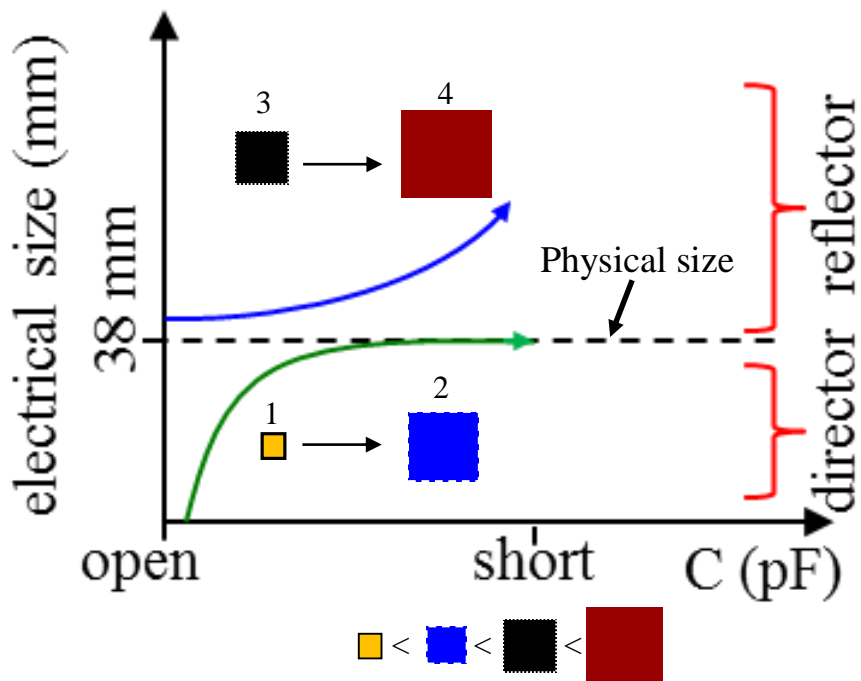
(b)

Figure 2-16. Behavior of the frequency-agile patch antenna proposed in chapter 2 vs. lumped capacitance value C: (a) resonant frequencies; (b) schematic diagram for the electrical size.

2.5. Summary

A novel approach for the design of a dual-band microstrip patch antenna using a capacitor-loaded slot has been proposed in this chapter. The capacitor-loaded slot is inductive at a band of lower frequencies and capacitive at a band of higher frequencies, leading to a dual resonance mechanism (two resonance conditions) of the microstrip patch. The proposed technique also shows the feasibility of an electronically reconfigurable dual-band operation whose tuning mechanism relies on a varactor diode. The frequency ratio is tuned from 1.45 to 1.93 with 0.31- 0.74 pF capacitance range, and 2-30 volts DC voltage. Similar radiation patterns at both bands are obtained because of the same resonant mode. The realized gain at the lower band (from 2.22 to 2.26 GHz) is 7 dBi with 89% efficiency, whereas at the higher band (from 3.24 to 4.35 GHz) it changes from 4.3 dBi to 5.5 dBi and the corresponding efficiency varies from 38% to 90%. Better efficiency could be obtained with advanced enabling technologies for fixed or variable capacitors that allow for higher quality factors. The attained gain values are higher than the current designs of tunable dual-band PIFA and slot antennas, making it a good candidate for base stations and terminals of wireless networks, including cognitive and software defined radio systems.

3. CIRCULARLY POLARIZED BEAM SCANNING RECONFIGURABLE MICROSTRIP YAGI-UDA ANTENNA

3.1. Introduction

The recent demand of compact wireless devices propels the development of pattern reconfigurable antennas, capable of changing their main beam direction in the real time, other than conventional antennas of fixed radiation pattern. This capability helps in avoiding noisy environment, and strengthening the signal detection from an intended target. Classically, beam steering or switching is realized with phased arrays, but it might be too large or complex to meet the demand of compactness, low power consumption, and low cost of the antenna terminals. Some research works proposed Yagi-Uda based microstrip antenna with linear polarized (LP) pattern reconfigurable feature, such as in [3]-[4], and [42]. However, these designs allows for beam switching along certain fixed directions, rather than continuous beam scanning. In a similar fashion, two microstrip Yagi-Uda antennas were placed orthogonally and double-fed with quadrature phase to allow for CP beam switching instead [5]. Other concepts have been utilized to establish beam switching as in [8]-[9], and [43]-[46].

Recently, continuous beam scanning has been achieved by loading the antenna with variable reactive elements [6], [7]. Nevertheless, the radiation beam with these designs is linearly polarized which is not suitable for some applications, such as the low-orbit vehicular

satellites, and aircrafts communication systems. In such systems, circular polarization is required, and it is desired to have an adjustable elevation coverage zone which mitigates fading or allows for terminal tracking. CP antenna with continuous beam scanning feature is very challenging and more research is required to develop a more practical and efficient antenna system. As mentioned earlier, many pattern reconfigurable antennas rely on the microstrip Yagi-Uda configuration, because it offers tilted beam with an excellent efficiency, reduced profile, and less design complexity in comparison with planar phased arrays that require complex feed network and larger areas [2]. Therefore, microstrip Yagi-Uda antenna turns to be a good candidate for attaining scannable CP beam. The conducted research efforts toward antenna with reconfigurable beam direction versus beam polarity are summarized in Table 3-I

Table 3-I. Research status for different types of reconfigurable beam direction antennas versus beam polarity.

		Beam direction	
		switched	**scanned**
Polarization	**LP**	mature in literature	few in literature (3)
	CP	few in literature (3)	none

This chapter presents a reconfigurable microstrip antenna design with continuous CP beam scanning. To the best of the authors' knowledge, this type of antenna design hasn't been reported in the literature before. It is based on a microstrip Yagi-Uda antenna of two similar square patches. One element is driven, and the other is parasitic. Four varactors with a proper DC biasing network are added to the parasitic patch, to allow for tuning its effective electrical size, and hence controlling the coupling between the driven and the parasitic patch. Because

the main beam direction is determined by the electrical size of the parasitic patch, electronic beam scanning is attained by changing the applied DC reverse biasing voltage (capacitance value). Operation at 2.45 GHz is selected as the design frequency throughout the chapter. The proposed design has been validated through experimental measurements of a fabricated antenna prototype.

3.2.   Operational Principle

CP microstrip Yagi-Uda antenna was proposed in [2], where the operational principle and the design rules were summarized. In light of that, the antenna geometry labeled with dimensions in Figure 3-1 is selected. It consists of two square patches; one is driven with two orthogonal feeds (patch 1), whereas the other is a parasitic (patch 2). The used substrate is Rogers RT/duroid 5880 of permittivity, $\varepsilon_r = 2.2$, thickness $h = 3.175$mm, and loss tangent $tan\delta = 0.009$. The antenna exhibits a tilted radiation beam whose main direction θ_m° is determined by the size L_r of the parasitic patch as illustrated by Figure 3-2, where θ_m° is the angle subtended between the y and z axis (elevation angle). The curves in Figure 3-2 are extracted using the full wave simulator Ansoft HFSS [36]. As can be observed, when the parasitic patch is smaller than
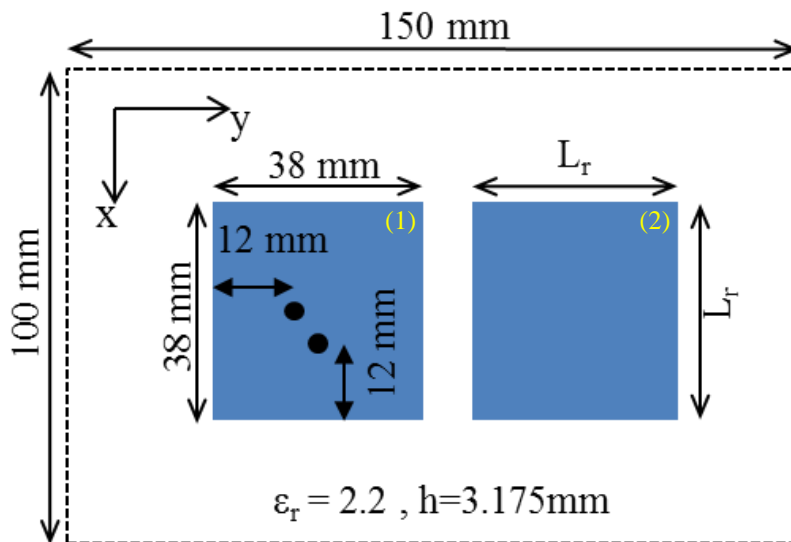
Figure 3-1. CP microstrip Yagi-Uda antenna geometry (units: mm).

39

the driven one ($L_r < L$), it acts as a director and the beam tilts toward the $+y$ direction. Whereas, if it is larger than the driven patch ($L_r > L$), it becomes a reflector and the beam tilts toward the
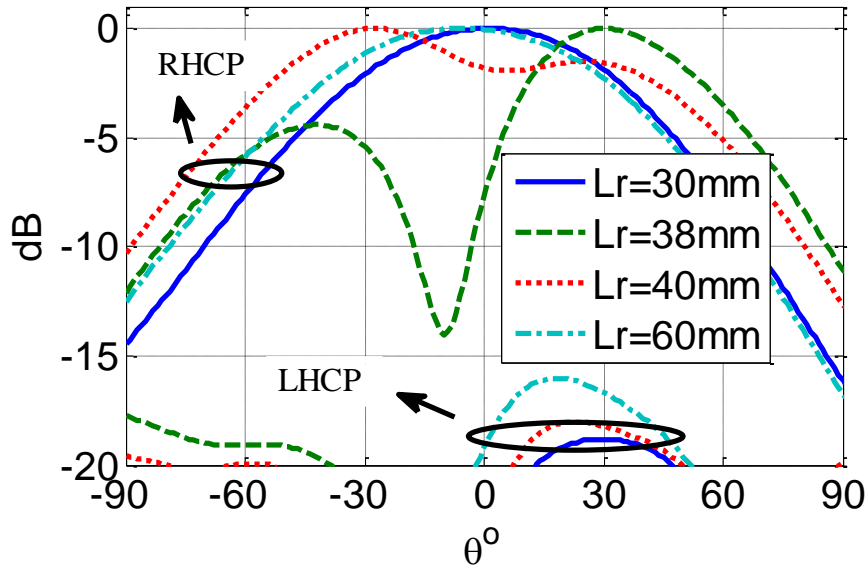
(a)
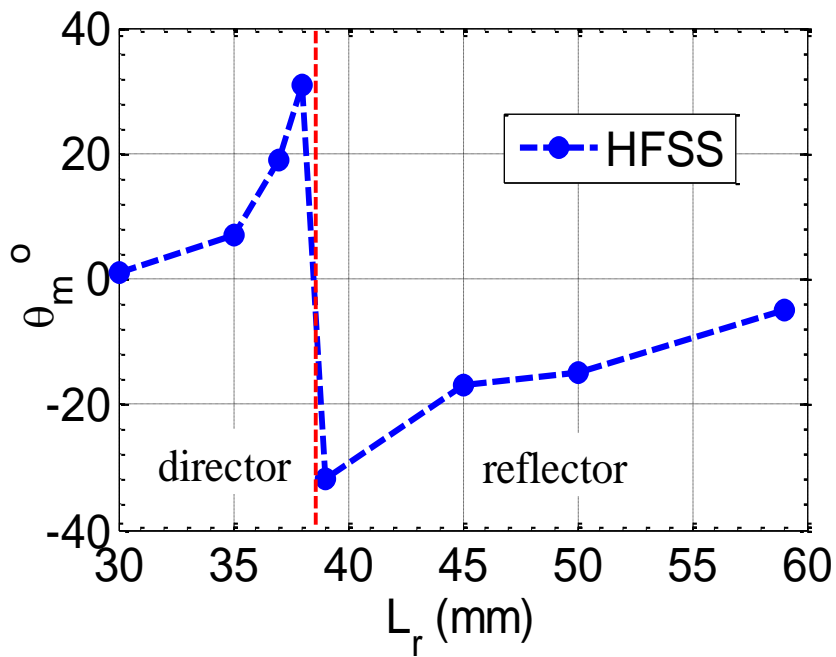
(b)

Figure 3-2. Simulated radiation patterns and beam directions θ_m° in the yz plane at 2.45 GHz vs. L_r: (a) radiation patterns; (b) beam directions.

y-direction. The maximum tilt angle is almost $30°$ in both $\pm y$ directions, and occurs when the parasitic patch size is close to the driven one. On the other hand, when the parasitic patch is too small or too large, it turns to be ineffective because its resonance is far from the resonance (operating frequency) of the driven patch, and the coupling between two patches is very weak. Therefore, the beam tilt angle at these cases approaches the broadside direction as if the radiation is only due to the driven patch. It is also noticed from Figure 3-2a, that the antenna inheres high SLL for beams with large tilt angles, such as in $L_r = 40$ mm ($-30°$).

According to [2], due to the different coupling effect at different size L_r of the parasitic patch, the differential phase between the orthogonal feeds needs to be adjusted other than $90°$ to acquire a good CP performance. Moreover, the probes feed positions also need to be moved independently for 50 Ω impedance matching at each port. These adjustments are impractical for a pattern reconfigurable design, and represent a real challenge in achieving scannable CP beam. To overcome this difficulty, the coupling mechanism between both patches has been carefully investigated. There exist two types of coupling between the two patches: *E*-plane coupling due to probe 1, and *H*-plane coupling due to probe 2 [47]. Let's define the relative phase shifts for the patches surface current (average value) due to the *E* and *H* planes coupling as β_e and β_h, respectively, such that:

$$\beta_e = \frac{1}{A}\left[\iint_A \angle J_{1y}(x,y)dx.dy - \iint_A \angle J_{2y}(x,y)dx.dy\right] \tag{3-1}$$

$$\beta_h = \frac{1}{A}\left[\iint_A \angle J_{1x}(x,y)dx.dy - \iint_A \angle J_{2x}(x,y)dx.dy\right] \tag{3-2}$$

$$A = L_r^2 \tag{3-3}$$

Where, $\angle J_{1x}$, and $\angle J_{2x}$ are the x-directed surface current phase (unit: rad) on patch 1 and patch 2 surfaces, respectively. $\angle J_{1y}$, and $\angle J_{2y}$ are the y-directed surface current phase on patch 1 and patch 2 surfaces, respectively.

Similarly, the current magnitude ratios α_e and α_h are defined as:

$$\alpha_e = \frac{\iint\limits_A |J_{2y}(x, y)| dx.dy}{\iint\limits_A |J_{1y}(x, y)| dx.dy} \tag{3-4}$$

$$\alpha_h = \frac{\iint\limits_A |J_{2x}(x, y)| dx.dy}{\iint\limits_A |J_{2x}(x, y)| dx.dy} \tag{3-5}$$

Where, $|J_{1x}|$, and $\angle |J_{2x}/$ are the x-directed surface current magnitude (unit: A/m) on patch 1 and patch 2 surfaces, respectively. $|J_{1y}|$, and $\angle |J_{2y}/$ are the y-directed surface current magnitude on patch 1 and patch 2 surfaces, respectively

The CP radiation condition is $\beta_e = \beta_h$, and $\alpha_e = \alpha_h$. Along the beam scanning range, this condition should be always satisfied to acquire a good CP radiation. Figure 3-3 shows the phase shift difference ($\beta_e - \beta_h$), as well as current ratio difference ($\alpha_e - \alpha_h$) between the E- and H-plane coupling versus different values of the parasitic patch size L_r, along with the separation distance s as a parameter. As can be seen when s = 4 mm the phase shift difference is minimized and almost constant. Meanwhile, the magnitude ratios (α_e, α_h) remain close to each other along the L_r variations. As such, with the optimized separation distance s = 4mm, no adjustments for the probes differential phase or positions would be required.
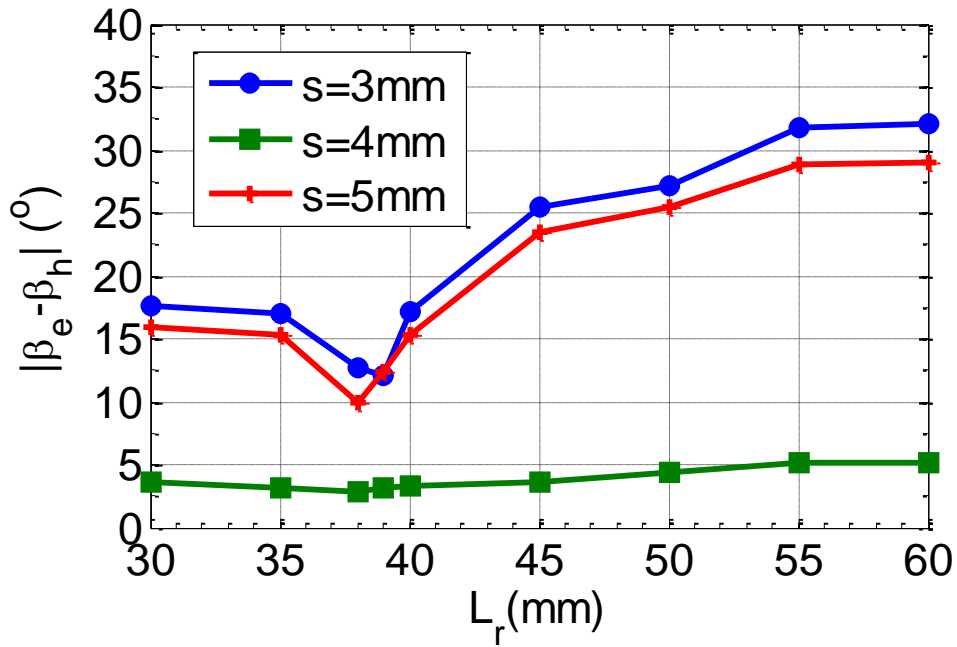
(a)
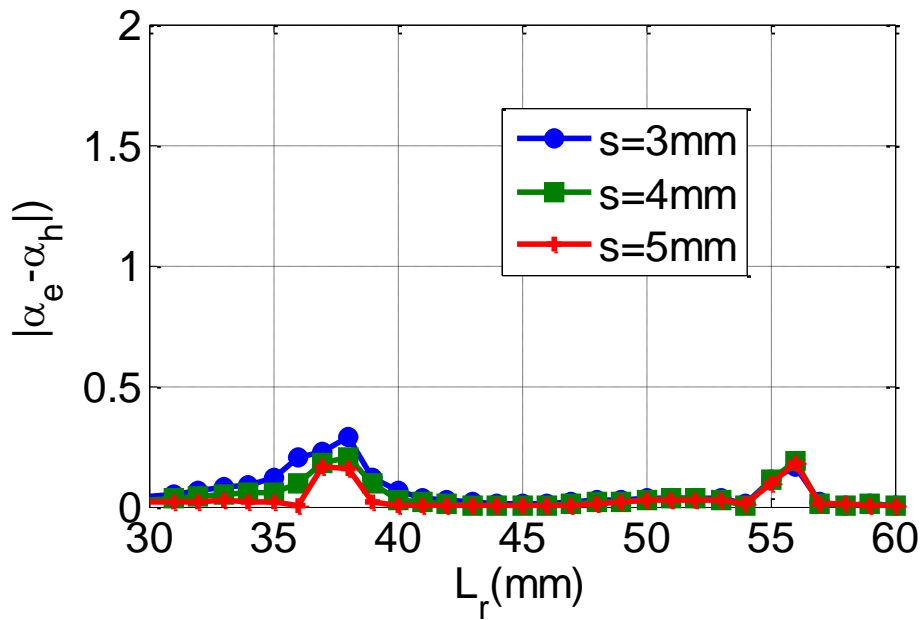
(b)

Figure 3-3. The phase shift and current ratio difference between the *E* and *H* plane coupling

vs. different L_r and *s* at 2.45 GHz: (a) phase shift difference; (b) current ratio difference.

3.3.   CP Patch Antenna with Reconfigurable Tunable Electrical Size

The previous section suggested the basic idea for scannable CP beam, which is to control the parasitic patch size that allows for controlling the coupling between the driven and parasitic patch, and hence determining the beam direction. The fundamental mechanism that provides changes in the electrical size of a microstrip patch antenna is the tuning of its resonant frequency. Frequency tuning is usually implemented with the adjustment of the patch physical dimensions. However, this method is not suitable for the electronically reconfigurable designs. Various techniques for electronic frequency-agility were developed in [21]-[24]. In such designs, the resonant frequency is modified by loading the antenna with varactors, which allow for changing the antenna overall capacitance electronically. Therefore, frequency-agile patch antenna applied to the CP microstrip Yagi-Uda antenna in Figure 3-1 could be used to control the mutual coupling, and change the scanning characteristics of the antenna radiation beam.

Frequency-agile microstrip patch antennas have two topologies regarding the varactor connection. The first topology is the parallel connection of the varactors across the patch radiating edge as in [21], [22]. The second topology uses the varactors to serially connect two halves of the patch as in [24], [48]. Since CP operation is looked for, the patch should be modified to accommodate both topologies as shown in Figure 3-4. As can be seen, the modification in the parallel connection is just adding two additional varactors to the other two radiating edges of the patch, which is simpler and easier to implement than for the serial connection. However, the parallel connection is disadvantaged over the serial connection in terms of the varactors values. Because the fringing capacitance at the radiating edge is smaller than the fringing capacitance at the centered separation gap, a higher tuning capacitance is required for the serial connection than for the parallel one to get the same change in the resonant frequency. This in turn permits the operation at higher frequency as the required tuning
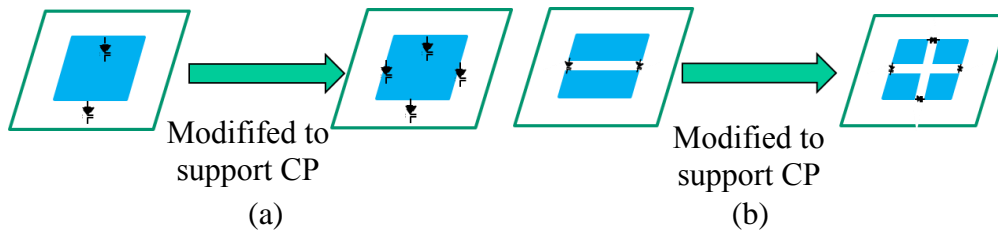
Figure 3-4. Schematic of frequency agility methods and its modification to support CP operation: (a) parallel varactor connection; (b) serial varactor connection.

capacitance decreases with increasing the frequency, and the small capacitance values are limited by the availability of the commercial off-shelf varactors. Therefore, serial connection is suggested [49]. On the other hand, the serial connection requires having centered crossed gap (patch divided into four quarters) with at least four varactors placed at the edges as shown in the figure. Such configuration imposes a complexity to implement the DC biasing network for the varactors, which complicates the prototyping process, and limits its practicality. Therefore, a new frequency-agile antenna design is necessary for the sake of simplicity and practicality of the proposed beam scanning antenna.

For the reasons and requirements discussed above, the frequency-agile antenna discussed in chapter 2 [50] has been used with some modification to support CP operation. In particular, the narrow rectangular slit in [50] is replaced with a square shaped slot as shown in Figure 3-5. The behavior of such devised antenna versus capacitance value is obtained with
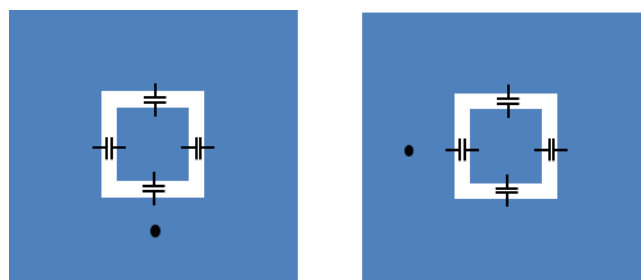
Figure 3-5. Patch antenna with a varactor loaded narrow square slot.
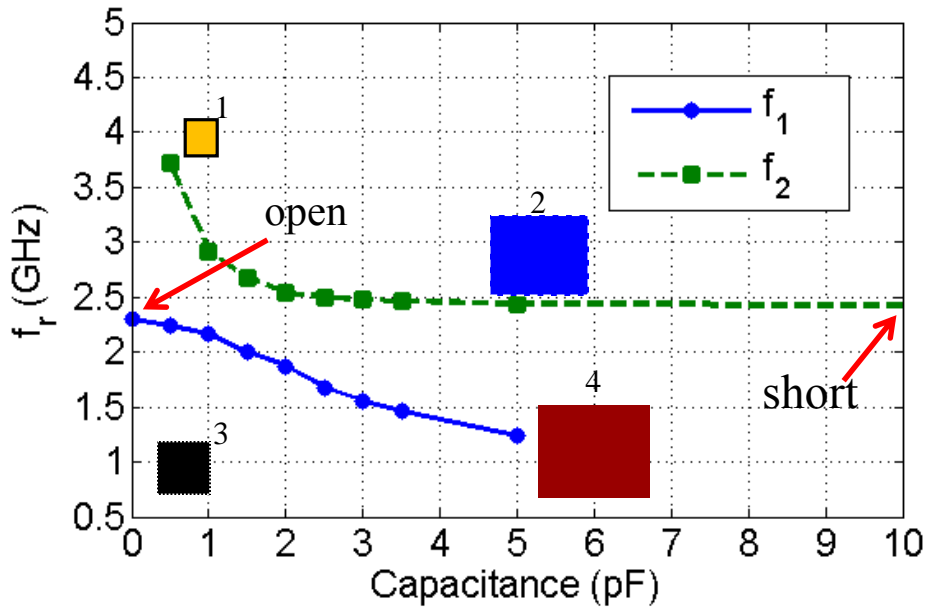
(a)
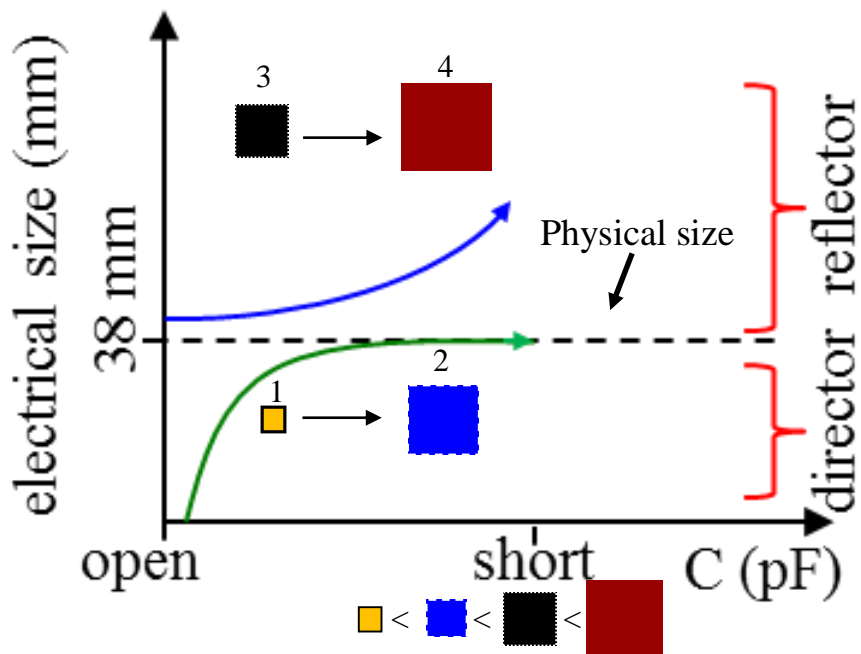
(b)

Figure 3-6. Behavior of the frequency-agile CP patch antenna proposed vs. lumped capacitance value C: (a) resonant frequencies; (b) schematic diagram for the electrical size.

is observed as expected, and hence, as discussed earlier in Section 2.4, the performance implies that the equivalent electrical size of that antenna behaves as illustrated schematically in Figure 3-6b. Therefore, the capacitance value change effectively tunes the electrical size of the patch. The new presented frequency-agile antenna can be easily modified to support CP without imposing complications to integrate the biasing circuit for the varactors, as will be discussed in the next section.

3.4. Beam-Scanning Reconfigurable CP Antenna

3.4.1. Antenna Design

The geometry of the proposed reconfigurable CP beam scanning microstrip Yagi-Uda antenna labeled with dimensions is shown in Figure 3-7. It is similar to the antenna in Figure 3-1, with the parasitic patch replaced by the frequency-agile patch antenna in Figure 2-1. However, that patch is modified to support CP as shown in Figure 3-7, where a narrow square slot is carved on its surface instead. Four varactors are placed in the middle of each side of the square slot, and a DC biasing circuit is integrated with the antenna as shown in the figure. The four varactors will be biased as unison with one control signal, which is connected to the inner part of the parasitic patch through a RF chock coil for RF/DC isolation. Regarding the completion of the DC path, the outer loop of the parasitic patch is grounded through a shorted $\lambda_g/4$ high impedance transmission line (TL) of thickness equal to 0.2 mm, where λ_g the guided wavelength at 2.45 GHz. The $\lambda_g/4$ TL acts as an RF choke at the parasitic patch edge, and hence the RF current on the patch is kept unperturbed. The TL is shorted to the ground through a metallic via. In order to attain the possible widest scanning range, the parasitic patch size is selected to be the same as the driven patch. This selection is according to the results in Figure 3-2b that make θ_m maximized when the parasitic patch size L_r is close to the driven patch. The separation gap s is selected, such.
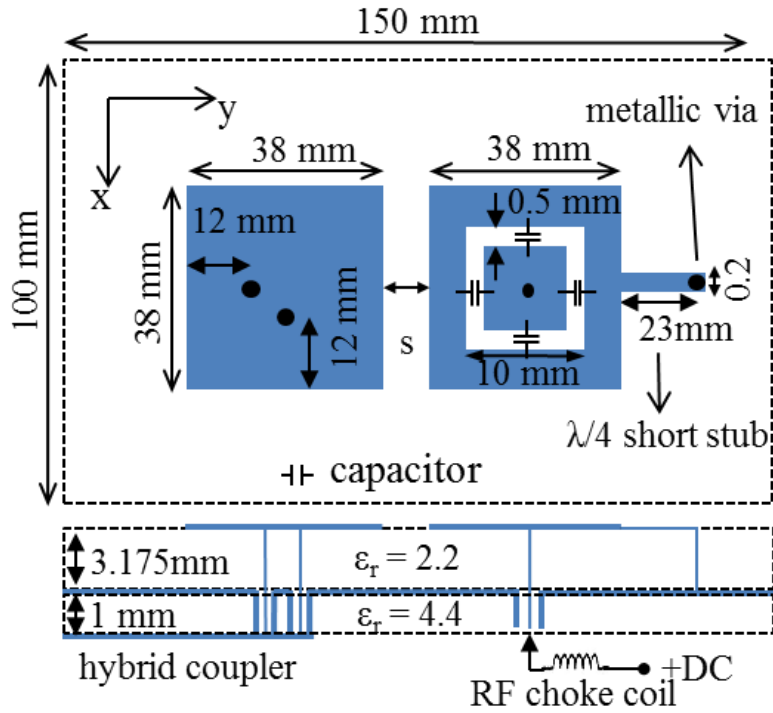
Figure 3-7. Geometry of the proposed reconfigurable CP beam scanning microstrip Yagi-Uda antenna.
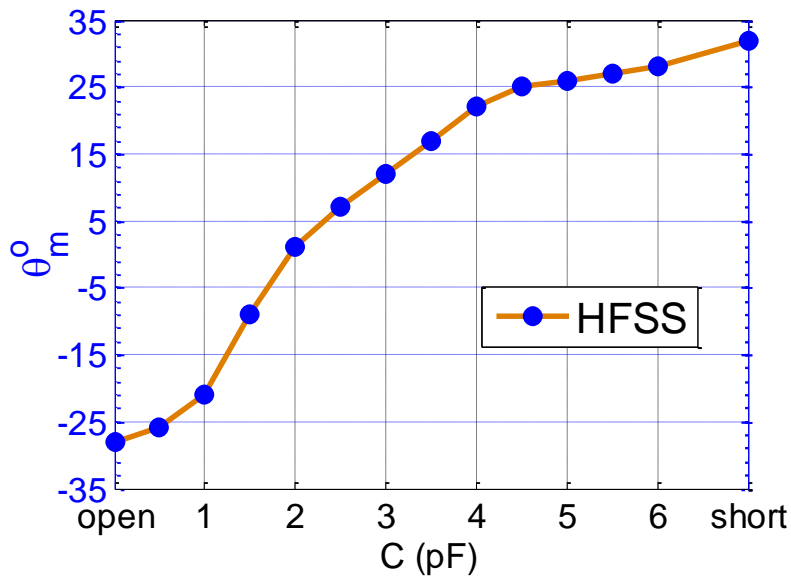
Figure 3-8. The simulated results for the main beam direction θ_m in the yz plane vs. C at 2.45 GHz.

that the E-plane (*yz*) coupling due to the left probe and H-plane (*yz*) coupling due to the

bottom probe are similar along the tuning range of the parasitic patch. Therefore, adjustments of the feeds differential phase other than 90°, or changing the probes positions for impedance matching are not needed during the beam scanning as needed in the fixed beam designs. Therefore, a 3 dB quadrature hybrid coupler can be used to feed the antenna, which will allow for switching the proposed antenna polarization from left hand to right hand and vice versa. The coupler is printed on the back side of the antenna over a FR4 substrate of $\varepsilon_r = 4.4$ and loss tangent $tan\delta = 0.02$.

Full wave simulation has been carried out for the proposed antenna shown in Figure 3-7 and the results for the main beam direction θ_m versus the capacitance value C are shown in Figure 3-8. As expected, beam scanning is observed upon changing C, where θ_m increases monotonically with C. The achieved scanning range is -28° to 32°. The curve manner is attributed to the behavior of the utilized frequency-agile antenna illustrated in Figure 3-6b as the following: when C is very small the parasite patch is effectively a reflector of a size slightly larger than its physical one. Although it has another electrical size as depicted by Figure 3-6b, it is too small to be effective. Thus, the main beam direction is in the $-y$ direction with large deflection (-28°). Upon increasing C, the reflector become larger and the tilt angle decreases till it reaches the broadside direction, where the reflector becomes ineffective. Meanwhile, the smaller size of the parasitic patch also becomes larger to be an effective director. Thus, the beam continuously tilts to the $+y$ direction till that smaller size approaches the physical size of the parasitic patch, and the deflection angle is maximum (32°). With the above explanation, the relation between θ_m and C in Figure 3-8 is consistent with the relation between θ_m and L_r in in Figure 3-2b.

3.4.1. Experimental Measurements

An antenna prototype has been fabricated and measured to validate the performance of the proposed design. A photo of the fabricated antenna prototype is shown in Figure 3-9. High quality varactor MHV505-19-1 by *Aeroflex Metelics* is used as a variable capacitance device [53]. It has a tuning capacitance of $0.458 < C < 6.642$ pF with $20 > V_{DC} > 0$ V DC reverse biasing voltage as shown in Figure 3-10. The tuning capacitance is sufficient for the achieved scanning range in Figure 3-8. The antenna is fed from the RHCP port, while the other port (LHCP) is terminated with a 50Ω matching load. If a LHCP is required, the coupler ports need to be switched.

The simulated and measured results for the normalized CP radiation patterns of the proposed antenna at four different DC voltages are shown in Figure 3-11. Good agreement is observed between the simulation and the measured results for the RHCP fields. The main beam direction θ_m changes with the applied DC voltages as anticipated. Within the 3 dB beam widths of the main beam lobes, the cross polarization level (LHCP) is less than -15.34 dB (axial ratio < 3 dB), which ensures the maintenance of the CP performance during the beam scanning. The CP performance is also maintained at all other DC voltages (scan angles). A variance is noticed between the simulated and measured results for the cross polarization level (LHCP). These discrepancies are considered due to following reasons: the existence of the biasing circuit in proximity of the antenna during measurement, the varactors parasitic effect that leads to a tolerance in the capacitance value C, the phase error introduced by the hybrid quadrature coupler, and the fabrication tolerance in the antenna prototype including the alignment, soldering, and the undesired air gaps between the layers that add additional errors. Even though differences between the simulated and measured results for the x-pol level exist, the full wave simulation model is

still a good guiding tool for predicting the antenna scanning performance at different biasing voltages. The antenna elevation coverage zone is defined as the intersection between the half power beam width (HPBW) angular region and the axial ratio beam width (ARBW) angular region. The former is set with the 3 dB level below the peak of the main CP radiation beam, whereas the latter is set with the 3 dB axial ratio level (-15.34 cross

RHCP

LHCP

$\lambda_g/4$

(a)

Input of the DC
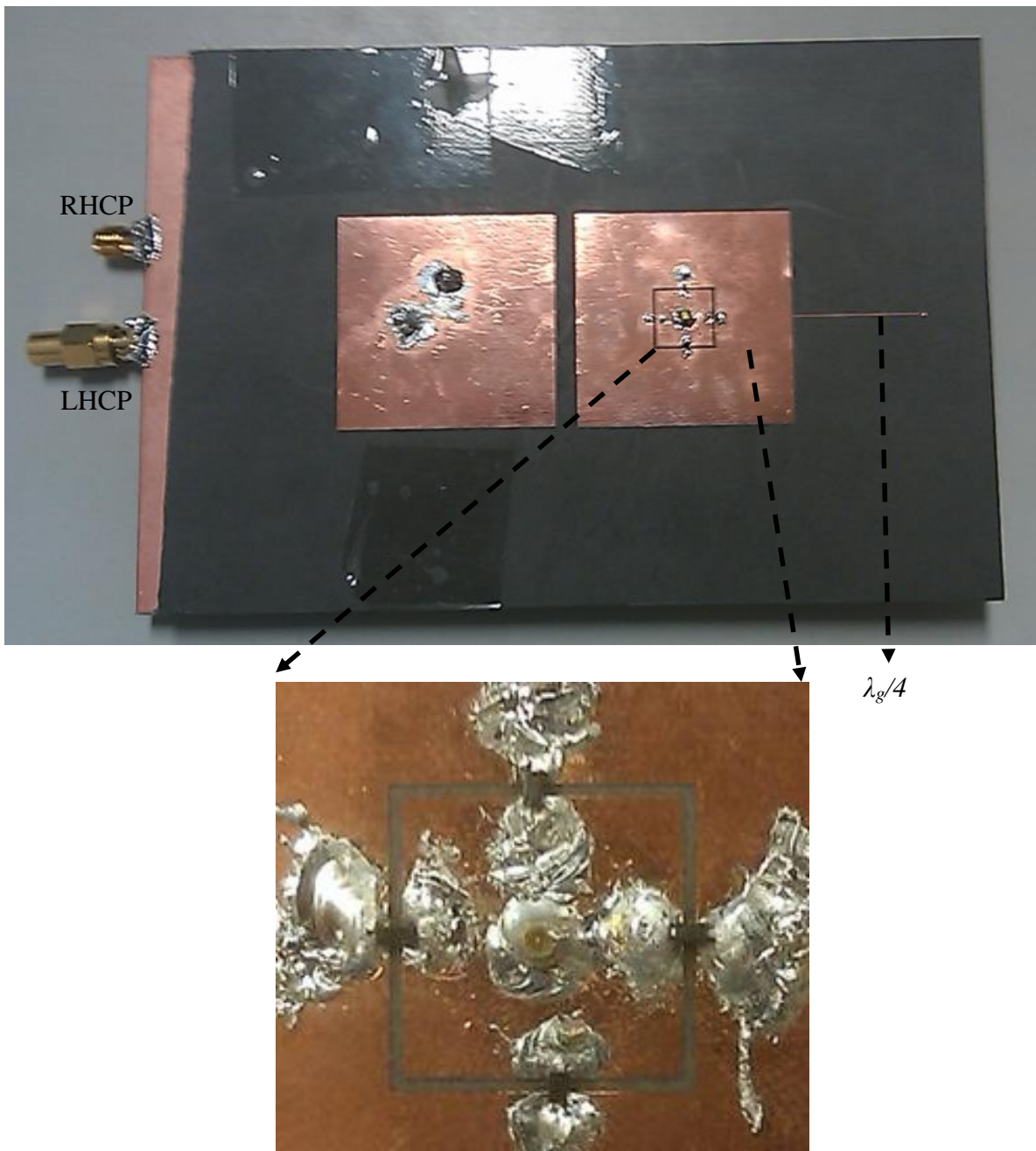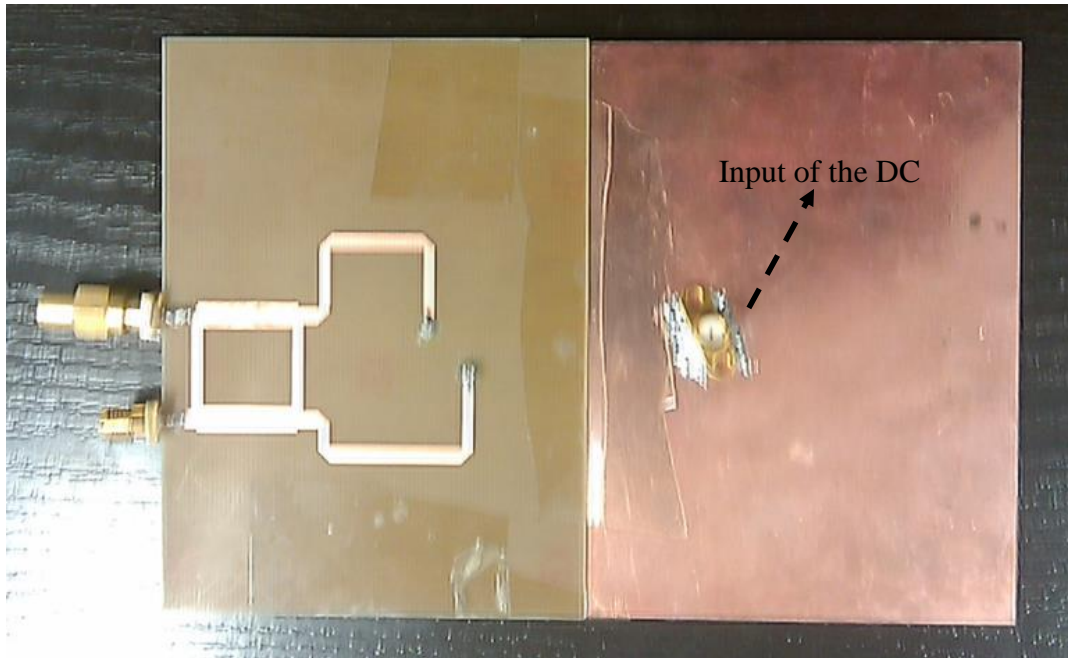
(b)

Figure 3-9. A photo of a the proposed reconfigurable CP beam scanning microstrip Yagi-Uda antenna prototype along with the associated tuning devices and biasing assemblies: (a) front view; (b) back view

polarized level). From the simulated and measured CP radiation patterns, the elevation coverage zone of the proposed antenna is recognized to be changing with applied DC voltages, and can be electronically adjusted.
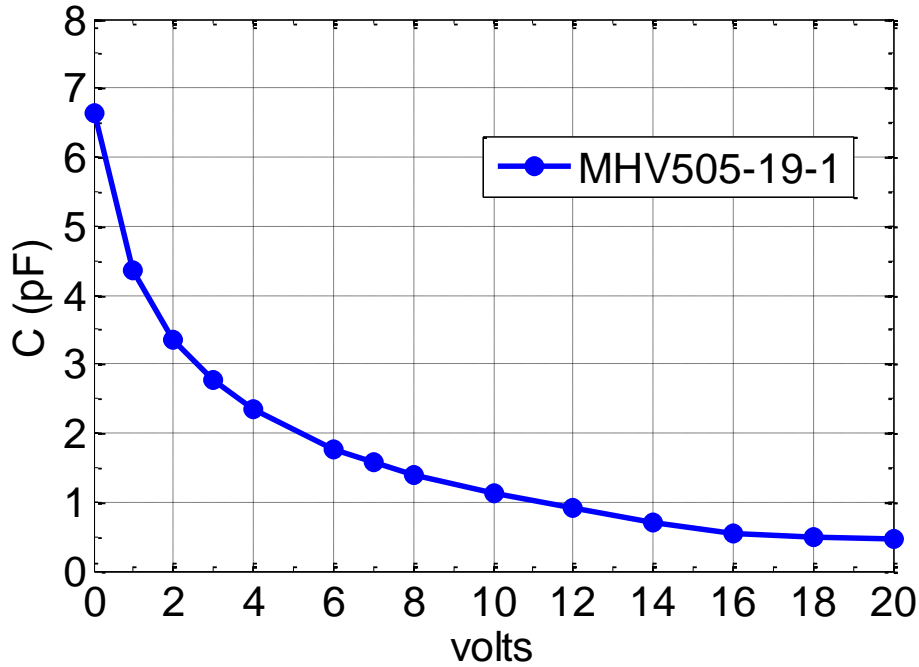
Figure 3-10. The capacitance values vs. the reverse biasing voltage of the MHV505-19-1 varactor by *Aeroflex Metelics* generated from the data provided by the manufacturer [53].

The main beam θ_m direction versus the reverse DC biasing voltages V is shown in Figure 3-12. It can be seen that both the simulated and measured curves are correlated and have the same trend, which is decreasing monotonically with the voltages as expected from Figure 3-8 and Figure 3-10. As observed before, a deviation exists in the measured scan angles from the predicted but it is clearer here in Figure 3-12. However, the full wave simulator with the approximated varactor model (pure capacitance) is still a good guiding tool for predicting, the beam scanned angles of the proposed antenna design at different biasing voltages.
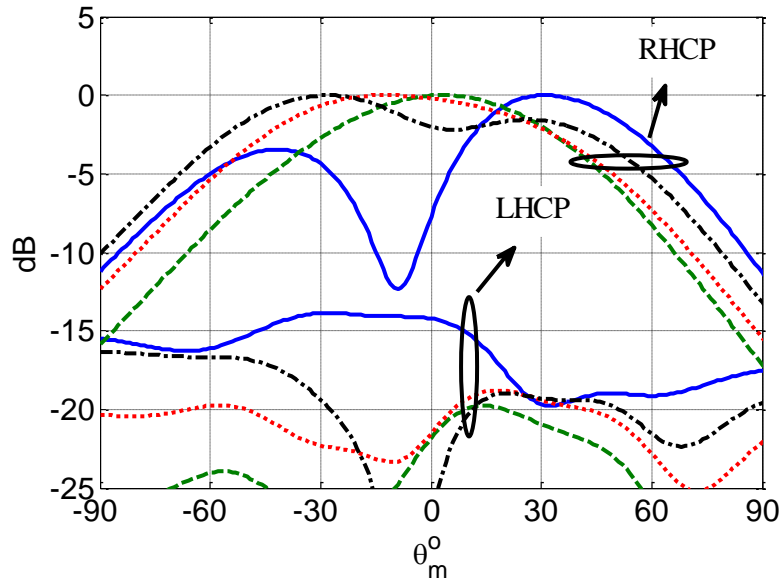
(a)
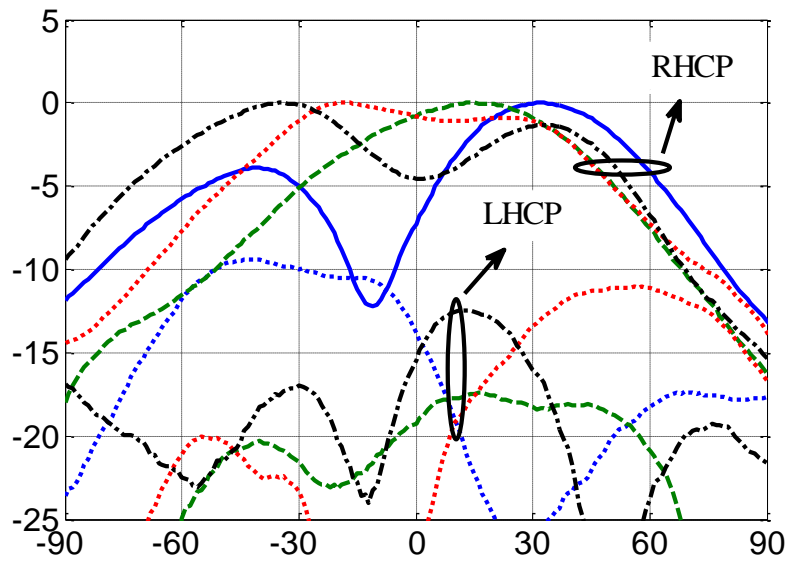
(b)

Figure 3-11. The normalized CP radiation patterns of the proposed antenna at 2.45GHz and different applied reverse DC biasing voltages: (a) simulations: solid line (0V, 31°), dashed line (4V, 3°), dotted line (8V, -12°), dashed-dotted line (20V, -28°); (b) measurements: solid line (0V, 32°), solid line (4V, 13°), solid line (8V, -17°), solid line (20V, -36°).
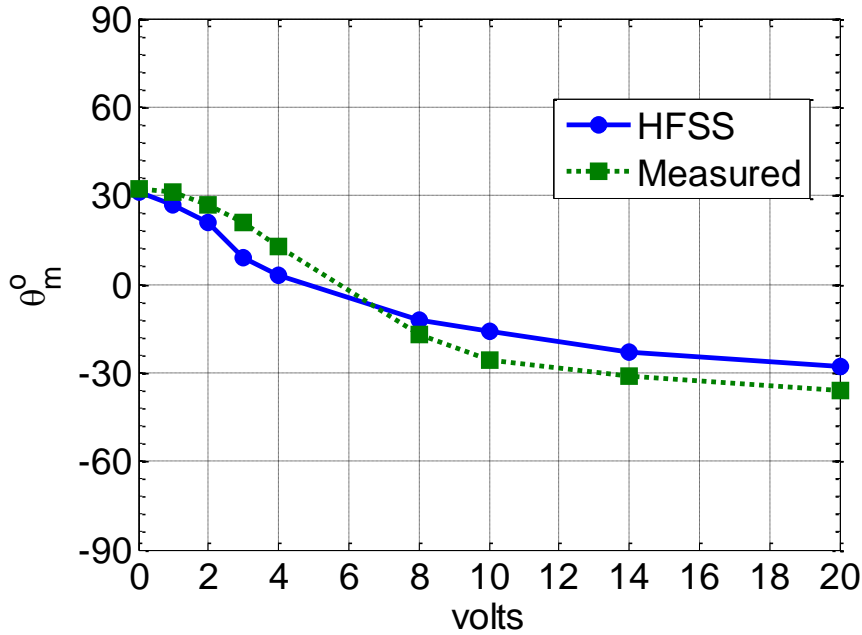
Figure 3-12. The simulated and measured results for the main beam direction θ_m versus the applied reverse DC biasing voltages at 2.45GHz.

The antenna realized circular gain versus the scan angle is shown in Figure 3-13 that reveals good accordance between the simulated and measured curves. The attained peak gain is 8.1 dBic with 2.4 dB variation along the scanning range. An estimate for the antenna efficiency is calculated using the simulated directivity and the measured realized gain. It decreases from 75.58% to 54% along the beam scanning, while the beam direction changes from the –y to the +y. This variation (decrease) in the efficiency is due to the inherent losses in the varactors that increases when the capacitance value increases (voltage decreases) [24], and in turn the beam scan angle θ_m. Better efficiency at low voltages (large scan angles θ_m) could be attained if a higher quality varactor is used. Newly emerged technologies are needed to enable higher quality varactors.

The reflection coefficient of the proposed antenna is in general dependent on the applied reverse DC biasing voltage. At 20V, the reflection coefficient from the RHCP port of the 3 dB hybrid coupler, while the other port is terminated with 50Ω is shown in
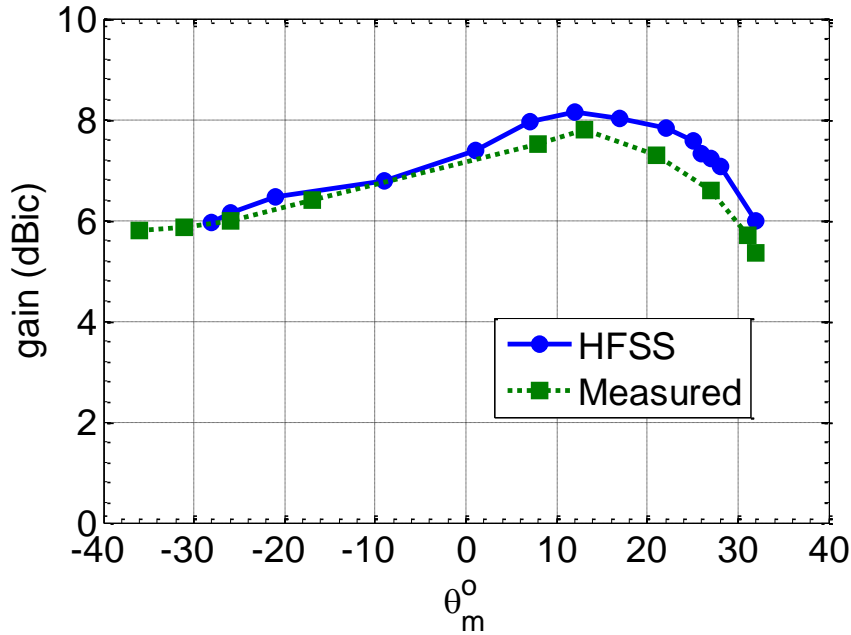
Figure 3-13. The simulated and measured realized circular gain versus the beam scan angles at 2.45 GHz.

Figure 3-14. From the figure, it is observed that the reflection coefficient is below -10 dB over a broadband of frequencies centered on 2.45 GHz. Similar performance is also found at all the other biasing voltages. The broadband impedance bandwidth is because of the hybrid coupler, where the reflections from the antenna add up out of phase and get cancelled.

CP antenna bandwidth is usually defined by the overlapped 10 dB return loss and 3 dB axial ratio bandwidths. However, the practical bandwidth of the antenna is limited by the beam squint, which is the fact that the beam shifts with frequency. This is because the main beam direction depends on the electrical size of the parasitic patch and the parasitic patch size is frequency dependent. Considering the proposed antenna elevation coverage is larger than 40°, a 5° beam squint is very acceptable and the antenna overall bandwidth could be defined. Figure 3-15 shows the simulated beam directions θ_m

versus the capacitance value at different frequencies. Accordingly, the achieved

bandwidth for the proposed antenna design is 2.425 - 2.475 GHz (2%).
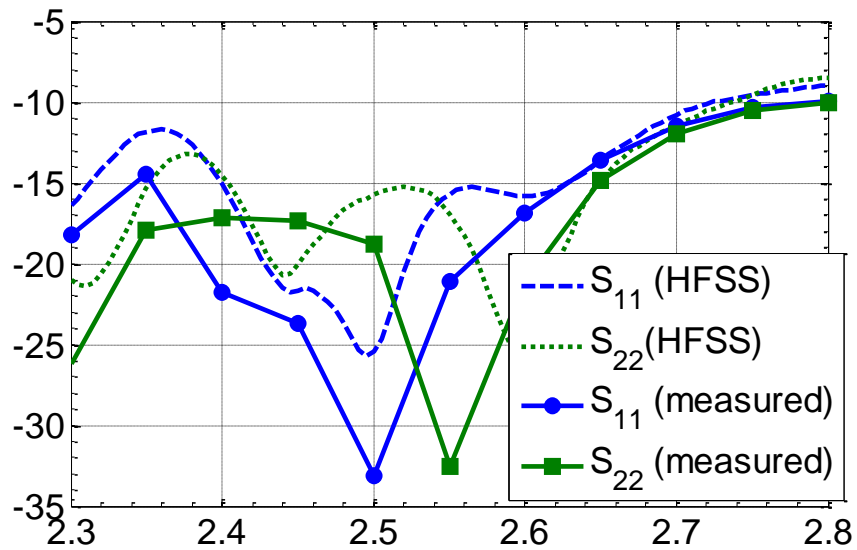
Figure 3-14. The reflection coefficient at 20 V from the LHCP /RHCP port, while the other

port is terminated with 50Ω.
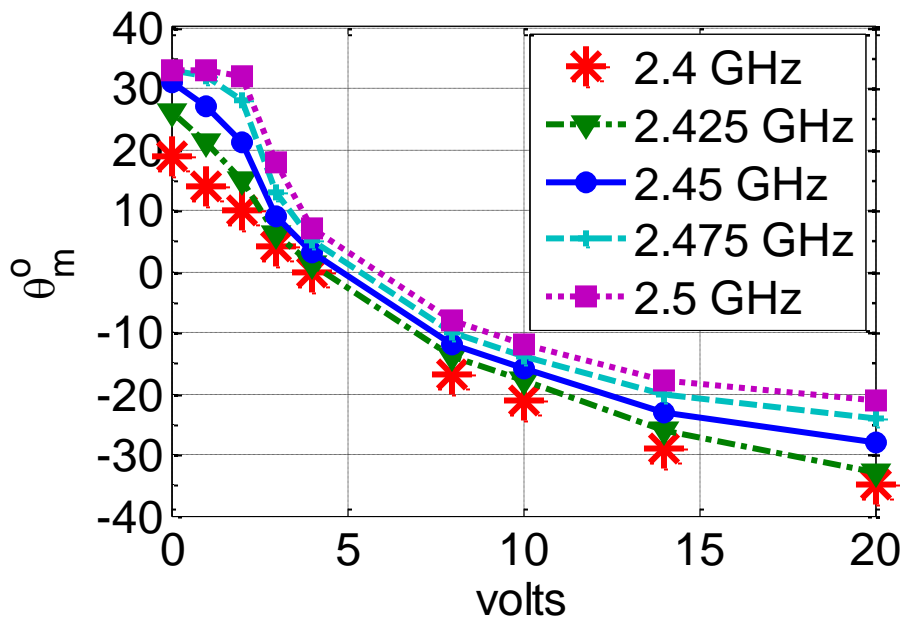
Figure 3-15. The beam scan angles vs. applied voltages at different frequencies swinging

around 2.45 GHz.

3.6. Summary

A novel design of a reconfigurable microstrip Yagi-Uda antenna for CP beam scanning is proposed. Electronic beam scanning is attained with the aid of four varactors and simple biasing network integrated into the parasitic patch. The varactors are of $0.48 – 6.642$ pF tuning capacitance with $0 – 20$ V DC voltages. The achieved scanning range is from $-36°$ to $32°$, and the attained peak gain value is 8.1 dBic with 2.4 dB gain variation along the entire scanning range. The antenna efficiency varies from 75.58% to 54%. Constant efficiency variation could be obtained with advanced enabling technologies for variable capacitor devices of higher quality factor. Low orbit vehicular satellites, aircrafts, tracking terminals, and remote sensing receiving systems are potential applications for the proposed antenna.

4. RECONFIGURABLE TWO-DIMENSIONAL BEAM SCANNING MICROSTRIP ANTENNA

4.1. Introduction

Continuing the development of pattern reconfigurable antennas capable of changing their main beam direction in real time, this chapter investigates and proposes microstrip antenna with two-dimensional beam scanning feature. Such antenna system is helpful to strengthen the signal detection from an intended target, or mitigate interference for applications such as, satellite, or land mobile tracking terminals. As discussed previously, phased arrays are the classical method for beam steering, but it might be too large or complex to meet the demand of compactness, simple implementation, or cost reduction. In [5], Yagi-Uda based microstrip antenna with a pattern reconfigurable in four quadrants is proposed, however it allows only for beam switching to fixed directions, rather than continuous beam scanning. In [6], [7] continuous beam scanning is achieved by loading the antenna with variable reactive elements. However, the radiation beam is allowed to be only scanned in the elevation plane (one-dimensional beam scanning). A summary for the conducted research efforts toward antennas with reconfigurable beam direction versus beam scan dimensions is listed in Table 4-I.

The proposed method for continuous two-dimensional beam scanning, exploits the reconfigurable parasitic patches of tunable electric size. The antenna geometry consists of two square parasitic patches, placed along the E and H-planes of a square probe-fed patch. A varactor diode with a proper DC biasing network is added to each parasitic patch, to effectively

Table 4-I. Research status for different types of reconfigurable beam direction antennas versus scan planes.

	Beam direction	
	switched	scanned
One-dimensional (elevation plane)	mature in literature	few in literature (3)
Two-dimensional (elevation and azimuth planes)	few in literature (3)	none

change its electrical size. Because the main beam direction is determined by the electrical size of the parasitic patches [2], [4], [5], electronic beam scanning is achieved by changing the applied DC voltage (capacitance value). Two DC control signals are required to scan the beam in two dimensions. The antenna design is validated through full wave simulations along with experimental measurements for a fabricated prototype, and excellent agreements are observed.

4.2. Operational Principle

The antenna geometry, shown in Figure 4-1, consists of three square patches. The substrate has thickness h=3.175 mm, and relative permittivity ε_r = 2.2. The ground plane size is 150 x 150 mm. One patch is fed with a probe and its dimensions are 38 x 38 mm. The other two are parasitic and placed to the top (H-plane) and right (E-plane) of the driven patch. When a parasitic patch is placed along the E or H plane of a driven patch at a small enough separation distance, the total radiation beam tilts away from the bore sight direction in that plane, due to the existing coupling between them [2]. Basically, if the parasitic patch size is smaller than or

equal to the driven one, it acts as a director and the beam tilts toward the direction of its side. The main beam tilt angle θ_m is determined by the size of the parasitic patch, and the maximum tilt angle occurs when the parasitic patch size is close to the driven one [52]. If the parasitic patch is also too small, the coupling becomes weak and loses its effect, therefore the main beam is in the broadside direction as the radiation is only due to the driven patch.

From Figure 4-1, when the size of the right parasitic patch (patch#2) is very small (L_{r1}=25mm), and top parasitic patch (patch#1) size is close to the driven patch size (L_{r1} = 37mm), the beam is directed toward the positive *y* axis with an elevation angle θ_m=32° (Case *A*). Upon the gradual enlargement of the right patch, the beam is scanned clockwise in the azimuth plane with a similar elevation angle (θ_m=32°). When the right patch size becomes equal to the top one, the azimuth angle $\phi_m = 45°$ (Case *B*). Then if the top patch size is gradually reduced, the beam continues to be scanned with a similar elevation angle (θ_m=32°) in the
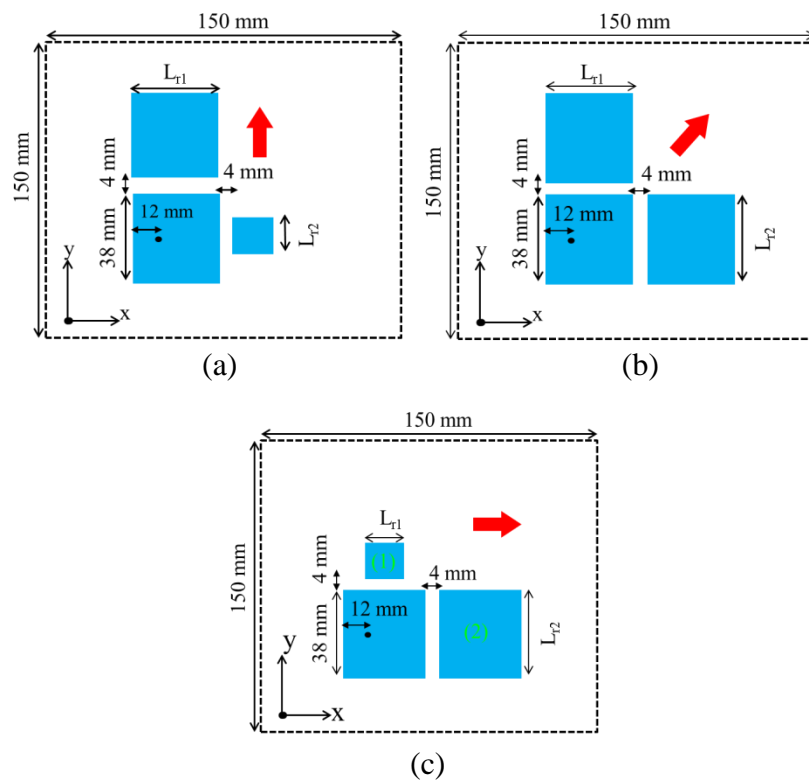
Figure 4-1. Microstrip patch antenna with two parasitic patches placed along the xz (*E*) and yz (*H*) planes: (a) case *A*; (b) case *B*; (C) case *C*.

61

Table 4-II. Simulated results for the beam directions vs. parasitic patches dimensions at 2.5 GHz.

	Top patch L_{r1} (mm)	Right patch L_{r2} (mm)	Direction (θ_m°, ϕ_m°) (degrees)
Case A	37	25	32°, 90°
	36	25	25°, 90°
Case B	37	37	32°, 45°
	36	36	25°,45°
Case C	25	37	32°, 0°
	25	36	25°, 0°

azimuth plane, clockwise direction, until its size becomes too small to be effective and case *C* is reached. Case *C* is the complement of Case *A*, at which the beam is directed toward the positive *x* axis. If the elevation angle is required to be reduced, the maximum value of the parasitic patches dimensions should be reduced further relative to the driven patch size. For instance, the antenna along cases *A*, *B*, and *C* with L_{r1}, or $L_{r2} = 36$mm leads the elevation angle θ_m to be 25° instead. Table 4-II summarizes the dimensions in mm of the geometrical parameters L_{r1} x L_{r1} and L_{r2} x L_{r2} along with the corresponding beam directions at three different cases. It should be also pointed that if both parasitic patches are quite small ($L_r = 25$mm), they becomes ineffective because of the weak coupling, and the beam is directed toward the broadside direction as discussed before. The results in Table 4-II are obtained with the aid of full wave simulation using HFSS [36].

The above elaborated mechanism is the principle to achieve two-dimensional beam scanning in both the elevation and azimuth planes. Indeed, if a tuning mechanism is introduced to the sizes of the parasitic patches, electronic beam scanning would be allowed.

4.3. Antenna Design and Performance

A patch antenna with a capacitor loaded slot proposed in chapter 2 [50], effectively provides the fundamental mechanism for tuning the electrical size. Detailed discussion on the

(a) (b)
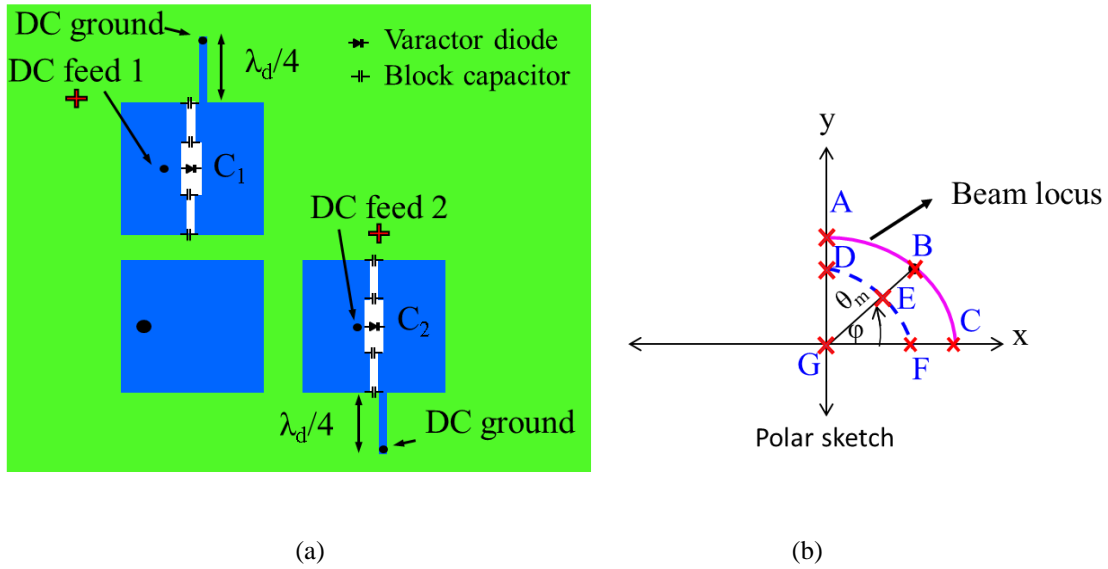
Figure 4-2. The proposed reconfigurable antenna for two-dimensional beam scanning along with the biasing assemblies, and the expected beam directions: (a) geometry; (b) sketch for the expected beam direction trajectory.

relation between the capacitance values C versus electrical size L_r exists in chapter 3 and illustrated in Figure 3-6 [52]. Therefore, the parasitic patches in Figure 4-1 are replaced with such antenna design, and the proposed reconfigurable antenna for 2D beam scanning is constructed as shown in Figure 4-2a. The dimensions of all the patches are 38 x 38 mm, whereas the slot of each parasitic patch is 20 x 0.5 mm. Two varactor diodes of capacitances C_1 and C_2 are placed in the middle of each slot along with the biasing circuits. The used varactor is MHV505-19-1 by *Aeroflex Metelics* [53] of capacitances $0.458 \leq C \leq 6.642$ pF with $20 > V_{DC} > 0$ V DC reverse biasing voltage as shown in Figure 4-3. Each parasitic patch is divided into two parts at its center by narrow slits of 0.2 mm width. The left part of the parasitic patches is fed with the DC signal through a metallic pin and a RF choke coil for RF/DC isolation. The right part is grounded through a shorted λ/4 transmission line to have high impedance at the patch edges. A Photo for the fabricated antenna prototype is shown in Figure 4-4.

The combinational change of the applied biasing voltage (capacitance value) to each

parasitic patch, allows for tuning their electrical size simultaneously, hence electronic beam scanning would be enabled as shown in Figure 4-2b, where a polar sketch for the beam direction trajectory is illustrated. The arc formed by points *A*, *B*, *C* represents beam scanning from $\phi_m = 0°$ to $90°$ with $\theta_m = 32°$. The arc *D*, *E*, *F* is similar to *A*, *B*, *C* but with $\theta_m = 25°$. Finally, points G represents the broadside direction. The voltage (capacitance) combination values associated with the beam direction are listed in Table 4-III. These capacitance values are depicted through full wave simulation as follow:

- At $C < 1.5$ pF, the parasitic patch electrical size is larger than its physical size, and it is effectively a reflector. Hence, values for C_1 & C_2 below 1.5 pF are abandoned.

- At $C = 1.5$ pF, the parasitic patch is ineffective and doesn't impact the radiation performance.

- At $C > 1.5$ pF, the parasitic patch electrical size starts smaller than its physical size, and continuously grows up with increasing C. It is effectively a director, and hence values for C_1 & C_2 should be above 1.5 pF.

- At $C > 3$ pF, antenna matching is quite poor.

According to the above findings, the permissible capacitance range is $1.5 < C < 3$ pF.
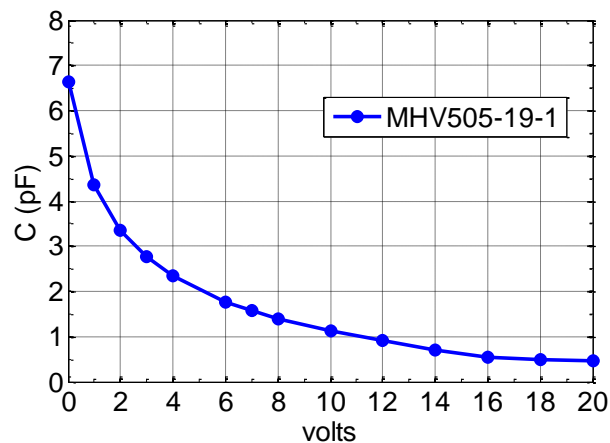
Figure 4-3. The capacitance values vs. the reverse biasing voltage of the MHV505-19-1 varactor by Aeroflex Metelics generated from the data provided by the manufacturer [53].

Figure 4-4. A photo for the proposed fabricated antenna prototype.

Table 4-III. Simulated results for the beam directions vs. voltage combinations at 2.5 GHz.

Case	V_1(volt)	V_2(volt)	Direction $(\theta_m^{\circ}, \phi_m^{\circ})$ (degrees)
A	7.5	3.5	$32^{\circ}, 90^{\circ}$
B	3.5	3.5	$32^{\circ}, 45^{\circ}$
C	3.5	7.5	$32^{\circ}, 0^{\circ}$
D	3.5	5	$23^{\circ}, 90^{\circ}$
E	5	5	$32^{\circ}, 45^{\circ}$
F	5	3.5	$23^{\circ}, 0^{\circ}$
G	7.5	7.5	$0^{\circ}, 0^{\circ}$
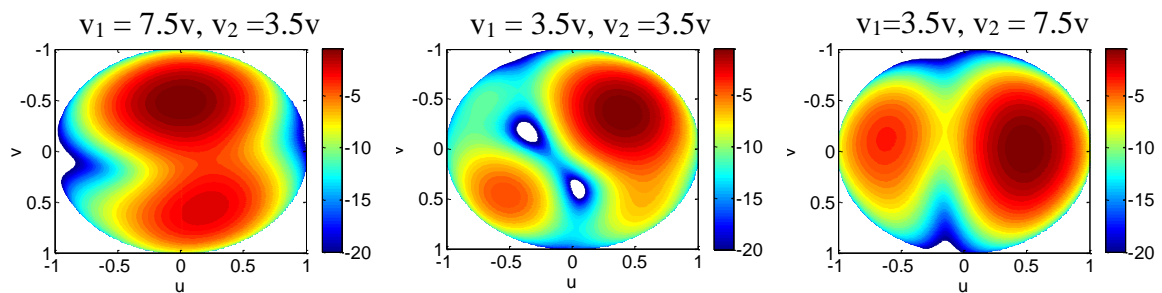
(a)
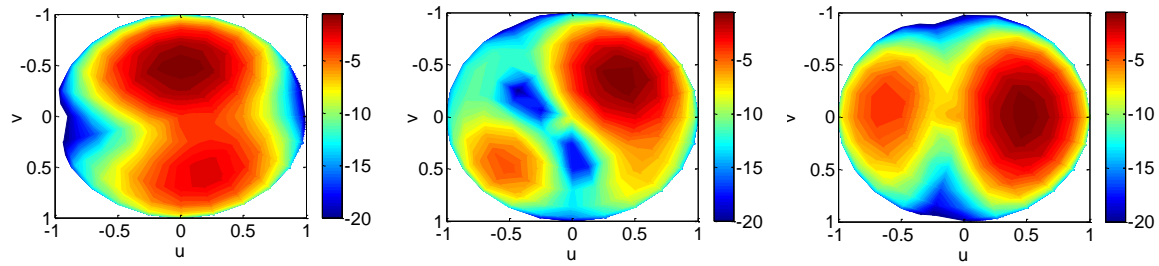
(b)
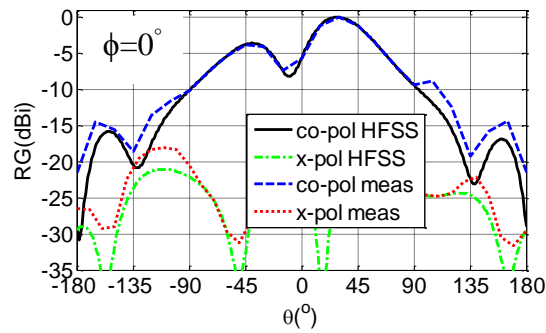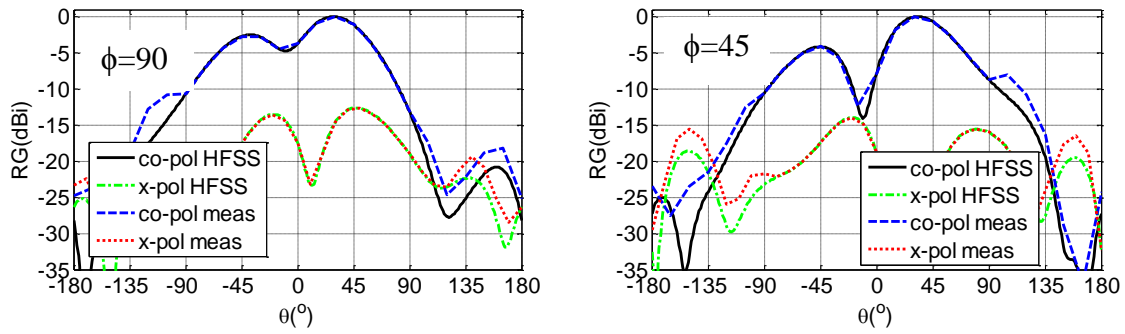
(c)

Figure 4-5. The simulated and measured projected co-pol 3D radiation patterns in the upper hemisphere space of the proposed antenna at different biasing voltage along the *A, B, C* arc, as well as the corresponding plan cuts of maximum radiation: (a) simulated 3D; (b) measured 3D; (c) simulated and measured plane cuts.

The 3D radiation pattern measurements for the proposed antenna are conducted inside an ETS-Lindgren far-field range, where the proposed antenna is mounted over a post of two rotational axis of motion. Several magnetic RF chocks are attached to the coaxial cable feeding the antenna under test to mitigate its spurious radiation, and minimize its effect on the

measured patterns. The radiation patterns at different combinations of biasing voltage along arcs *ABC*, *DEF*, and point *G*, are shown in Figure 4-5, Figure 4-6, and Figure 4-7 respectively. Excellent agreement is observed between the simulated and measured results. As can be seen from Figure 4-5, the beam is rotating from $\phi_m = 0°$ to $90°$ with $\theta_m \sim 32°$ due to the corresponding biasing voltage combinations as expected. The maximum side lobe level (SSL) is -2.8 dB occurs at case *A*, and cross polarization (x-pol) level within the beam width of the major beam is < -10 dB for all cases. Similar behavior for the beam is seen in Figure 4-6 but with smaller elevation angle $\theta_m \sim 25°$, and much lower x-pol and SLL. The presented results implied two-dimensional beam scanning in the top right quadrant of the upper hemispherical space up to $32°$.

(a)

(b)

(c)
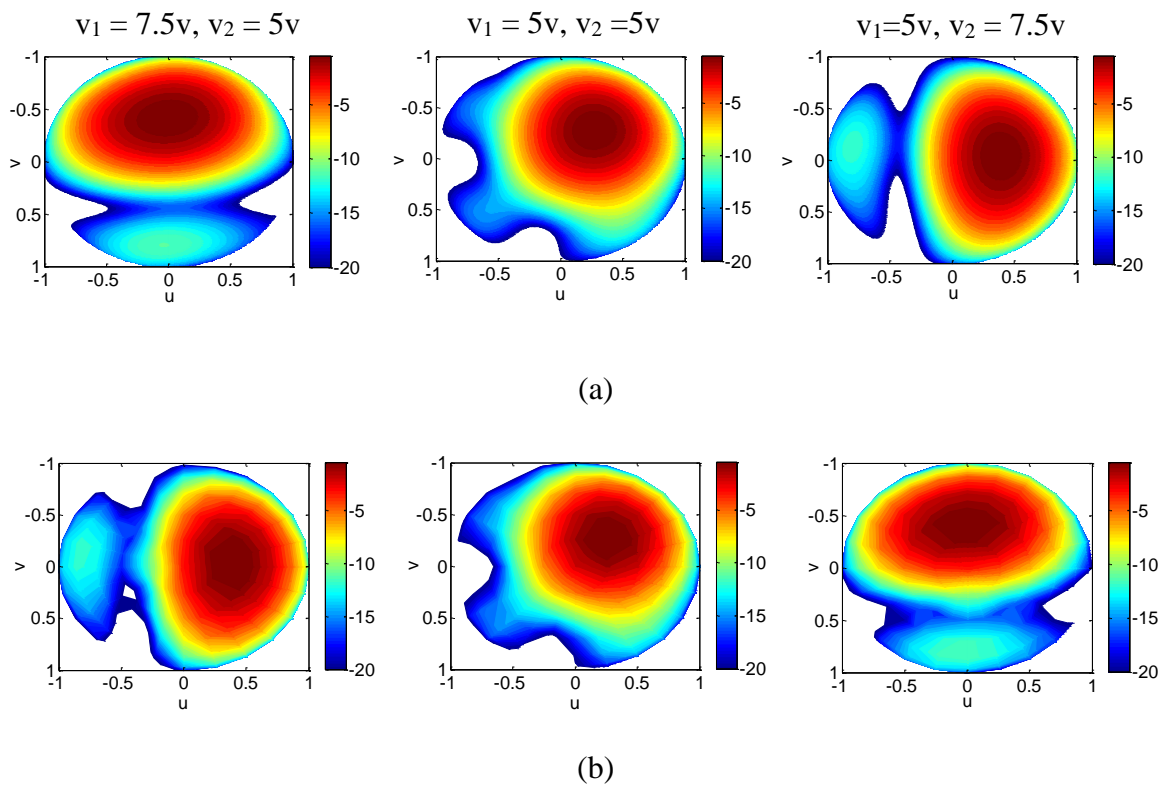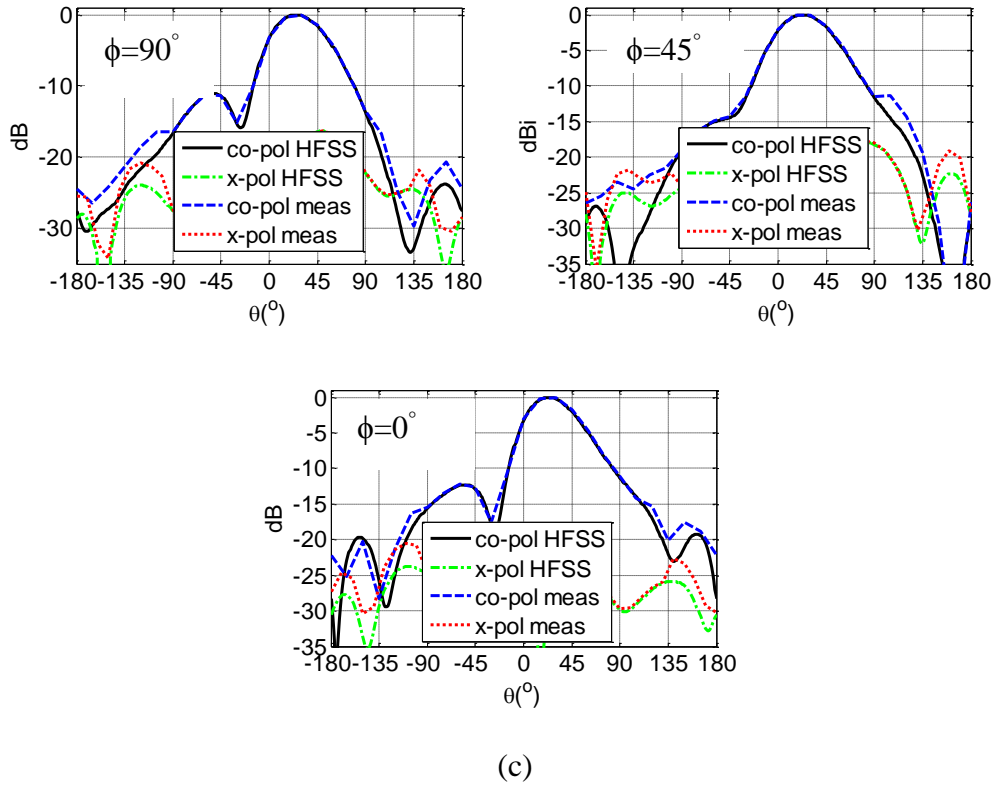
Figure 4-6. The simulated and measured projected co-pol 3D radiation patterns in the upper hemisphere of the proposed antenna at different biasing voltage along the *D, E, F* arc, as well as the corresponding plan cuts of maximum radiation: (a) simulated 3D; (b) measured 3D; (c) simulated and measured plane cuts.

$v_1 = 7.5v, v_2 = 7.5v$

(a)   (b)
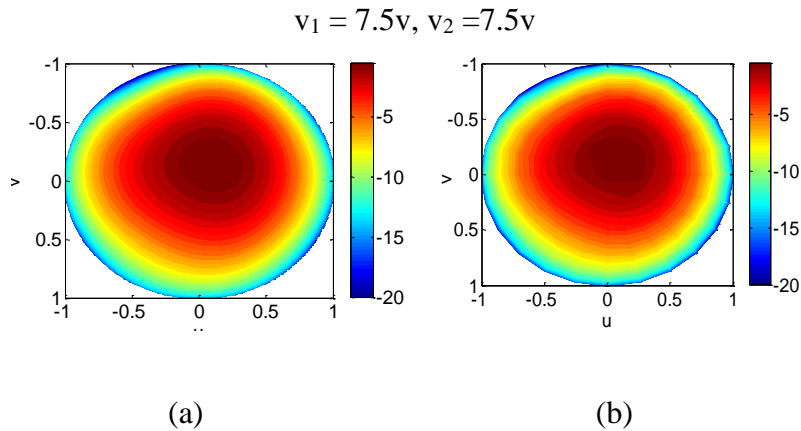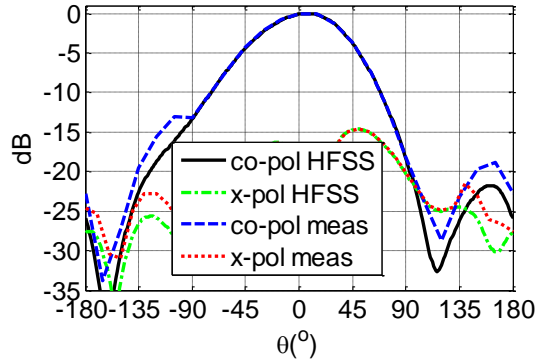
(c)

Figure 4-7. The simulated and measured projected co-pol 3D radiation pattern in the upper hemisphere space of the proposed antenna at the broadside direction (point G) along with the plan cut in yz plane with v1, v2 =7.5 volts: (a) simulated 3D pattern; (b) measured 3D pattern; (c) simulated and measured plane cut.

Table 4-IV. Antenna measured gain and efficiency at 2.5 GHz.

Cases	v_1(volt)	v_2 (volt)	Gain (dBi)	Efficiency (dB)	Efficiency (%)
A	7.5	3.5	8.37	-0.62	86.7
B	3.5	3.5	8.14	-0.82	82.7
C	3.5	7.5	8.29	-0.65	86
D	7.5	5	8.70	-0.54	88
E	5	5	8.95	-0.63	86.4
F	5	7.5	8.68	-0.55	88.1
G	7.5	7.5	8.1	-0.29	93
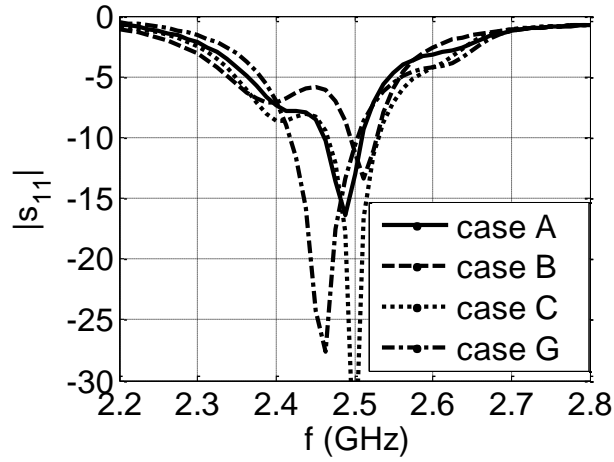
(a)
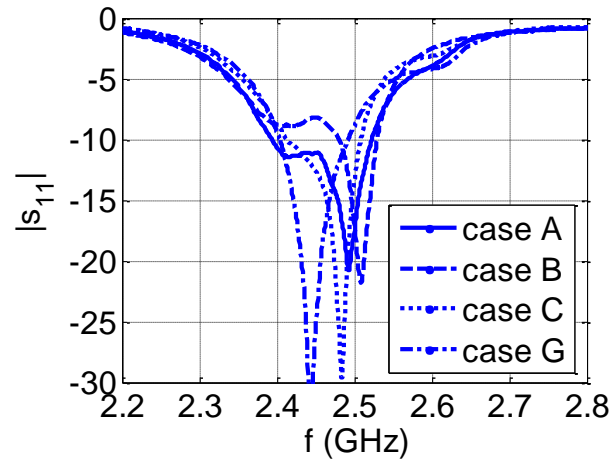
(b)

Figure 4-8. The simulated and measured results for the reflection coefficient of the proposed antenna at different cases of the scanned beam due to the corresponding voltage combination: (a) simulated; (b) measured.

The measured antenna gain, and efficiency along the scanning range are listed in Table 4-IV. The attained peak gain is 8.95 dBi with 0.8 variations across the tuning range. The corresponding efficiencies vary from -82% to 93 %. Case *C* has the least efficiency since it acquires highest coupling effect, and capacitance values among all cases. This lead to the

highest current excited on the parasitic patches that in turn go through the varactors and increase the I^2R losses.

The antenna reflection coefficient at different cases of the scanned beam due the biasing voltage combination is shown in Figure 4-8. Good correlation between the simulated and measured results is observed. The return loss for case *G* is very similar to the driven patch by itself alone, because the parasitic patches at that case are quite small and coupling is insignificant. For the other cases, *A*, *B*, and *C* the coupling is more significant, and hence a slight shift in the resonant frequency occurs, whereas other close resonant frequency is also introduced as observed from the curves. The refection coefficient magnitude ($|S_{11}|$) is less than -8 dB for all cases from 2.39 to 2.5 GHz. Although the antenna bandwidth is usually defined by certain threshold for the reflection coefficient (-10, -8, or -6 dB), it is limited by the stability of the beam scanning performance presented above. Indeed the beam scan angle shifts with frequency because as discussed in section II, the main beam direction depends on the electrical size of the parasitic patch, which is frequency dependent. Given that the proposed antenna beamwidth is larger than 40°, a 5° shift of the scan angle is quite acceptable and the antenna overall bandwidth could be defined accordingly. The 5° shift occurs within 2.425 to 2.475 GHz, and hence the achieved bandwidth for the proposed antenna design is about 2%.

4.4. Summary

A new design of a reconfigurable microstrip antenna with continuous 2-dimensional beam scanning patch has been proposed, using tunable size parasitic patches method. Electronic beam scanning is attained with the aid of varactors and proper biasing network integrated into the parasitic patch. The achieved scanning range is from 0° to 32°, 0° to 90° in the elevation and azimuth planes, respectively. The peak gain value is 8.5 dBi with less than 1 dB variation across the entire scanning range. The proposed antenna doesn't require feed

network, variable phase shifter, or attenuators as in phased arrays, making it simpler to implement and more cost effective. Vehicular satellite, and land mobile receiving system are one of the potential applications for the proposed antenna.

It is worthwhile to mention that using the parasitic patches in their reflective mode (C_1 and/or $C_2 < 1.5$ pF) along with their directive mode (C_1 and $C_2 > 1.5$ pF), could attain full azimuth beam scanning instead of only from $0°$ to $90°$. However, the radiation beam in the reflective mode has high SLL as discussed earlier in section 3.2, and shown in Figure 3-2a. Indeed, in some cases (combination of C_1 and/or $C_2 < 0.5$ pF) the SLL combines with the main lobe leading to a broad radiation beamwidth. This could be interesting for applications that require azimuth steering for specific plane cut (with broad beamwidth) of the beam, other than steering the radiation beam maximum (beam direction).

Meanwhile, full azimuthal beam steering could be allowed if two more parasitic patches with two varactors and their biasing assemblies are placed to the left and bottom of the driven patch as shown in Figure 4-9 . All the parasitic patches have same dimensions, and equidistant from the driven patch. The two added parasitic patches should be operated in the directive mode to avoid high SLL as discussed.
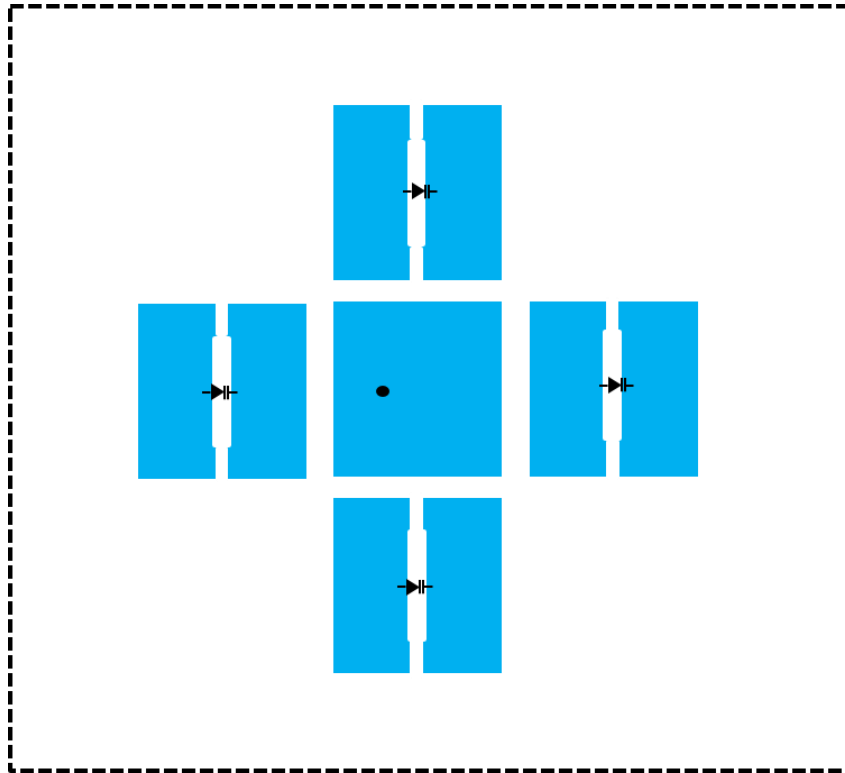
Figure 4-9. The suggested reconfigurable antenna with full azimuth scanning.

5. TUNABLE BEAMWIDTH MICROSTRIP ANTENNA

5.1. Introduction

Antenna terminals with dynamic control over their radiation beamwidth have been paid significant attention by the modern wireless network operators (e.g. Wi-Fi, UMTS) in the recent few years. The deployments of such antenna systems allow accommodating the dynamic behavior for the subscribers' number in certain spot without reducing the quality of service (link reliability, data rate, and traffic capacity) [1]. On the other hand, they are also beneficial for remote sensing from airborne surfaces and radar applications, where a radiation beam spot independent of the antenna altitude is desired. One direct method to enable this feature is to use an antenna array with full control on each element excitation magnitude and phase, using variable/switchable phase shifters, attenuators, amplifiers, etc. However, such solution is complex, and of high implementation cost for some application, such as indoor Wi-Fi antenna terminals that are very cost sensitive.

An array fed with a switchable network such that different numbers of elements are excited along the switching states, where the directivity (beamwidth) is controlled [54], could be a cheaper and simpler alternative. Other method uses a switchable parasitic ring surrounding a patch antenna to modify the excited surface waves' behavior, and hence changes the radiation beamwidth [55]. The designs in [54], and [55] however, don't provide continuous tuning of the beamwidth as they depend only on switching mechanisms. Recently, an electronic dynamic focusing for the antenna beam is proposed in [56], where a reconfigurable partial reflecting surface (PRS) is placed over the antenna to focus its radiation, depending on the PRS

74

reflectivity. Nevertheless it is of quite large volume, and with too many varactors, which increases the implementation cost, challenges the biasing circuits' integration, and limit its practicality for deployment.

In this chapter, a reconfigurable microstrip antenna with a tunable beamwidth feature is proposed. The method is based on the placement of two reconfigurable parasitic patches with tunable electrical size to the left and right of a probe-fed patch along the *H*-plane (xz). A varactor diode with a proper DC biasing network is added to each parasitic patch to allow for the tuning of its electrical size. Therefore, the effective aperture size of the entire antenna can be controlled and electronic tuning of the beamwidth is achieved by changing the applied DC voltage (capacitance value). Experimental measurements have been conducted on a fabricated antenna prototype to validate the proposed concept.
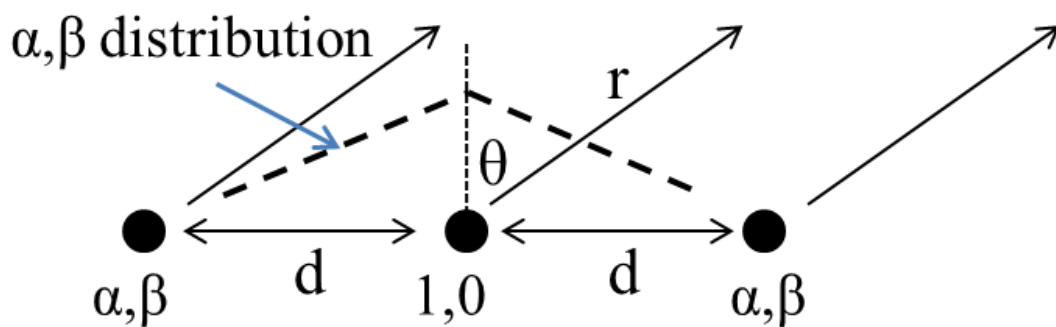
Figure 5-1. Three elements antenna array with even distribution for the excitation phase and magnitude around the center element.

5.2. Operational Principle

5.2.1. Three elements array with even magnitude and phase excitation

(a)

(b)   (c)
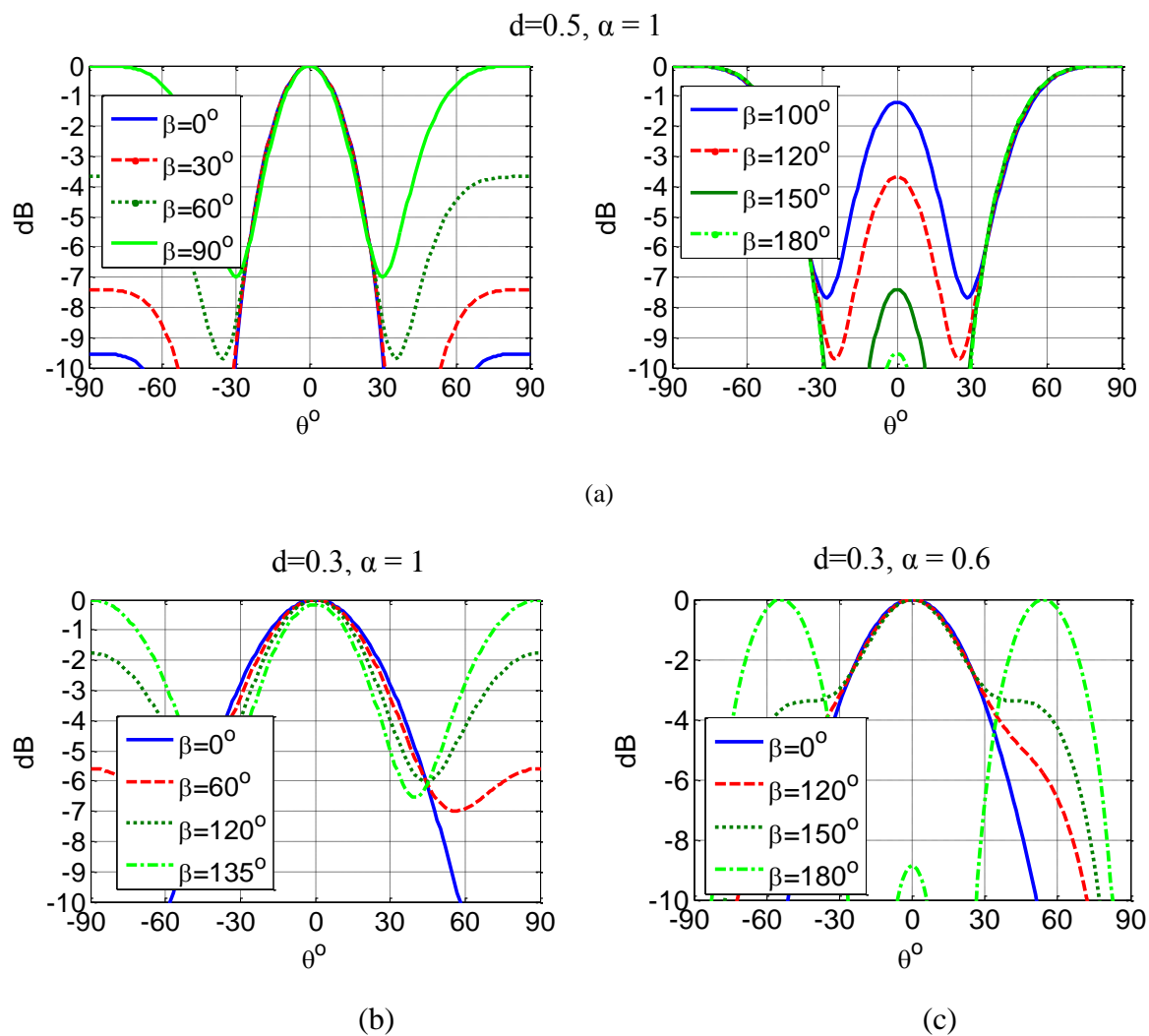
Figure 5-2. The computed total radiation pattern for three isotropic sources array with even distribution for different excitation magnitude α, and phase β at different separation distance d: (a) d = 0.5, α = 1; (b) d = 0.3, α = 1; (c) d = 0.3, α = 0.6.
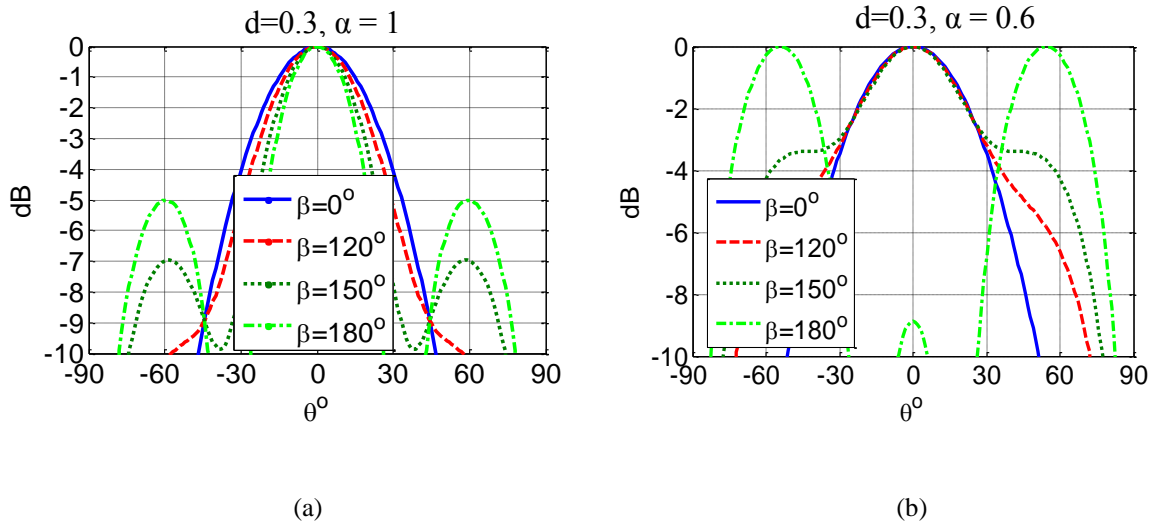
Figure 5-3. The computed total radiation pattern for an even array of three sources whose elements pattern is cosθ at different excitation magnitude α, and phase β.

Figure 5-1 shows an antenna array of three elements with even distribution for the excitation phase and magnitude around the center element. The distribution then is either uniform or triangular. The total radiation pattern of such array can be computed with the array theory through multiplying the array factor by the element factor, such that:

$$P(\theta) = f(\theta).\left(\alpha e^{j(-kd\sin\theta+\beta)} + 1 + \alpha e^{j(-kd\sin\theta+\beta)}\right) \tag{1}$$

where, α is the current ratio, β is the deferential phase (with respect to the center element), and $f(\theta)$ is the element pattern. The results at different parameters are shown in Figure 5-2a. As can be seen, at half wave length separation distance $d = \lambda/2$, with $\beta < 90°$, the 3dB beamwidth is unchanged, but the SLL at the end fire directions increases as β increases, till two grating lobes appears when $\beta = 90°$. With $\beta > 90°$, the end fire lobes continue to exist, but the bore sight lobe directivity decreases as β increases, which inspires the idea for a tunable beamwidth design.
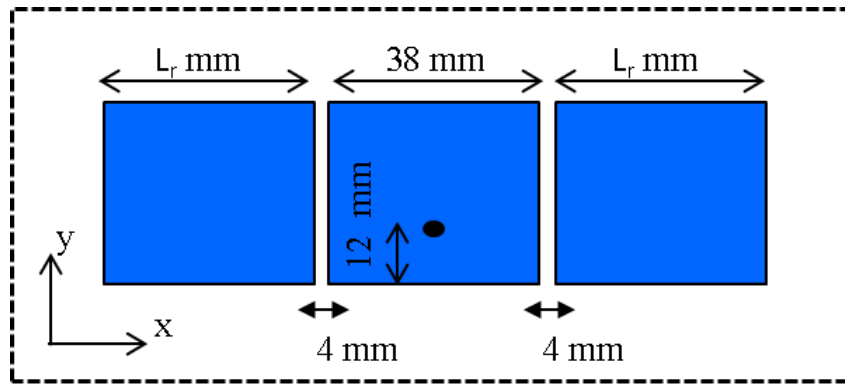
(a)
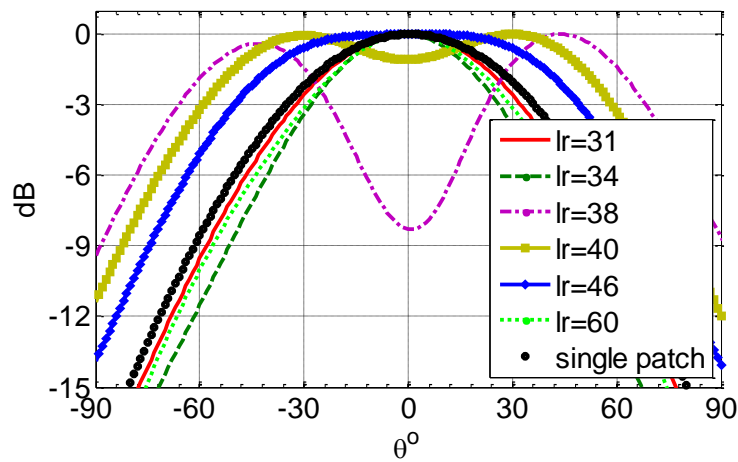
(b)

Figure 5-4. A probe-fed patch antenna with two parasitic patches along the xz plane (H-plane): (a) geometry; (b) radiation patterns in the xz plane at different sizes *Lr* (mm) of the parasitic patches at 2.45 GHz.

At a smaller separation distance $d = 0.3\lambda$, the 3dB beamwidth variation with β is more significant as shown in Figure 5-2b, where the grating lobes start to appear at $\beta = 133°$ instead of 90°. On the other hand, when $\alpha < 1$, the directivity (beamwidth) variation for the bore sight lobe becomes more pronounced, making α an additional parameter beside β for changing the beamwidth. Now if a *cos(θ)* element pattern is used as an element pattern in (1), the resulted patterns are shown in Figure 5-3. The beamwidth is similarly controlled by

changing the phase shift β, and current ratio α as expected, but the grating lobes are suppressed because of the element pattern. However, at some value for $\alpha < 1$, a difference beam could be obtained at high values of β close to 180°. The previous study inspires the idea for designing a tunable beamwidth antenna. It simply suggests simultaneous control for the magnitude and phase distributions in an array of tightly packed three directive antenna elements.

5.2.2. Antenna Topology

The antenna geometry shown in Figure 5-4a, consists of three square patches printed on a substrate of $\varepsilon_r = 2.2$, and thickness $h = 3.175$ mm. The center patch is excited with a probe feed, whereas the other patches are parasitic. The parasitic patches are of equal sizes. The substrate size is 200 x 100 mm, backed with a metallic ground plane of the same size. As the parasitic patches are placed closely to the driven patch, mutual coupling occurs and electric currents are induced on the surface of the parasitic patches [2]. Because of the symmetry, the induced currents on both parasitic patches are equal but with different magnitude and phase from the driven patch surface current. Consequently, the entire antenna geometry represents a three-element array discussed in the previous section, whose amplitude (α) and phase (β) distributions are symmetrically even around the center driven patch. The size of the parasitic patches (L_r) controls the coupling strength, which in turns defines the values of α, β distribution for the induced currents. The radiation pattern in the H-plane (xz) changes with L_r as shown in Figure 5-4b. These results are extracted through full wave simulation using HFSS [36]. As can be seen, when L_r is very small ($L_r \leq 31$ mm) the radiation beamwidth is similar to the driven patch by itself without the parasitic patches. This is due to the weak coupling, where no energy is captured by the parasitic patches and hence they don't contribute to the radiation. When L_r increases, the coupling becomes more

significant, and the beam becomes more directed. When L_r is close to the driven patch size (38 mm), unsurprisingly a difference beam exists. This agrees with the array theory analysis for a three-element array with an even α, and β distribution discussed in the previous section. The analysis depicts a difference beam at some α, and β values as shown in Fig. 3b. On the other hand, broader beamwidth is achieved when L_r becomes larger than 38 mm. Then it shrinks gradually with the increase of L_r and tends to approach the primary case at which the coupling is weak again.

5.3. Tunable Beamwidth Design

According to the above discussion, an electronic dynamic control over the radiation beam spot would be allowed, if a tuning mechanism for the parasitic patches size is introduced. Indeed a patch antenna with a capacitor loaded slot proposed in chapter 2 [50] effectively provides the fundamental mechanism for tuning its electrical size. The relation between the capacitance C versus the electrical size L_r is illustrated in chapter 3 [52]. Therefore, the parasitic patches in Figure 5-4a are replaced with such antenna, and the proposed reconfigurable antenna with a tunable radiation beamwidth is constructed as shown in Figure 5-5. The dimensions of all the patches are 38 x 38 mm, whereas the slot of each parasitic patch is 20 x 0.5 mm. Two varactors are placed on each slot along with their integrated biasing circuitry. The used varactor is MHV505-19-1 by *Aeroflex Metelic* [53] of capacitances $0.458 \leq C \leq 6.642$ pF with $20 > V_{DC} > 0$V DC reverse biasing voltage as shown in Figure 5-6. To avoid DC shortage, each parasitic patch is divided at its center into two parts by narrow slits of 0.2 mm width. Two 68 nF *murata* capacitors of package size 0603 are placed on each slit for RF continuity. For the RF/DC isolation, the top part of each parasitic patch is fed with a DC signal through a resistive thin film as RF choke printed over the substrate as shown in the Figure 5-5. The bottom part of the parasitic patch is also grounded using the same method. The resistive lines are implemented
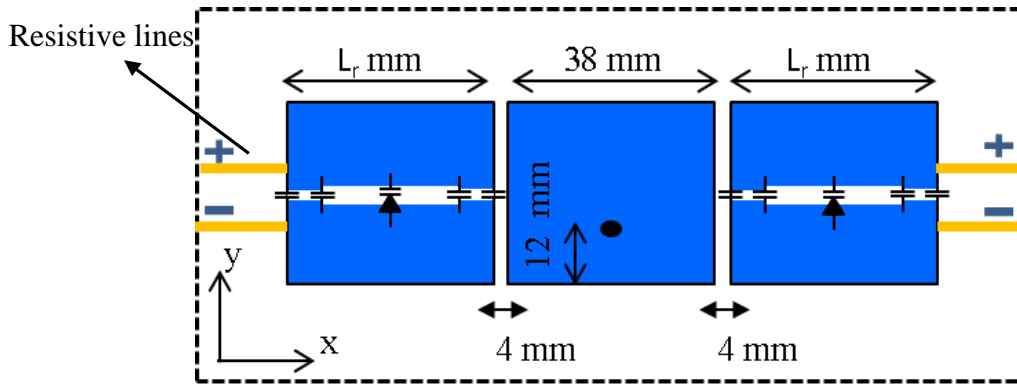
Figure 5-5. The geometry of the proposed reconfigurable antenna with an electronic tunable radiation beamwidth along with the biasing assemblies.
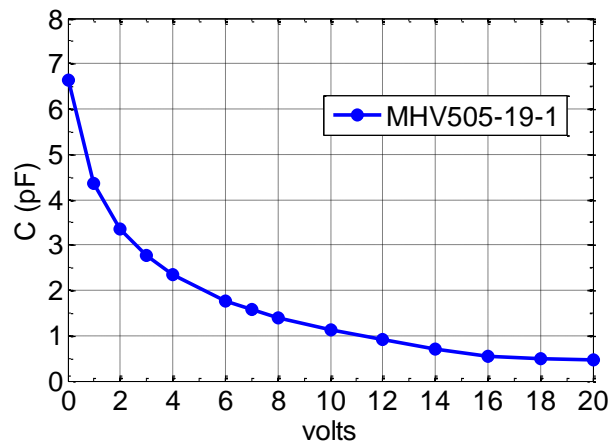
Figure 5-6. The capacitance values vs. the reverse biasing voltage of the MHV505-19-1 varactor by *Aeroflex Metelics* generated from the data provided by the manufacturer [53].

Figure 5-7. A photo for the proposed antenna fabricated prototype.

using conductive graphite isopropanol base material [57], which has been recently proven to be effective, and simpler to implement for RF circuits design [57]. Both varactors are biased simultaneously, hence one DC control signal is required for the entire antenna. The change in the applied biasing voltage (capacitance value) allows for tuning the parasitic patches electrical size, hence the radiation beamwidth. A photo for the fabricated antenna prototype is shown in Figure 5-7.

(a)

(b)
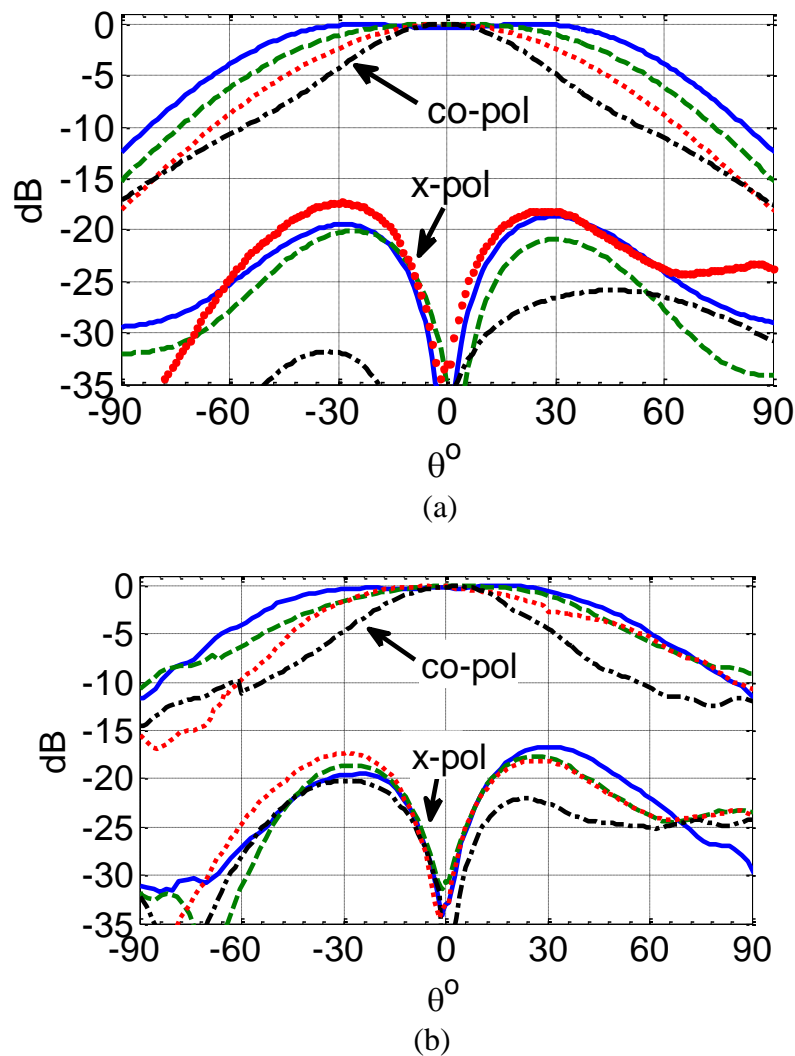
Figure 5-8. The simulation and measured radiation patterns in the xz plane for the proposed antenna at 2.475 GHz. Solid line (17V), dashed line (11V, 3°), dotted line (7.5V), dashed-dotted line (5V): (a) simulation; (b) measured.
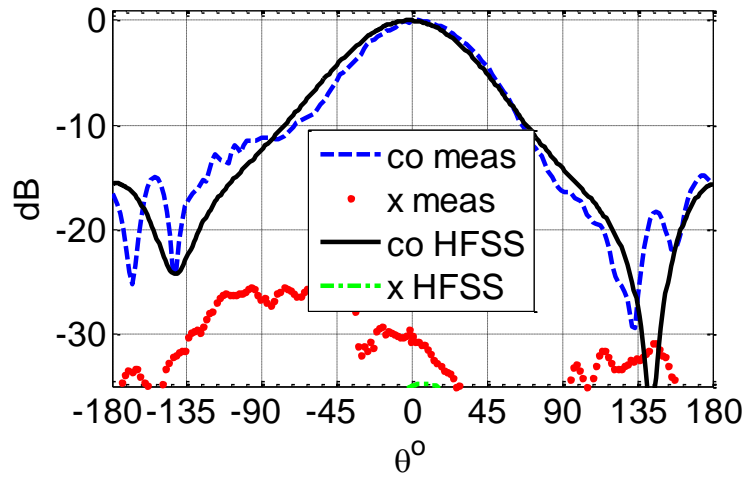
Figure 5-9. The simulation and measured radiation pattern in the yz plane for the proposed antenna with a biasing voltage of 11 volt.
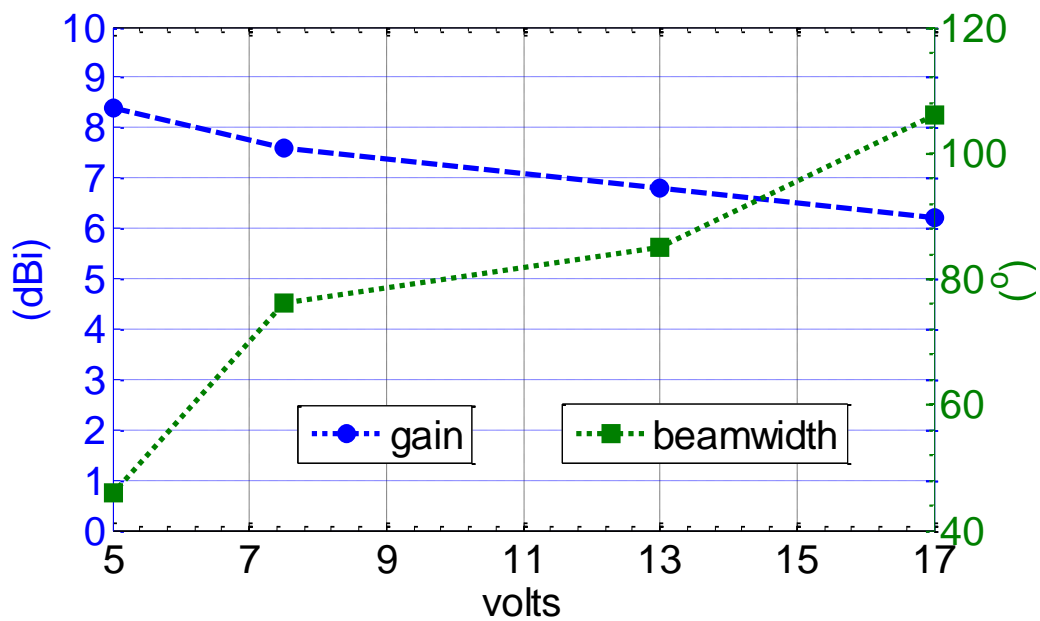
Figure 5-10. The measured gain and beamwidth of the proposed antenna along the different biasing voltage.

The simulation and measured results for the antenna upper half radiation patterns in the xz plane (H-plane) at different biasing voltages (capacitance value) are shown in Figure 5-8. Good agreement between simulated and measured results is observed. From the figure the

beamwidth changes from 48° to 108° by changing the applied voltage from 5 to 17 volts. The cross polarization level is below -15 dB within the 3dB beamwidth along the tuning range. The upper half radiation pattern (-90° to 90°) is only presented in the figures to be more clear, given that the back radiations are larger than 10 dB below the peak at the broadside direction. On the other hand, the radiation patterns in the yz plane (E-plane) along different biasing voltages are not changed, because the effective antenna aperture in such plane is not altered by changing the parasitic patch size. Indeed, the patterns are similar to the pattern of a single patch. For brevity, the pattern in the yz plane at 11v is selected to be presented in Figure 5-9.

The measured realized gain, and beamwidth of the proposed antenna along the tuning range are shown in Figure 5-10. The realized gain decreases from 8.4 to 6.2 dBi as the voltage increases from 5 to 17 Volts. The gain results are in correlation with the voltage-beamwidth relation previously discussed and shown in Figure 5-8. The efficiency of the proposed antenna has been also estimated along the tuning voltages using the measured realized gain and the simulated directivity, and found to be varying from 79% to 86% as the voltage increases. This variation is due to the inherent I^2R losses of the varactors variation, which is a voltage dependent (losses decreases as voltage increases) [24]. Better efficiency especially at low biasing voltage could be attained if higher quality varactors are used. Newly emerged technologies are needed to enable higher quality varactors.

The reflection coefficient for the antenna at different voltages is shown in Figure 5-11. Slight discrepancies are observed between the simulation and measured results. The discrepancies are thought to be mainly due to the resistive lines, which is not included in the simulation and the uncertain defects in the fabricated prototype that add additional errors. The reflection coefficient, as can be seen from the figures, is equal or below -10 dB at 2.45 GHz. The antenna bandwidth is usually defined by the return loss -10 or -8 dB level, however the
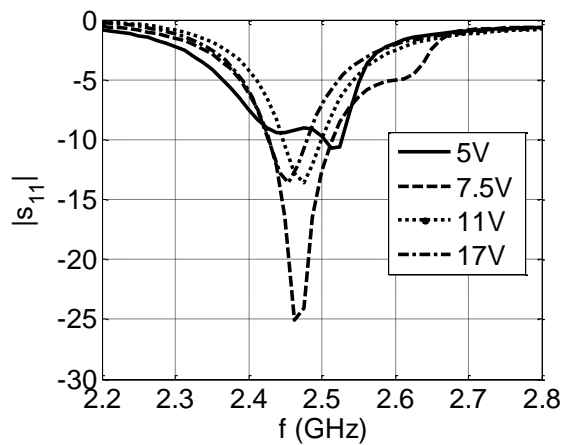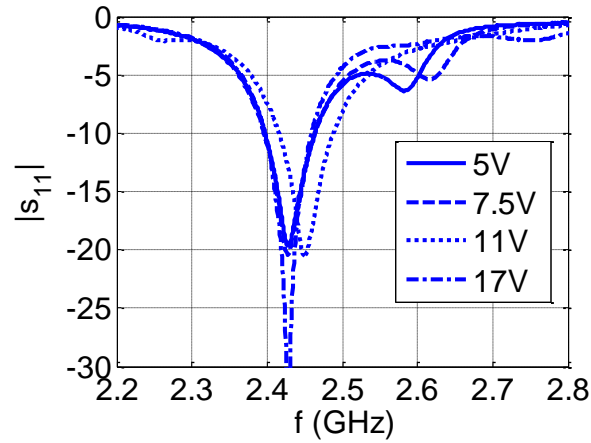
Figure 5-11. The reflection coefficient for the proposed antenna at different biasing voltages: (a) measured; (b) simulated.

frequency dependency for the antenna radiation specifications including beamwidth impose other bandwidth limitation. It is found that antenna radiation performance is maintained within 2.41- 2.46 GHz (2%).

5.4. Summary

A new type of a reconfigurable microstrip antenna with tunable radiation beamwidth is proposed. The design methodology is to modify the antenna effective aperture through tunable size parasitic patches using a novel tuning mechanism. Two varactors with simple integrated

biasing are used as tuning devices. The achieved beamwidth tuning range is from 48° to 108° in the H-plane. The required capacitance range is from 0.5 pF to 2 pF. Within the tuning range, the antenna gain changes from 6.2 to 7.2 dBi, whereas the efficiency varies from 60% to 86%. A better efficiency could be obtained with advanced enabled technologies for variable capacitor devices of higher quality factors. The proposed antenna is compact and simple to implement compared to array with full control over excitation magnitude and phase.

In a similar fashion, the radiation beamwidth in the E-plane, could be enabled with two parasitic patches of reconfigurable size placed along the E-plane. However, careful consideration should be taken because of the asymmetry existence due to the probe feed in that plane. Studying the performance of this case is left for future research work.

6. CONCLUSION AND FUTURE WORK

6.1 Conclusions

The dissertation investigated, and addressed the design, analysis, implementation, and measurements for pattern reconfigurable microstrip antennas with tunable radiation characteristics. Such antenna system can continuously tune its radiation specification, such as beam direction, beam width, etc., in real time. A new methodology to achieve this capability has been first introduced, which is the reconfigurable parasitic elements of tunable electric size, then it is used and applied to devise several novel antenna designs, each with different tunable beam feature.

The first chapter surveyed different designs of pattern reconfigurable antennas using two methods: *parasitic elements*; and *non-parasitic elements*. An illustration for the difference between the two methods, and how the first one is more practical and amenable to achieve tunable radiation characteristics exists. An overview for the dissertation in form of flow chart is also presented.

The second chapter proposes a new configuration for a microstrip antenna, which is a patch with a varactor/capacitor loaded slot at its center. Such configuration has been analyzed with circuit model, and it suggests a new approach for dual-band design using lumped capacitor. A dual-band operation with tunable frequency ratio using one varactor is also showed to be feasible. The antenna exhibits frequency ratio tuning from 1.45 to 1.93 with capacitance ranges from 0.31 to 0.74 pF. The gain at the lower band is 7dBi with 88% efficiency, whereas

at the higher band is 4.92 dBi (average), with 69% (average) efficiency along the tuning range. The proposed antenna provides higher gain values than its PIFA, and slot antenna counterpart designs. Stationary antenna terminals in wireless networks with enabled software defined radio, is one of the potential application for the proposed antenna. Because frequency agility provides the fundamental mechanism for controlling the electrical size, the proposed antenna could be seen as a tunable size patch antenna, whose electrical size is effectively allowed to be electronically adjusted using one varactor diode. The relation between the patch electrical sizes versus varactor capacitance value is concluded

In Chapter 3, CP beam scanning antenna is offered. The concept of using a reconfigurable parasitic element of tunable electrical size to attain CP beam scanning is introduced and validated. The proposed antenna is a microstrip Yagi-Uda antenna with two elements. The first element is a square patch driven with two probe feeds of quadrature phase for CP excitation. The second element is a parasitic square patch with a narrow square-shaped slot carved on its surface. This parasitic patch is a modified version of the one discussed in chapter two to support CP operation. The parasitic patch is adjacent to the driven patch with a small separation distance (4 mm). Four varactor diodes are placed on the middle of each side of the square slot to facilitate tuning of its electrical size. The parasitic patch electrical size is allowed to be effectively tuned by varying the applied reverse DC biasing voltage to the varactors (capacitance value). The CP beam direction is scanned from -36° to 32° with gain variation from 5.7 to 8.2 dBic, and efficiency from 54% to 75.58% along the scanning range. The required capacitance range is from 0.458 to 6.642 pF.

In chapter 4, continuous two-dimensional beam scanning antenna is proposed exploiting the same methodology but with two reconfigurable parasitic patches of tunable electric size, each is controlled independently. The proposed antenna consists of two orthogonal crossed Yagi-Uda antenna configuration. The driven element is a square patch

excited with a probe coaxial feed. The other two parasitic patches are closely placed along the *E & H* planes of the driven patch. Each parasitic patch has a narrow rectangular slit at its center, where a varactor diode is placed to allow for tuning its electrical size. The beam direction is permitted to be scanned in both the elevation and azimuth planes. The achieved scan range in the elevation plane is from 0° to 32°, whereas in azimuth plan is from 0° to 90°, with capacitance ranges from 1.5 to 2.5 pF. Matching the effective parasitic patches size to the corresponding beam direction is also presented in details. Along the scanning range, the attained gain changes from 8.1 to 8.9 dBi, and efficiency changes from 86% to 93%. The beam-scanning antennas in chapter 3, and 4 are candidates for satellite communication, remote sensing, and terminal tracking receiver systems.

In chapter 5, a microstrip antenna, with a dynamic control over the radiation beam focusing (tunable beamwidth) is proposed, where two adjustable size parasitic patches are used in a different fashion to acquire this feature. The antenna consists of a square patch excited by a coaxial probe feed, and other two square parasitic patches placed on both sides of the driven along its H-plane. Each parasitic patch has a narrow slit at its center loaded with lumped varactor diode to tune its electrical size. Upon changing the parasitic patches size, the antenna effective aperture is altered, and hence the beamwidth in the H-plane is controlled. An analysis with array theory is used to predict and estimate the acquired beam shapes. The achieved beamwidth tuning range is from 52° to 108°, whereas the gain changes from 6.5 to 8.1 dBi. The proposed antenna with dynamic zooming (focusing) capability is potential for wireless networks infrastructure to accommodate more efficiently their dynamic traffic demand. It is also beneficial for remote sensing from airborne surfaces. The implementation of the proposed antenna is simple, low cost, and compact.

A flow chart summarizing the dissertation conclusion is shown in Figure 6-1.
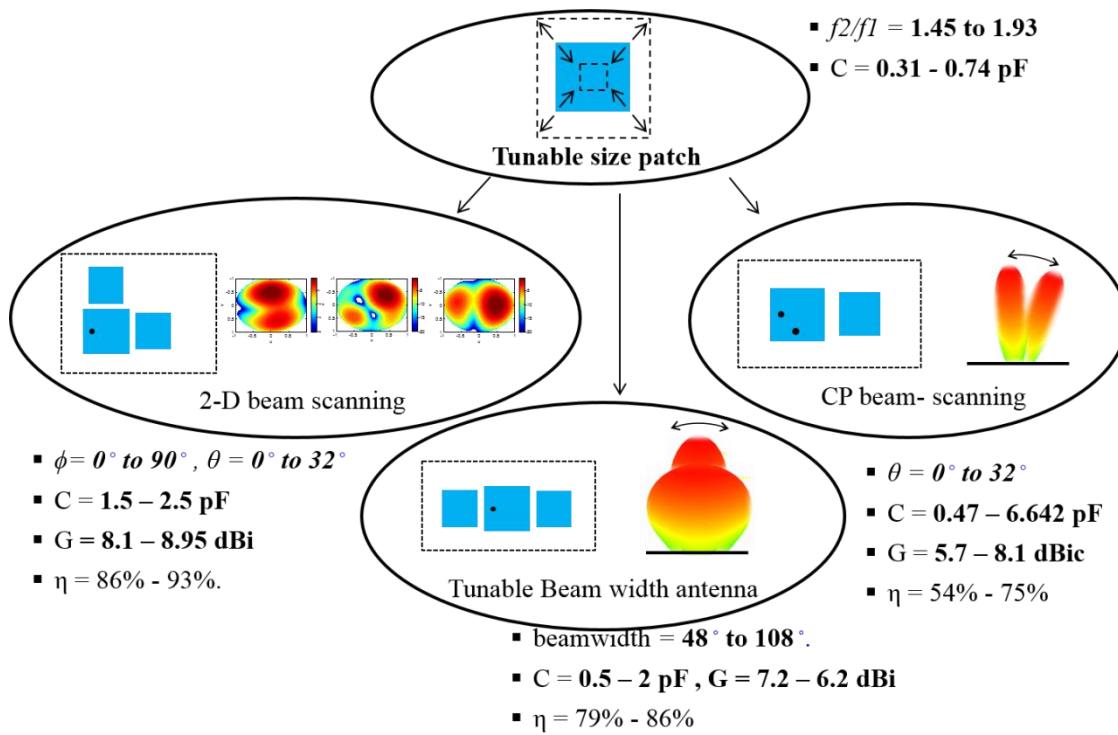
Figure 6-1. A flow chart summary for the dissertation conclusion.

6.2 Future Work

After all, more investigations and future research work are still required for the dynamic control over some, or combinations of the radiation beam specifications, for example:

- The beam scanning in azimuth plane from 0° to 360° with smaller size antenna solution.

- The antenna beamwidth to be tunable in both the *E* and *H* - planes, other than *H*-plane only.

- The down tilt angle of a conical (monopole-like) beam antenna, which would be much desired for wireless access points to change its cell coverage size, and hence adapt with the dynamic changes in traffic demand.

- Omni-to-directional beam antenna, with the ability to steer the beam direction, and control beamwidth. Such antenna would be attractive for stationary terminals in MIMO system, where uncorrelated multi-radio streams are required at the client equipment. An example for a scenario where such antenna system is required is as follows: an omni pattern is

desired for broadcast messages to all the clients. Directional pattern is desired during the communication with specific client(s), because it reduces interference and provide higher gain, and hence better SNR, or SNIR. On the other hand, steering the multiple beam directions (in MIMO case) could improves de-correlation between the radio streams, and hence higher throughput. Finally, the beam width as an additional parameter would enhance the overall performance.

BIBLIOGRAPHY

[1]   "MIMO and Smart antennas for Mobile Broadband Systems.", 4G Americas, October 2012. www.4gamericas.com

[2]   J. Huang and A. C. Densmore, "Microstrip Yagi Array Antenna for Mobile Satellite Vehicle Application," *IEEE Trans. Ant. Propag*., vol. 39, no. 7, pp. 1024–1030, 1991.

[3]   S. Zhang, G. Huff, J. Feng, and J. Bernhard, "A Pattern Reconfigurable Microstrip Parasitic Array," *IEEE Trans. Ant. propag*., vol. 52, no. 10, pp. 2773-2776, October, 2004.

[4]   X. Yang, B. Wang, W. Wu, and S. Xiao, "Yagi Patch Antenna with Dual-Band and Pattern Reconfigurable Characteristics," *IEEE Ant. Wireless Propag. Lett*., vol. 6, pp. 168-171, 2007.

[5]   X. Yang, B. Wang, S. Yeung, Q. Xue, and K. Man, "Circularly Polarized Reconfigurable Crossed-Yagi Patch Antenna," *IEEE Ant. Propag Mag.*, vol. 53, no. 5, pp. 65-80, October 2011.

[6]   Lijun Zhang, Fan Yang, and Atef Z. Elsherbeni, "Analysis and Design of a Reconfigurable Dual-Strip Scanning Antenna," *IEEE AP-S Int. Antenna and Propag. Symp. Digest,* 2009.

[7]   R. L. Li, V. F. Fusco, and R. Cahill, "Pattern Shaping Using a Reactively Loaded Wire Loop Antenna," *IEE Proc. Microw., Antennas Propag.*, vol. 148, pp. 203–208, Jun. 2008.

[8]   C. Jung, M. Lee, G. Li, and F. Flaviis, "Reconfigurable Scan-Beam Single-Arm Spiral Antenna Integrated with RF-MEMs Switches," *IEEE Trans. Ant. Propag.*, vol. 54, no. 2, pp. 455–463, Feb. 2006.

[9]   J. Sarrazin, Y. Mahé, S. Avrillon, and S. Toutain, "Pattern Reconfigurable Cubic Antenna," *IEEE Trans. Ant. Propag.*, vol. 57, no. 2, pp. 310–317, Feb. 2009.

[10]   S. Nikolaou, R. Bairavasubramanian, C. Lugo, I. Carrasquillo, D. Thompson, G. Ponchak, J. Papapolymerou, and M. Tentzeris, " Pattern and Frequency Reconfigurable Annular Slot Antenna Using PIN Diodes," *IEEE Trans. Ant. Propag.*, vol. 54, no. 2, February 2006.

[11]   S. Maci, B. B. Gentili, P. Piazzesi, and C. Salvador, "Dual Band Slot-Loaded Patch Antenna," *IEEE Ant. Propag. Mag.,* vol. 39, no. 6, pp. 13-20, Dec. 1997.

[12]   K. B. Hsieh and K. Wong, "Inset Microstrip-Line-Fed Dual-Frequency Circular Microstrip Antenna and Its Application to a Two-Element Dual-Frequency Microstrip Array," *IEEE Microw. Antennas Propag. Symp. digest,* vol. 147, pp. 359–361, Oct. 1999.

[13]   S. T. Fang and K. L. Wong, "A Dual Frequency Equilateral Triangular Microstrip Antenna with a Pair of Two Narrow Slots," *Microw. Opt. Technol. Lett.,* vol. 23, pp. 82–84, Oct. 1999.

[14]   D. Lorens, P. Otero, and C. C. Penalosa, "Dual-Band, Single CPW Port, Planar Slot Antenna," *IEEE Int. Antennas and Propagation Symp. Digest.,* pp. 137–139, 2003

[15]   C. Wang, J. Lee, and R. Huang, "Experimental Studies of a Miniaturized CPW-fed Slot Antenna with The Dual-Frequency Operation," *IEEE Ant. Wireless Propag. Lett.,* vol. 2, pp. 151–154, 2003.

[16]   T. Morioka, S. Araki, and K. Hirasawa, "Slot Antenna with Parasitic Element for Dual Band Operation," *IET Electron. Lett.,* vol. 33, pp. 2093–20 944, December 1997.

[17]   K. Virga and Y. Rahmat-Samii, "Low-Profile Enhanced-Bandwidth PIFA Antennas for Wireless Communications Packaging," *IEEE Trans. Microw. Theory Tech.*, vol. 45, no. 10, pp. 1879–1888, Oct. 1997.

[18]   K. L. Wong, *Compact and Broadband Microstrip Antennas*, New York: Wiley, 2002.

[19]   K. P. Ray and Girish Kumar, "Tuneable and Dual-Band Circular Microstrip Antenna with Stubs." *IEEE Trans. Ant. Propag.*, vol. 48, no. 7, July 2000.

[20]   Y. Tawk, J. Costantine, K. Avery, and C. G. Christodoulou, "Implementation of a Cognitive Radio Front-End Using Rotatable Controlled Reconfigurable Antennas', *IEEE Trans. Antennas Propag.*, vol. 59, no. 5, pp. 1773–1778, May 2011.

[21]   D. Schaubert, F. Farrar, A. Sindoris, and S. Hayes, "Microstrip Antennas with Frequency Agility and Polarization Diversity", *IEEE Trans. Ant. Propag.*, vol. 29, no. 1, pp. 118-123, Jan. 1981

[22]   P. Bhartia and I. J. Bahl, "Frequency Agile Microstrip Antennas," *Microw. J.*, pp. 67–70, Oct. 1982.

[23]   F. Yang, Y. Rahamt-Samii, "Patch Antennas with Switchable Slots (PASS) in Wireless Communications: Concepts, Designs, and Applications," *IEEE Ant. Propag. Mag.,* vol 47, no. 2, pp. 13-29, April 2005.

[24]   S. Hum, and H. Xiong, "Analysis and Design of a Differentially-Fed Frequency Agile Microstrip Patch Antenna," *IEEE Trans. Ant. propag.,* vol. 58, no. 10, pp. 3122-3130, Oct. 2010.

[25]   P. Panayi, M. Al-Nuaimi, and I. Ivrissimtzis, "Tuning Techniques for Planar Inverted-F Antenna," *Electron. Lett.*, vol. 37, no. 16, pp. 1003–1004, Aug. 2001.

[26]   A. Sheta and S. Mahmoud, "A Widely Tunable Compact Patch Antenna," *IEEE Antennas Wireless Propag. Lett.*, vol. 7, pp. 40–42, 2008.

[27]   V. A. Nguyen, R. A. Bhatti, and S. O. Park, "A Simple PIFA-Based Tunable Internal Antenna for Personal Communication Handsets," *IEEE Antennas Wireless Propag. Lett.*, vol. 7, pp. 130–133, 2008.

[28]   A. Sheta and M. Alkanhal, "Compact Dual-Band Tunable Microstrip Antenna for Gsm/DCS-1800 Applications," *IET Proc. Microw. Ant. Propag.*, vol. 2, no. 3, pp. 274–280, Apr. 2008.

[29]   S.-K. Oh, H.-S. Yoon, and S.-O. Park, "A PIFA-Type Varactor-Tunable Slim Antenna with A PIL Patch Feed for Multiband Applications," *IEEE Antennas Wireless Propag. Lett.*, vol. 6, pp. 103–105, 2007.

[30]   N. Karmakar, "Shorting Strap Tunable Stacked Patch PIFA," *IEEE Trans. Ant. Propag.*, vol. 52, no. 11, pp. 2877–2884, Nov. 2004.

[31]   A. Mak, C. Rowell, R. Murch, and C. Mak, "Reconfigurable Multiband Antenna Designs for Wireless Communication Devices," *IEEE Trans. Ant. Propag.*, vol. 55, no. 7, pp. 1919–1928, July 2007.

[32]   M. Komulainen, M. Berg, H. Jantunen, E. Salonen, and C. Free, "A Frequency Tuning Method for a Planar Inverted-F Antenna," *IEEE Trans. Ant. Propag.*, vol. 56, no. 4, pp. 944–950, Apr. 2008.

[33]   N. Behdad and K. Sarabandi, "A Varactor Tuned Dual-Band Slot Antenna," *IEEE Trans. Antennas Propag.,* vol. 54, no. 2, pp. 401–408, Feb. 2006.

[34]   N. Behdad and K. Sarabandi, "Dual-Band Reconifgurable Antenna with a Very Wide Tunable Range," *IEEE Trans. Antennas Propag.,* vol. 54, no. 2, pp. 409–416, Feb. 2006.

[35]   W. J. R. Hoefer, ''Equivalent Series Inductance of a Narrow Transverse Slit in Microstrip,'' *IEEE Trans. Microwave Theory Tech.*, vol. 25, no. 10, pp. 822-824, Oct. 1977.

[36]   High Frequency Structure Simulation (HFSS), Version 13, Ansoft Corp. Canonsburg, PA, 2010.

[37]   K. Carver and J. Mink, "Microstrip Antenna Technology," *IEEE Trans. Antennas Propag.*, vol. 29, no. 1, pp. 2–24, 1981.

[38]   K. Gupta, R. Garg, I. Bahl, P. Bhartia, *Microstrip Lines and Slotlines*, 2nd ed, MA: Artech House, 1996.

[39]   X. Zhang, F. Yang, "Study of a Slit Cut on a Microstrip Antenna and Its Applications," Microw. Opt. Technol. Lett., vol 18, no. 4, pp. 297-300, July 1998.

[40]   Data sheet of Skyworks varactor diodes SMV1405-SMV1430 Series: Plastic Packaged Abrupt Junction Tuning Varactors

[41]   L. J. Chu, "Physical Limitations on Omni-Directional Antennas," *J. Appl. Phys.*, vol. 19, pp. 1163–1175, Dec. 1948.

[42]   P. F. Wahid, M. A. Ali, and B. C. DeLoach, "A Reconfigurable Yagi Antenna for Wireless Communications," *Microw. Opt. Tech. Lett.*, vol. 38, no. 2, pp. 140–141, July 2003.

[43]   K. J. Vinoy, K. A. Jose, V. K. Varadan, and V. V. Varadan, "Hilbert Curve Fractal Antennas with Reconfigurable Characteristics," in Proc. *IEEE MTT-S Int. Microw. Symp. Digest*, vol. 1, 2001, pp. 381–384..

[44]   G. H. Huff and J. T. Bernhard, "Integration of Packaged RF-MEMS Switches with Radiation Pattern Reconfigurable Square Spiral Microstrip Antennas," *IEEE Trans. Ant. Propag.*, vol. 54, no. 2, pp. 464–469, Feb. 2006.

[45]   S. Chen, J. Row, and K. Wong, "Reconfigurable Square-Ring Patch Antenna with Pattern Diversity," *IEEE Trans. Ant. Propag.*, vol. 55, no. 2, pp. 472–475, Feb. 2007.

[46]   S. Wu and T. Ma, "A Wideband Slotted Bow-Tie Antenna with Reconfigurable CPW-to-Slot line Transition for Pattern Diversity," *IEEE Trans. Antennas Propag.*, vol. 56, no. 2, pp. 327–334, Feb. 2008.

[47] C. A. Balanis, Antenna Theory Analysis and Design, 2nd ed. Hoboken, NJ: Wiley-Interscience, p. 814, 2005.

[48] N. Fayyaz, S. Safavi-Naeini, E. Shin, and N. Hodjat, "A novel electronically tunable rectangular patch antenna with one octave bandwidth," *Proc. IEEE Canadian Conf. on Electrical and Computer Engineering*, May 1998, vol. 1, pp. 29–31.

[49] S. Hum, M. Okoniewski, and R. Davies, "Modeling and Design of Electronically Tunable Reflectarrays," *IEEE Trans. Ant. Propag.*, vol 55, no. 8, pp. 2200-2210, August 2007.

[50] A. Khidre, Xiao Liu, F. Yang, and A. Z. Elsherbeni, "Reconfigurable Dual-Band Patch Antenna with a Varactor-Loaded Slot" *IEEE AP-S Int. Antenna and Propag. Symp. Digest,* July 2012.

[51] A. Khidre, F. Yang, and A. Z. Elsherbeni, "A Patch Antenna with A Varactor-Loaded Slot for Reconfigurable Dual-Band Operation," *IEEE Trans. Ant. Propag.* 2013. (under review).

[52] A. Khidre, F. Yang, and A. Z. Elsherbeni, "Reconfigurable Microstrip Yagi-Uda Antenna with a Scannable Circularly Polarized Beam," *IEEE AP-S Int. Antenna and Propag. Symp. Digest*, July 2012.

[53] Data sheet of *Aeroflex Metelics* varactor diodes MHV505-19-1 Series: Hyper Abrupt Tuning Diode, Microwave. www.aeroflex.com

[54] O. Lafond, M. Caillet, B. Fuchs and M. Himdi, *Microwave and Millimeter Wave Technologies Modern UWB antennas and equipmen*t, Intech, 2010, p. 129.

[55] K. Lee, R Rojas, and N. Surittikul, "A Pattern-Reconifgurable Microstrip Antenna Element," *Micro. and Optical Tech. Lett*., vol. 48, no. 6, pp.1117-1119, June 2006.

[56]   T. Debogovic, J. carrier, and J. Bartolic, "Partially Reflective Surface Antenna With dynamic Beamwidth control," *IEEE Ant. Wireless. Propag.Lett..,* vol. 9, pp. 1157-1161, 2010.

[57]   Ted Pella, Inc., Redding, CA, "Technical notes, PELCO conductive graphite isopropanol based," 2009 [Online]. Available: http://www.tedpella.com

[58]   J. Kovitz, H Rajajopalan, Y. Rahmat-Sami, "Practical and Cost-Effective Bias Line Implementations for Reconfigurable Antennas," *IEEE Anennas Wireless Propag. Lett.,* vol. 6, pp. 1552-1555, 2012.

[59]   C. A. Balanis, *Antenna Theory Analysis and Design*, 2nd ed. Hoboken, NJ: Wiley-Interscience, p. 283, 2005.

[60]   P. Jarske, T. Sramaki, S. K. Mitra, and Y. Neuvo, "On the properties and design of nonuniformly spaced linear arrays," *IEEE Trans. Acoust., Speech, Signal Process.*, vol. 36, no. 3, pp. 372–380, Mar. 1988.

[61]   V. Murino, A. Trucco, and C. S. Regazzoni, "Synthesis of unequally spaced arrays by simulated annealing," *IEEE Trans. Signal Process.*, vol. 44, no. 1, pp. 119–123, Jan. 1996.

[62]   T. L. Roach and J. T. Bernhard, "Investigation of Sidelobe Level Performance in Phased Arrays with Reconfigurable Elements", in *IEEE AP-S Int. Antenna and Propag. Symp. Digest*, pp. 403-406, 2006.

[63]   S. Zhang and J. T. Bernhard, "Performance Study of a reconfigurable microstrip parasitic array (RMPA) Phased Array," *IEEE AP-S Int. Antenna and Popag. Symp. Digest*, pp. 403-406, 2006.

[64]   S.Xiao, Y. Y. Bai, B. Z. Wang, and S. Gao, "Scan Angle Extension By Array With Pattern Reconfigurable Elements," *Applied Computational Electromagnetics Society (ACES) Journal*, vol. 24, no. 5, pp. 453-457, October, 2009.

[65]   J. Wu, C. Chang, T. Chin, S. Huang, and S. Chang, "Sidelobe Level Reduction in Wide-Angle Scanning Array System Using Pattern-Reconfigurable Antennas," *IEEE MTT-S Int. Microwave Symp. Digest,* pp. 1274-1277, 2010.

[66]   Y. Y. Bai, S. Xiao, B. Z. Wang, and S. Gao, "Two Dimensional Pattern Scanning by Linear Phased Array with Pattern Reconfigurable Elements," *Applied Computational Electromagnetics Society (ACES) Journal*, vol. 25 no. 2, pp. 144-148, October, 2010.

[67]   A. Khidre, F. Yang, and A. Z. Elsherbeni, "Reconfigurable Microstrip Antenna with Two-Dimensional Scannable Beam" *IEEE AP-S Int. Antenna and Propag. Symp. Digest,* July 2013.

[68]   A. Khidre, F. Yang, and A. Z. Elsherbeni, "Reconfigurable Microstrip Antenna with Tunable Radiation Beamwidth" *IEEE AP-S Int. Antenna and Propag. Symp. Digest,* July 2013.

[69]   A. Khidre, F. Yang, and A. Z. Elsherbeni, "Radiation Characteristics of Linear Phased Arrays Consisting of Beam Scanning Reconfigurable Antenna," in *IEEE Micro., Ant., Propag., and EMC Tech. for Wireless Comm. Symp. Digest.* pp. 140-143, Nov. 2011.

[70]   A. Khidre, F. Yang, and A. Z. Elsherbeni, "Circularly Polarized Beam Scanning Microstrip Antenna using A Reconfigurable Parasitic Patch of Tunable Electrical Size," *IEEE Trans. Ant. Propag*. 2013 (Under review).

LIST OF APPENDICES

APPENDIX A: THE RESONANT FREQUENCIES FOR A

PATCH WITH A CAPACITOR LOADED SLOT

A1. Introduction

This appendix presents in details the resonant frequencies calculations for the patch antenna with a capacitor loaded slot proposed in chapter 2 shown in Figure A-1a. As discussed in chapter 2, the transmission line (TL) theory along with the wheeler incremental volume concept are used for the circuit model deduction shown in Figure A-1b. Accordingly, the appendix is divided into two parts:

➢ The first part presents the calculation for both L_s and L_c of Figure A-1b through applying the wheeler volume concept.

➢ The second part deduces the resonance condition solution to estimate the resonant frequencies.

A2. L_c and L_s calculations

L_c is the inductance due to the current detouring around the slot. If the patch is seen as two halves, each is a microstrip line of width $w/2$, and intercepted by a narrow slit of width $w_s/2$ as shown in Figure A-2a. Therefore, the inductance due to the current going around the narrow slit could be calculated directly using equation (A1), which is deduced by the wheeler volume concept [35]. Z_w and Z_{w-ws} in (A2) are the air characteristic impedances for microstrip lines of widths w and $w-w_S$, respectively.
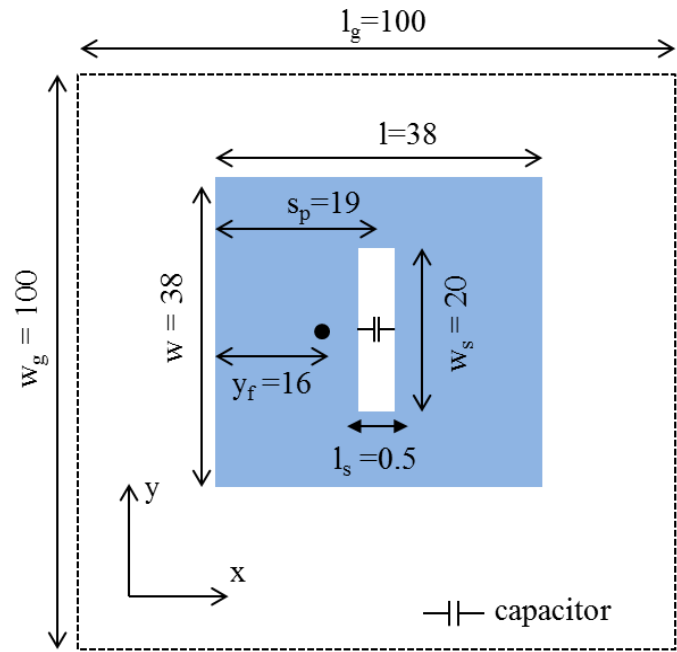
(a)
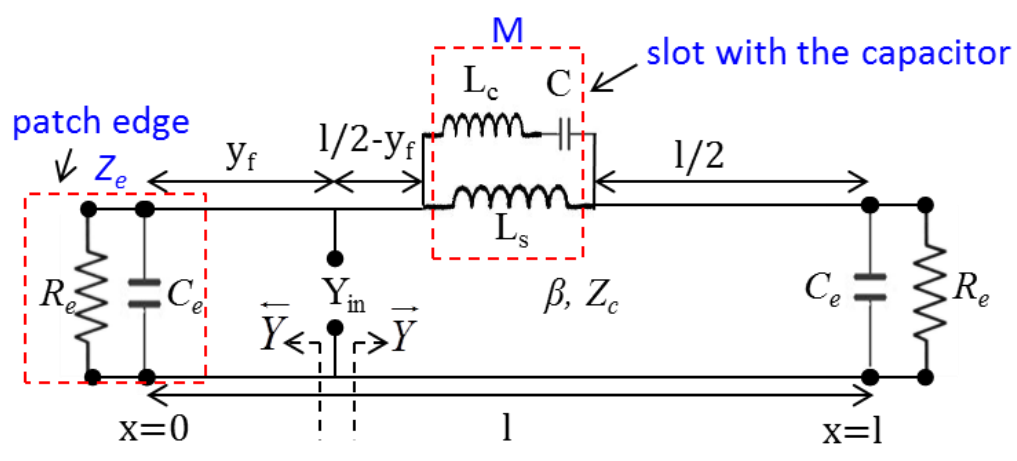
(b)

Figure A-1. A patch antenna with a capacitor loaded slot along with its equivalent circuit model: (a) geometry; (b) circuit model

(a)   (b)
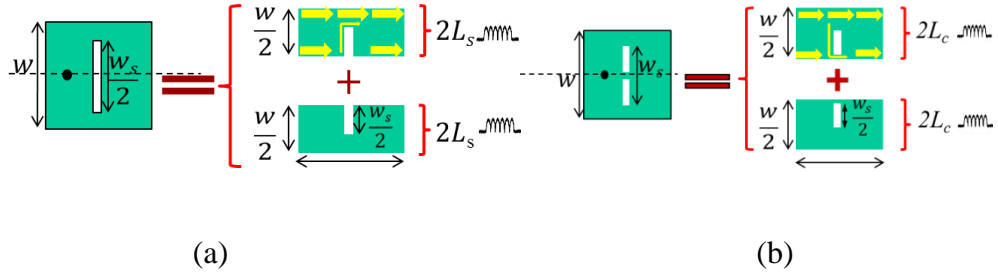
Figure A-2. A schematic diagram to illustrate how the wheeler volume concept is applied to calculate the slot inductance (L_s), and the series inductance to the capacitor.

$$L_s = \frac{h\pi\mu_o}{4}\left(\frac{w^{'}-\delta^{'}}{w^{'}}\right)^2$$

(A1)

$$w^{'} = \frac{h}{Z_w}\sqrt{\frac{\mu_o}{\varepsilon_o}} \quad , \quad \delta^{'} = \frac{h}{Z_{w-ws}}\sqrt{\frac{\mu_o}{\varepsilon_o}}$$

(A2)

L_c is the inductance due the current going through the capacitor as shown in Figure A-2b, which could be calculated using wheeler volume concept in a similar way to L_s. The patch is seen again as two microstrip lines of width $w/2$, each intercepted by a narrow slit of width $w_s/2$. However, the current path is different from the L_s case as shown in Figure A-2b. Therefore, equation (A1) is modified to (A3) to calculate L_c :

$$L_c = \frac{h\pi\mu_o}{4}$$

(A3)

A3. Resonant Frequencies

After calculating L_s, and L_c of Figure A-1b, the resonant frequencies are computed by applying the resonance condition at an arbitrary datum along the transmission line using equation (A4).

$$\mathrm{Im}\left\{Y_{in}\left(f_r,C\right)\right\} = \mathrm{Im}\left\{\overleftarrow{Y}+\overrightarrow{Y}\right\} = 0.$$

(A4)

Y_{in} is the total input port admittance, $\vec{Y}$ is the right input admittance, and $\overleftarrow{Y}$ is the left input admittance. For simplicity, the datum is taken at the patch center, where $y_f = l/2$. Then the left admittance could be calculated using equation (A5):

$$\therefore \overleftarrow{Y} = Y_c \frac{Y_e + jY_c \tan(\beta l / 2)}{Y_c + jY_e \tan(\beta l / 2)}. \tag{A5}$$

where, Y_c is the characteristic impedance of the microstrip TL whose width is w, and it is given as [37] :

$$Y_c = \frac{\sqrt{\varepsilon_{eff}}\left[\dfrac{w}{h} + 1.393 + 0.667\ln\left(\dfrac{w}{h} + 1.444\right)\right]}{120\pi}. \tag{A6}$$

β is the effective propagation constant for a quasi TEM mode along the microstrip TL, and it is given as [37]:

$$\beta = \frac{\omega}{c}\sqrt{\varepsilon_{eff}} \ , \ \varepsilon_{eff} = \frac{\varepsilon_r + 1}{2} + \frac{\varepsilon_r - 1}{2}\left(1 + 12\frac{h}{w}\right)^{-\frac{1}{2}}. \tag{A7}$$

Y_e is the admittance for the radiating slot at each of the patch edges. It is composed of parallel combination of the slot radiation resistance R_e and slot capacitance C_e.

$$Y_e = \frac{1}{R_e} + j\omega C_e \tag{A8}$$

R_e and C_e are both given in [38] as follows:

$$R_e = \frac{I}{120\pi^2} \ , \ \text{where } I \text{ is the integral:} \tag{A9}$$

$$I = \int_0^\pi \left[\frac{\sin\left(\dfrac{\beta_o w}{2} \cos\theta\right)}{\cos\theta} \right]^2 \sin^3\theta \, d\theta \tag{A10}$$

$$= -2 + \cos(\beta_o w) + \beta_o w S_i(\beta_o w) + \frac{\sin(\beta_o w)}{\beta_o w}$$

β_o is the air propagation constant for TEM wave:

$$\beta = \frac{\omega}{c} \tag{A11}$$

and $S_i(x)$ is Fresnel integral:

$$S_i(x) = \int_0^x \sin(t^2).dt \tag{A12}$$

$$\omega C_e = \frac{w}{120\lambda_o}\left[1 - 0.636\ln(\beta_o h)\right] \tag{A13}$$

The right admittance is calculated using equation (A14):

$$\overline{Y} = Y_c \frac{Y_e + jY_c \tan(\beta l / 2)}{Y_c + jY_e \tan(\beta l / 2)} \square Y_M = \frac{Y_M.Y_c \dfrac{Y_e + jY_c \tan(\beta l / 2)}{Y_c + jY_e \tan(\beta l / 2)}}{Y_M + Y_c \dfrac{Y_e + jY_c \tan(\beta l / 2)}{Y_c + jY_e \tan(\beta l / 2)}}. \tag{A14}$$

$$\overline{Y} = \frac{Y_M Y_c Y_e + jY_M Y_c^2 \tan(\beta l / 2)}{Y_M Y_c + jY_e Y_M \tan(\beta l / 2) + Y_c Y_e + jY_c^2 \tan(\beta l / 2)}. \tag{A15}$$

Y_M is the admittance for the combination M shown in Figure A-1, and it is deduced in

equation (A15):

$$Y_M = \frac{1}{j\omega L_s} + \left(\frac{1}{j\omega L_c - \dfrac{j}{\omega C}} \right) = -j\,\frac{\omega^2 L_s C + \omega^2 L_s C - 1}{\omega L_s \left(\omega^2 L_s C - 1 \right)}. \tag{A16}$$

$$Y_{in} = \frac{Y_c Y_e + jY_c^2 \tan(\frac{\omega}{c}\sqrt{\varepsilon_{eff}}\,l/2)}{Y_c + jY_e \tan(\frac{\omega}{c}\sqrt{\varepsilon_{eff}}\,l/2)} + \frac{Y_M Y_c Y_e + jY_M Y_c^2 \tan(\frac{\omega}{c}\sqrt{\varepsilon_{eff}}\,l/2)}{Y_M Y_c + jY_e Y_M \tan(\frac{\omega}{c}\sqrt{\varepsilon_{eff}}\,l/2) + Y_c Y_e + jY_c^2 \tan(\frac{\omega}{c}\sqrt{\varepsilon_{eff}}\,l/2)}. \tag{A17}$$

The resonant frequencies of the antenna in Figure A-1 are obtained with two ways:

1. The zeroes of the imaginary part of equation (A17), which solving for its zeroes is a transcendental equation that needs to be solved numerically.

$$Im\{Y_{in}\} = 0$$

2. The maxima of the real part of equation (A17), which could be calculated by finding the zeroes of equation (A17) first derivative. Solving for the zeroes of equation (A17) first derivative is also a transcendental equation that requires numerical solution.

$$d\,\frac{\mathrm{Re}\{Y_{in}\}}{df} = 0$$

APPENDIX B: RADIATION CHARACTERISTICS OF LINEAR PHASED ARRAYS CONSISTING OF BEAM SCANNING RECONFIGURABLE ANTENNA

B1. Introduction

Extensive research work is conducted on phased array because of its potentials in numerous applications such as, radars and wireless communication systems. The major advantage it provides is the high gain electronically scanned beam, however great challenges are still facing the phased array system. One of these challenges that the beam suffers is the SLL and the grating lobes, when the beam is scanned away from broadside especially at the end fire direction. The SLL is considered one of the critical considerations in phased array design. In general, it is minimized by non-uniformly weighting the elements' excitation amplitude, or by changing their relative position [59], following certain optimization algorithms that have been developed for this goal [60], [61]. These methods rely on modifying the array factor, thus increasing the implementation complexity of the beam forming circuitry and the whole system. Other challenging point in phased array design is the two-dimensional beam scanning with linear arrays. Normally, for beam scanning in the whole angular space, planar phased array is necessary. Planar phased array gives a pencil beam, and requires two dimensional phase distribution across the elements. Therefore, it might be complex and high cost without the need of such narrow beam. On the other hand, linear phased array has a fan beam that could be scanned only in one plane with one dimensional phase distribution along

the elements. If a beam-scanning reconfigurable antenna element is placed in phased array, it will provide an additional degree of freedom, which is shaping the element pattern other than the array factor. This would help in:

- Reducing the side lobe level at wider scanning angle, and acquire a more efficient amplitude tapering.

- Overcoming the difficulty of two-dimensional beam scanning with linear phased arrays (E-plane aligned) as will be discussed in a later section.

Investigations is carried out on linear phased array with pattern reconfigurable antenna elements to improve the SLL, in comparison to linear phased array of fixed beam antennas [62]-[64]. In [62], and [64], the switchable three strips antenna in [3] is used. This element has three switchable states; at one state the beam has a broadside direction, whereas in the other two states the beam is deflected to two directions at ±45˚. In a similar fashion, [64] used a newly proposed pattern reconfigurable rectangular monopole antenna with three switchable states. Those elements don't allow for continuous beam scanning, rather than switching along fixed directions, and hence limit the scanning range of the phased array.

The two-dimensional beam scanning with linear phased array has been attempted in [66], where the element in [3] is used. Therefore the beam is scanned in one plane through elements' phase progression, whereas it is switched in the orthogonal plane to directions at ±30˚. Recently, an antenna with a continuous beam scanning feature has been proposed in [6], where such feature was enabled with the aid of lumped reactive loadings. The beam direction is controlled according to the reactive loading value, allowing for continuous beam scanning within certain range [-40˚, 30˚].
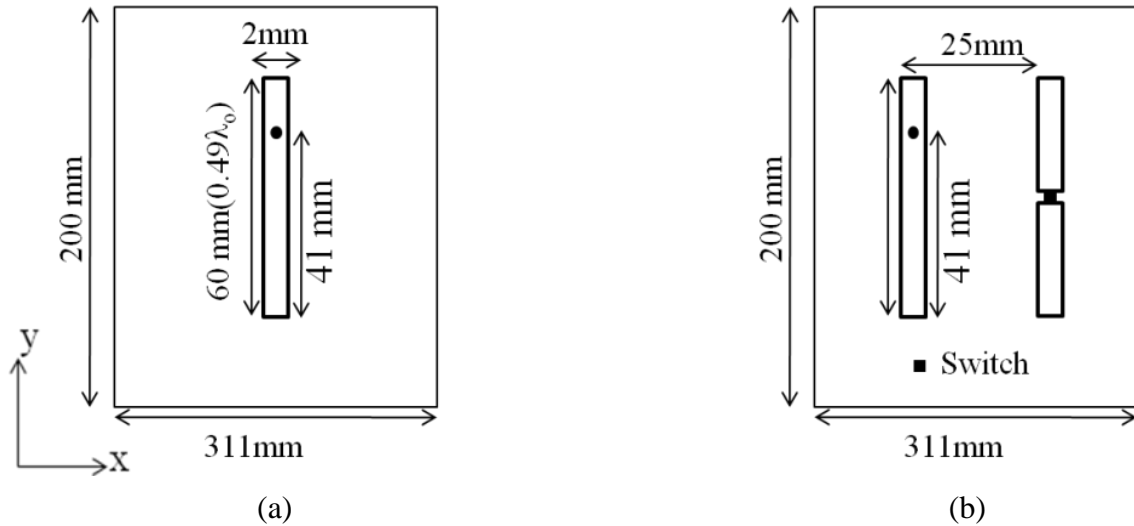
Figure B-1. (a) Single strip antenna; (b) dual-strip beam scanning antenna.

This Appendix presents a study on using beam scanning antenna element in linear phased array to reduce SLL, and compare it to an array of antennas with fixed broadside beam. Furthermore, a study on two-dimensional continuous beam scanning of E-plane aligned phased array using the same approach is also presented.

B2.   Dual-Strip Beam Scanning Antenna Element

The dual-strip beam scanning antenna proposed in [6] is the one that will be used throughout this study but with altered dimensions. The geometry of the antenna is shown in Figure B-1a, whereas Figure B-1b shows single strip antenna that exhibit fixed broadside radiation beam. Dual-strip beam scanning antenna consists of two parallel strips each of 2mm width, one is driven with coaxial pin feed, and the other is a parasitic. The antenna is built over an air substrate with 10mm thickness above a perfect electric conducting ground plane. A gap 2mm $\times$ 2mm is inserted on the middle of the parasitic strip to allow for placing, either RF PIN diode switch or a variable reactive loading (capacitor or inductor). If a switch is placed, the antenna would have two possible states; ON state, where the antenna beam is directed to 12˚ in xz plane, and OFF state, where its beam is directed to -24˚ in xz plane. Simulation results

for the reflection coefficient of the dual strip antenna in its two switching states, compared with the single strip antenna are shown in Figure B-2. The simulated radiation patterns of the corresponding antennas configuration are also shown in Figure B-3. On the other hand, if a varicap or variable inductor is placed at the gap instead, beam scanning feature in xz plane would rather exist. With full EM simulations, Figure B-4, and Figure B-5 show how the beam direction of the dual-strip antenna changes in the xz plane, with the capacitance and inductance value, respectively. All simulations are carried out using Ansoft HFSS [36].
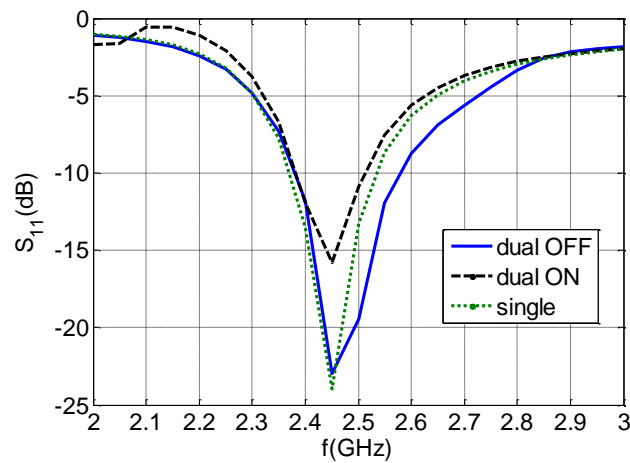

Figure B-2. The simulated S_{11} of the dual strip antenna in both ON/OFF state vs. the single strip antenna.
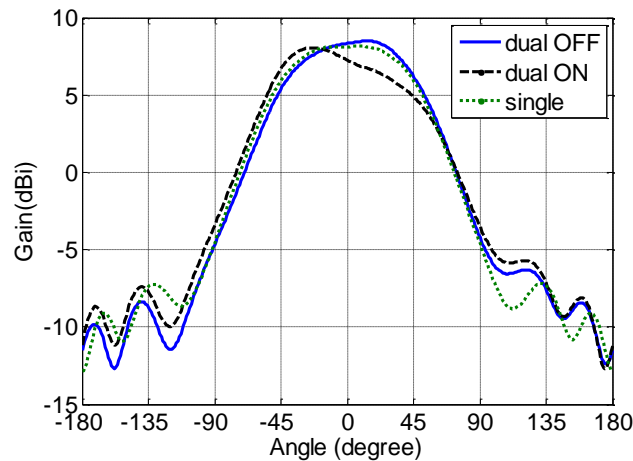

Figure B-3. The simulated radiation pattern of the dual strip antenna in both the ON/OFF state vs. the single strip antenna.
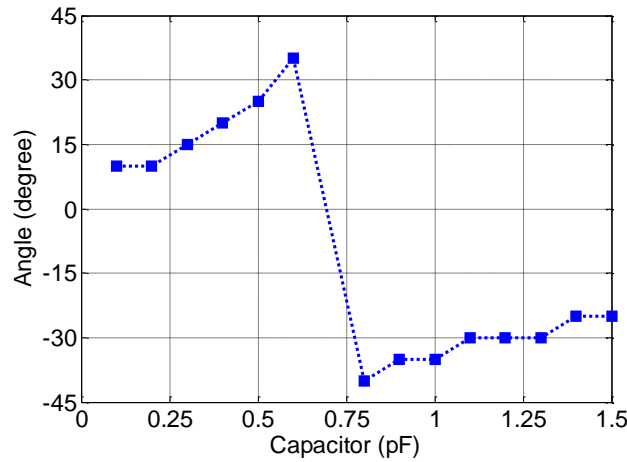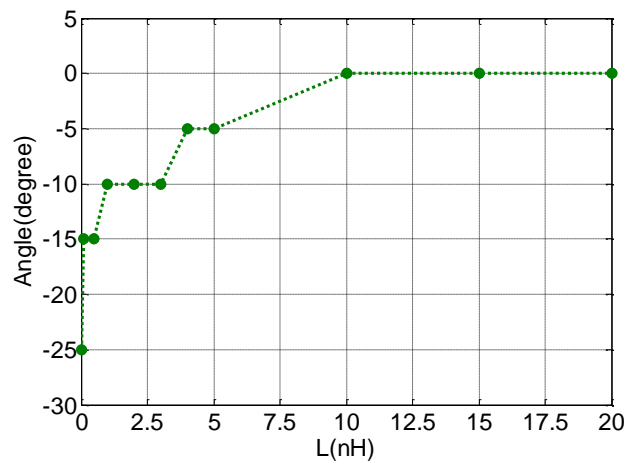
Figure B-4. Scan angle vs. capacitance value.

Figure B-5. Scan angle vs. inductance value.

B3.   H-plane Aligned Linear Phased Array: SLL Reduction

The above two antennas; single strip, and dual strip, are packed in a 4×1 H-plane aligned array as shown in Figure B-6. The separation between elements in both arrays is 0.5 λ_0, and their progressive phase shift is 'β'. Changing the value of β, would scan the beam in the xz plane. Figure B-7 shows the SLL versus the scan angle of both arrays. The blue curve is for the array of single strip antennas, while the other two curves are for the array of dual strip antennas in both ON and OFF states. It is clear that, in the ON state, at angles < -8˚, the array of dual strip elements, has lower SLL than the array of single strip elements.
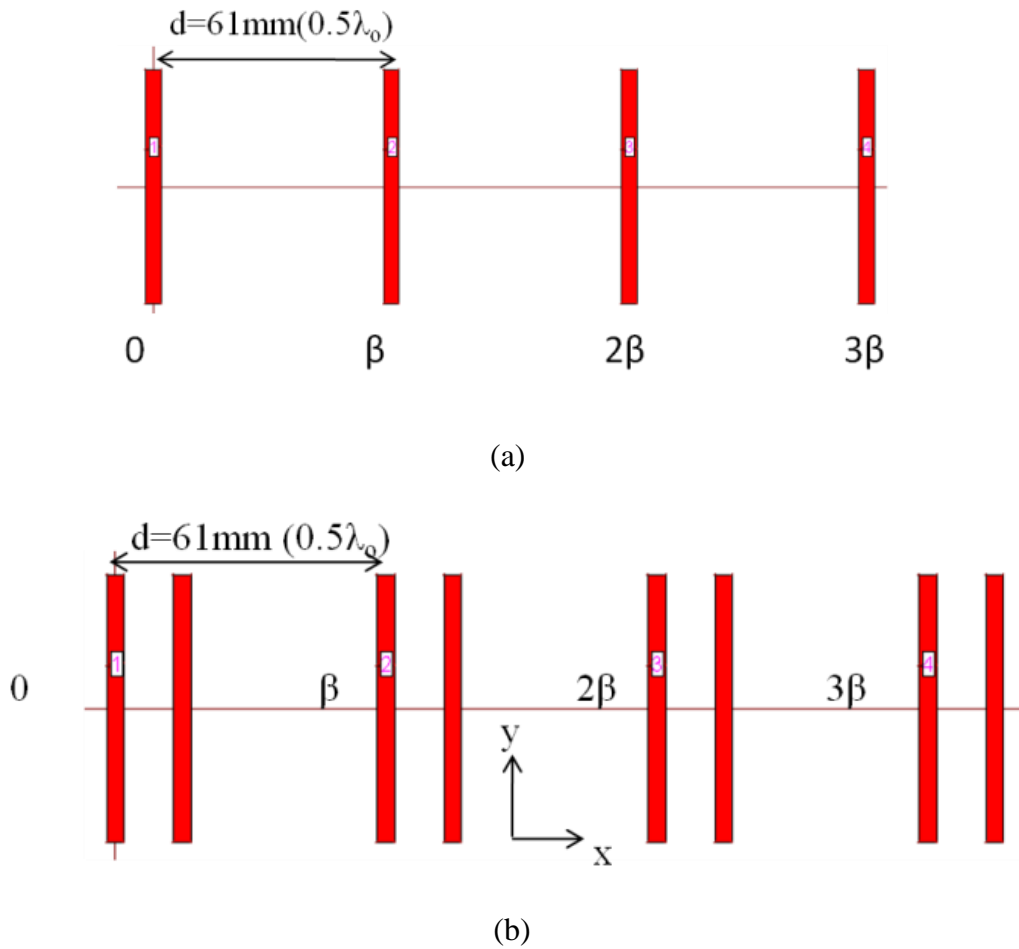
Figure B-6. 4×1 H-plane array (a) dual strip beam scanning element (b) single strip fixed beam element.

Whereas, at angles > -8°, it is higher. In the OFF state, dual strip antenna array has a quite similar performance as the single strip array at angles ≥ 0°, but at angles < 0° it is worse. Therefore, for SLL reduction, dual strip array should be used in the ON state at scan angles ≤ -8°, and in the OFF state at scan angles ≥ -8°. This defines what is called a combined state of the dual strip antenna array, at which the SLL due to the array of dual-strip antenna in the combined state is lower than single strip antenna array as shown in Figure B-8.

One can conclude from this study is to improve the SLL at wider scanning angles, varactor should be used instead of RF switches, because it forces the radiation beam of the dual strip antenna to deflect to a higher angle values in both +x and -x directions. An example to

better elaborate the idea, if lower SLL is needed at angles ≤ -30˚, the dual-strip array should be

operated with varactors tuned to a value around 1.25 pF. At 1.25 pF, the antenna element has

a -30˚ tilted beam. On the other hand, if lower SLL is need at angles ≥ +30˚, the varactors
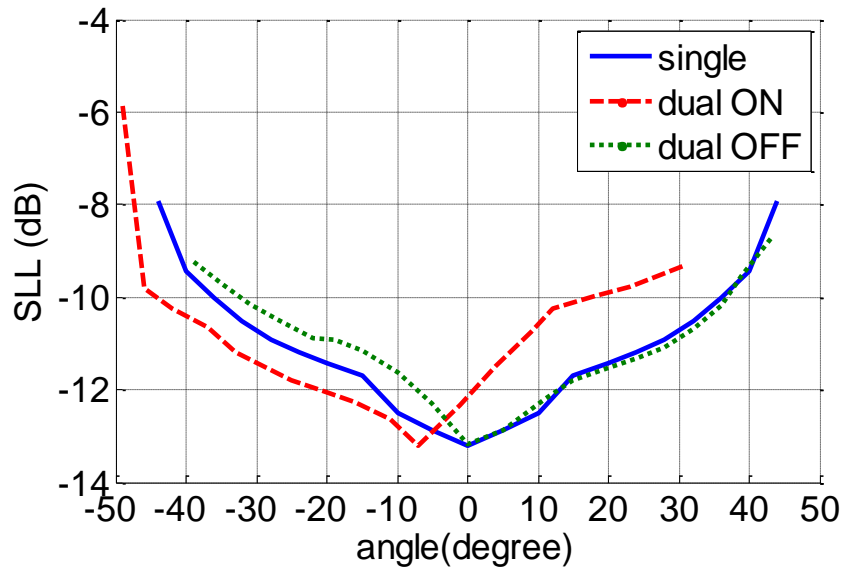
should be tuned around 0.5pF.

Figure B-7. SLL vs. scan angle for H-plane phased array of dual strip beam scanning element

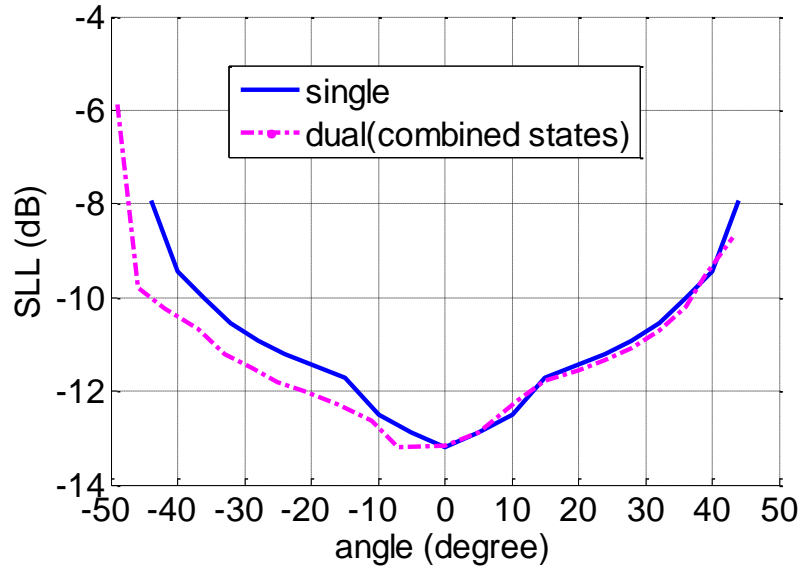compared to single strip fixed beam one.

Figure B-8. SLL vs. scan angle for both single strip array and dual strip array in the combined state (ON/OFF).

B4. E-plane Aligned Linear Phased Array: Two-Dimensional Beam Scanning

In this section, the dual-strip antenna is packed in a 1×4 E-plane aligned array, and the elements are placed $0.57\lambda_0$ away from each other as shown in Figure B-9. The idea behind scanning the beam in xz and yz planes is based on the following:

1. Scanning the beam in yz plane through modifying the elements' phase shift progression β_y as depicted by the array theory.

2. Scanning in the xz plane by tilting the element's beam direction in the same plane.

The latter could happen via tuning the varactor mounted over the antennas. For instance, if all the varactors are tuned to 1.25pF and (β_y) is set to zero, the radiation pattern will deflect to -30˚ in the xz plane, and 0˚ in the yz plane, as shown in Figure B-10. Furthermore, if β_y is set to any value, other than zero, two dimensional beam scanning will be obtained. The beam

direction θ_m in the yz plane could be predicted using the array theory as described by equation (B1).

$$\sin(\theta_m) = -\frac{\lambda_0 \cdot \beta_y}{2\pi.d}.$$ (B1)

For example, if β_y is set to -60˚, θ_m would be 17˚. Figure B-11 shows the radiation pattern due to an array of dual strip antennas, with progressive phase shift -60˚ and the varactors are tuned to 1.25pF. It is observed that, the beam's direction in xz plane is -30˚, which is due to the tilted beam of the dual strip elements. Whereas, the beam direction in the yz plane is 15˚, which is due to the elements' phase shift progression and agrees well with the array theory prediction. Figure B-12 shows two different prospective 3D view of the fan beam produced by the linear array.
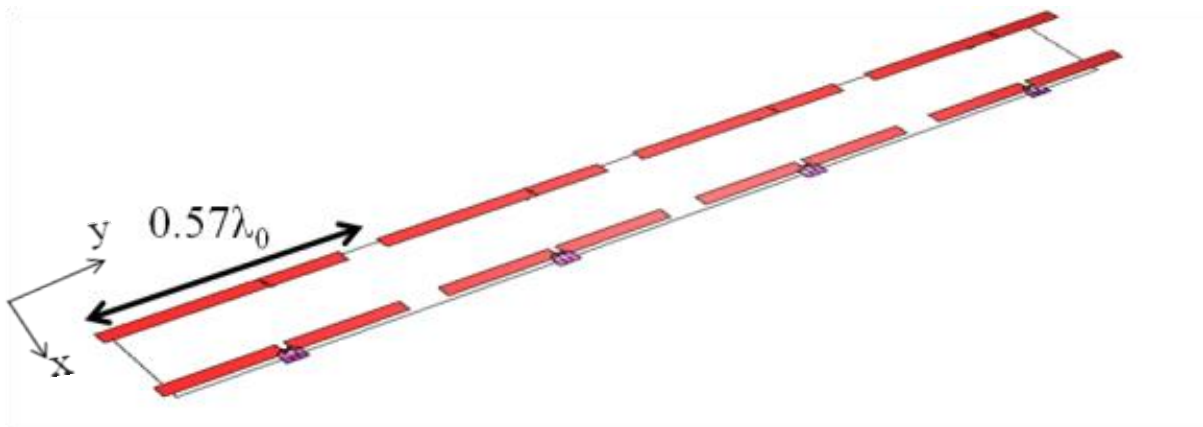

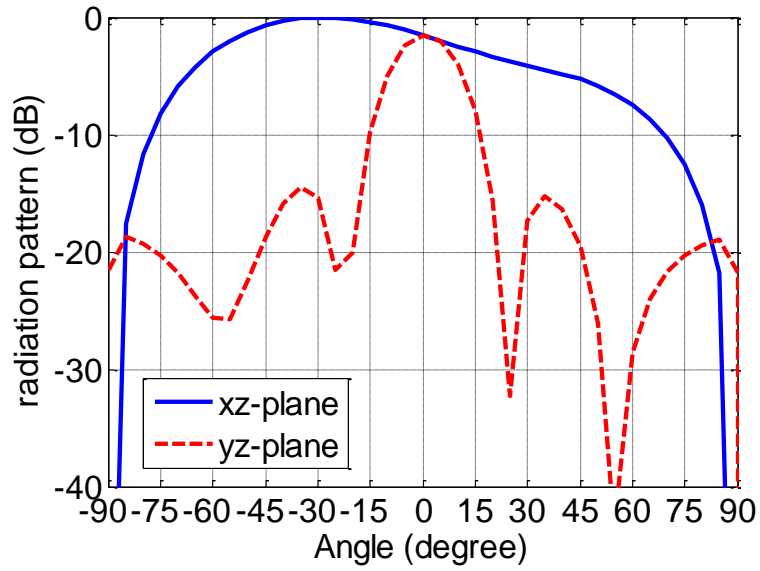Figure B-9. E-plane array for dual strip beam scanning antenna.

Figure B-10. The radiation patterns of the 1×4 E-plane array of dual strip antenna with 1.25 pF capacitance value.
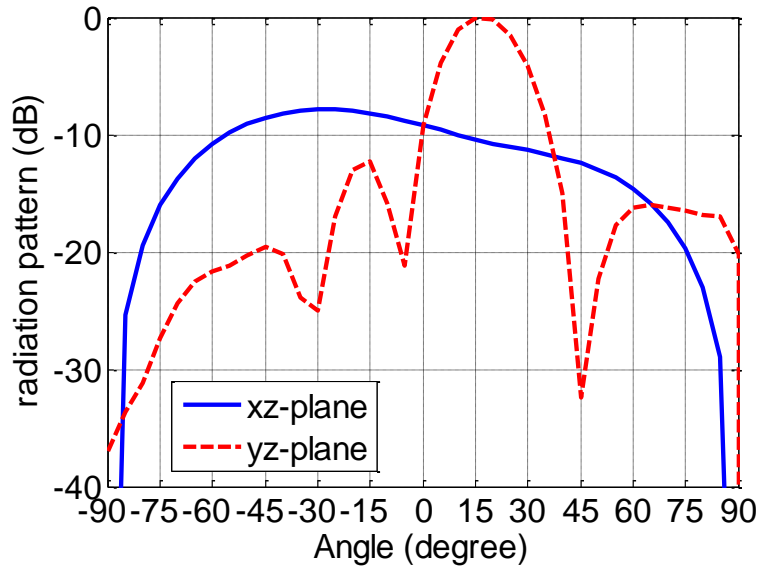

Figure B-11. The radiation pattern of the 1×4 E-plane array of dual strip antenna with 1.25 pF capacitance value and progressive phase -60˚.
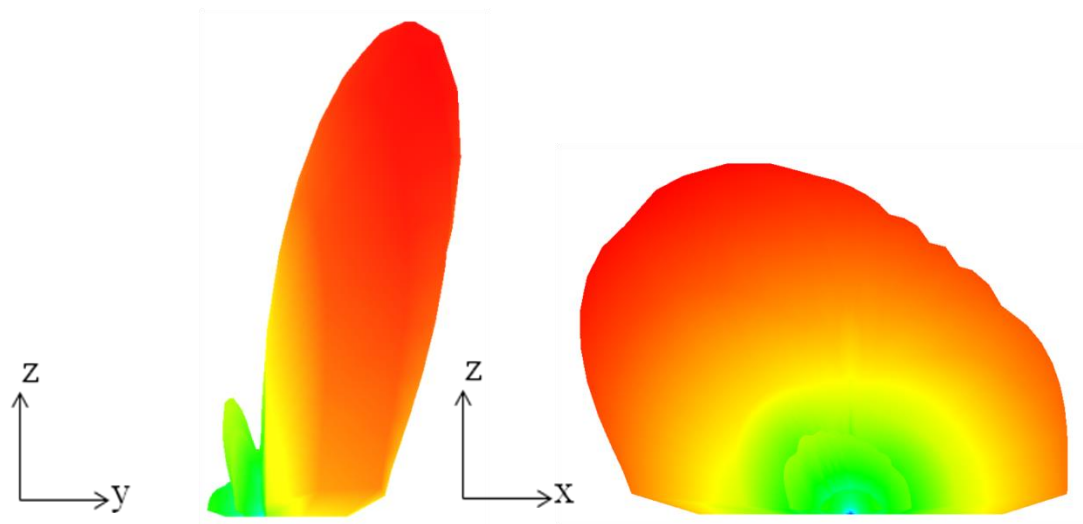
Figure B-12. Different 3D prospective view of the fan beam due to the E-plane phased array of dual strip antenna with -60˚ progressive phase shift and capacitance of 1.25pF.

B5.   Conclusion

Reconfigurable antennas with beam scanning feature enabled by varactors or variable inductors could enhance the performance of linear phased array, compared to the conventional array of fixed beam antennas. For the H-plane phased array, beam scanning reconfigurable antennas could help in reducing the SLL at wider scanning angles. The 1 dB SLL reduction is obtained by an array of dual-strip elements operating in the ON state (-24˚ tilted beam). For the E-plane phased array, beam scanning reconfigurable antennas allow two dimensional scanning of fan beams, which is impossible with the conventional linear phased arrays. Scanned beam with 15˚ in the yz plane, and -30˚ direction angle in the xz plane is obtained, using an array of dual strip elements with 1.25pF capacitance. The experimental verification for this theoretical study plus investigations on using lumped elements in the H-plane phased arrays for more SLL reduction will be continued in the future.

APPENDIX C: LIST OF PUBLICATIONS

Conferences:

[1]   A. Khidre, K. F. Lee, F. Yang, and A. Z. Elsherbeni, "Circularly Polarized E-Shaped Patch Antenna for Wireless Applications," *in URSI Radio Science Meeting Digest, Toronto, Canada,* July 2010.

[2]   A. Khidre, K. F. Lee, A. Z. Elsherbeni, and F. Yang, "E-shaped Patch Antenna with Reconfigurable Circular Polarization for Wireless Applications", *in ACES Int. Rev. of Prog. in Applied Comp. EM, Digest*, pp. 822-826, July 2010.

[3]   A. Khidre, K. F. Lee, F. Yang, and A. Z. Elsherbeni, "Wideband Dual-Beam Microstrip Antenna for Wireless Communication," *URSI Radio Science Meeting Digest,* Spokane, Washington, July 2011.

[4]   A. Khidre, F. Yang, and A. Z. Elsherbeni, "Radiation Characteristics of Linear Phased Arrays Consisting of Beam Scanning Reconfigurable Antenna," *IEEE Micro., Ant., Propag., and EMC Tech. for Wirless Comm. Symp. Digest.* pp. 140-143, Nov. 2011.

[5]   A. Khidre, F. Yang, and A. Z. Elsherbeni, "Reconfigurable Dual-Band Patch Antenna with a Varactor-Loaded Slot" *IEEE AP-S Int. Ant. and Propag. Symp. Digest,* July 2012.

[6]   A. Khidre, F. Yang, and A. Z. Elsherbeni, "Reconfigurable Microstrip Yagi-Uda Antenna with a Scannable Circularly Polarized Beam" *IEEE AP-S Int. Ant. and Propag. Symp. Digest,* July 2012. (honorable mentioned)

[7]   A. Khidre, F. Yang, and A. Z. Elsherbeni, "Reconfigurable Microstrip Antenna with Two-Dimensional Scannable Beam" *IEEE AP-S Int. Antenna and Propag. Symp. Digest*, July 2013.

[8]   A. Khidre, F. Yang, and A. Z. Elsherbeni, "Reconfigurable Microstrip Antenna with Tunable Radiation Beamwidth" *IEEE AP-S Int. Antenna and Propag. Symp. Digest*, July 2013.

[9]   A. Abdelrahman, A. Khidre, F. Yang, and A. Elsherbeni, "Transmitarray Antenna Design using Slot-Type Element," *IEEE AP-S Int. Antenna and Propag. Symp. Digest*, July 2013.

[10]   A. Khidre, F. Yang, and A. Z. Elsherbeni, "Reconfigurable Microstrip Antennas with Dynamic Radiation Patterns," *IEEE AP-S Int. Antenna and Propag. Symp. Digest*, July 2014.

Journals:

[1]   A. Khidre, K. F. Lee, F. Yang, A. Elsherbeni "Wide Band Circularly Polarized E-Shaped Patch Antenna for Wireless Applications," *IEEE, Antennas Propag., Mag.*, vol. 52, no. 5, pp. 219-229, October 2010.

[2]   A. Khidre, K. F. Lee, F. Yang, A. Z. Elsherbeni, "Circular Polarization Reconfigurable Wideband E-Shaped Patch Antenna for Wireless Applications," *IEEE Trans. Ant. Propag.*, vol. 61, no. 2, pp. 960-964, Feb. 2013.

[3]   A. Khidre, K. F. Lee, F. Yang, A. Z. Elsherbeni, "Wide Band Dual-Beam U-Slot Microstrip Antenna," *IEEE Trans. Ant. Propag.*, vol. 61, no. 3, pp. 1415-1418, March. 2013.

[4]   A. Khidre, F. Yang, and A. Z. Elsherbeni, "A Patch Antenna with a Varactor-Loaded Slot for Reconfigurable Dual-band Operation," *IEEE Trans. Ant. Propag*. (under revision)

[5]   A. Khidre, F. Yang, and A. Z. Elsherbeni, "Circularly Polarized Beam Scanning Microstrip Antenna Using A Reconfigurable Parasitic Patch of Tunable Electrical Size," *IEEE Trans. Ant. Propag*. (under revision)

[6]   A. Khidre, F. Yang, and A. Z. Elsherbeni, "Tunable Beamwidth Microstrip Antenna," in preparation to *IEEE Ant. Wireless Propag. Lett*.

[7]   A. Khidre, F. Yang, and A. Z. Elsherbeni, "Two-Dimensional Beam Scanning Microstrip Antenna Using Reconfigurable Parasitic Patches of Tunable Electrical Size," in preparation to *IEEE Trans. Ant. Propag*.

VITA

Ahmed Khidre received his B.Sc. in electrical engineering from Ain Shams University, Cairo, Egypt, in 2006. He completed also all the required coursework toward M.Sc. of EE by 2009 at the same university as a part time student. From 2006 to 2007, he was employed at Ericsson Egypt Ltd. From 2007 to 2009, he was appointed as a teacher assistant at the electrical engineering department of Misr International University (MIU), where he tutored, and mentored several courses/labs of the EE curriculum. He joined The University of Mississippi in 2009 as a research assistant and graduate student in the center of applied electromagnetic systems research (CEASR), where he earned his MSc in 2012. Mr. Khidre experience has broaden, and enriched during his graduate study program through several academic/industrial internships, including *research intern* at *Magdeburg University*, Magdeburg, Germany (summer 2009), *senior visiting scholar* at *Tsinghua University*, Beijing, P. R. China (fall 2011), *antenna engineer intern* at *Apple Inc.*, Cupertino, CA, USA (fall 2012- spring 2013), and *R&D engineer intern* at *Aruba Networks Inc.*, Sunnyvale, CA, USA (summer 2013).

Mr. Khidre, is currently employed as *Antenna/RF hardware engineer* at *Aruba Networks Inc.* (R&D unit), He is also a technical reviewer for multiple refereed journals in the field of applied electromagnetics, including *IEEE Transaction on Antennas and Propagation*, *IET Microwave, Antennas, and Propagation*, *PIER*, *JEMWA*, and *ACES*. His research interest includes microstrip antennas, reconfigurable antennas, tunable microwave circuits, beam scanning antennas, UWB and MIMO Wireless systems, FDTD, RF MEMs, and MMIC.